The aeroelastic tailoring of a high aspect-ratio composite structure

TN van den Bosch

23289767

Dissertation submitted in fulfilment of the requirements for the degree *Magister in Mechanical Engineering* at the Potchefstroom Campus of the North-West University

Supervisor: Dr. A.S. Jonker

September 2014

It all starts here ™

NORTH-WEST UNIVERSITY
YUNIBESITI YA BOKONE-BOPHIRIMA
NOORDWES-UNIVERSITEIT
®

The aeroelastic tailoring of a high aspect-ratio composite structure

THE AEROELASTIC TAILORING OF A HIGH ASPECT-RATIO COMPOSITE STRUCTURE

By

Taeke van den Bosch

23289767

Supervisor : Dr. A.S. Jonker

Year : 2014

Department : Mechanical Engineering

ABSTRACT

The aim of this investigation was to review literature for the most suitable aeroelastic tailoring analysis tools for long slender composite structures, and integrate them into an aeroelastic tailoring process.

The JS1C Revelation is a high performance sailplane made from modern composites, mostly carbon fibre. This has the advantage of being more rigid than traditional engineering materials, thereby reducing the effects of the twisting deflections on these long slender structures due to aerodynamic loads. The implementing of aeroelastic tailoring can create bend-twist couples for performance improvements. Composites enable the use of aeroelastic tailoring to improve gliding performance. Flaperon 3 of the JS1C 21 m was used as the design problem for aeroelastic tailoring.

Aeroelastic tailoring was done by analysing the flaperon structure at the different layup angles to determine the correct design point to tailor the structure to improve aerodynamic performance at thermalling and cruise, but mostly cruise since it accounts for 70% of the flight time.

The composite structure analysis tool has the objective to get results during concept design. This directed the line of research of analysis tools to a solution method of two dimensional cross-section mesh properties projected onto a one dimensional beam. The literature of Hodges had good verification and published data on the analysis tools.

The analysis tools comprised of three programs that were not very user friendly. Thus the author compiled a Matlab program as a user interface tool to run the three programs together. The aeroelastic tailoring process systematically works through the known design variables and

objectives, which are given as inputs to the analysis tool. The analysis tool plots the coupling data versus layup angle. From this the best layup angles for a sought-after bend-twist couple is used to aeroelastically tailor the wing.

The composite structure analysis tool's accuracy was verified by analysing cantilever beam deflections and comparing the results with hand calculations and SolidWorks Simulation FEM results. The analysis tool's accuracy was further verified by comparing the aerodynamic torsional load's twist deflections with thin walled tube theory.

The analysis tool was validated by applying a torsional load at the tip of a JS1C production Flaperon 3 in an experimental setup and then comparing this result with the Flaperon 3 modelled in the analysis tool. These comparisons also ensured that the model's composite material properties and the meshing of the flaperon cross-sectional properties were correct.

This aeroelastic tailoring was validated with the advantage of then being used to improve the aerodynamic performance of the JS1C Revelation 21 m tip's flaperon. This improvement could be made by making use of a tailored bend-twist couple to reduce the effect of the aerodynamic load's twist deflections.

A test sample of the JS1C 21 m flaperon 3 was used to validate aeroelastic tailoring. The test sample was designed to be 1 m in length and have all the specified tailoring coupling characteristics that could improve the aerodynamic performance of the JS1C 21 m flaperon 3. The test sample was manufactured according to Jonker Sailplanes manufacturing standards and experimentally set up with the same applied deflections as in the analysis tool. The calculated bend-twist values and the experimental setup results were similar with a negligible difference, assuming small displacements and an aspect ratio greater than 13; this confirmed that the PreVABS/VABS/GEBT composite structure analysis tool could be used in aeroelastic tailoring to predict and design the bend-twist couple needed to improve the aerodynamic performance of the JS1C 21 m.

While the twist behaviour of Flaperon 3 was improved by the tailored bend-twist couple, it was still necessary to add pre-twist as well, to fully address the effects of twisting by aerodynamic forces.

UITTREKSEL

Die doelstelling van hierdie ondersoek was om die nodige gereedskap te bekom aan hand van beskikbare literatuur, ten einde lang dun balkstrukture, van saamgestelde materiaal vervaardig, te analiseer en uiteindelik in te lyf by ‘n proses om sulke strukture met pasgemaakte eienskappe te ontwerp onderworpe aan aerodinamiese kragte.

JS1C Revelation is ‘n hoëwerkverrigtingsweeftuig en is grotendeels vervaardig van moderne veselopleggings, veral koolstofvesel. Hierdie werkstowwe beskik oor hoër starhede en sterkte as tradisionele materiale, wat aanleiding gee tot voordele soos ‘n vermindering in wringing onder die invloed van aerodinamiese belastings. Indien die opleggings doelontwerp word, kan eieskappe soos buig-wringkoppels in die struktuur lei tot verdere verbetering in die werk verrigting van onder andere sweeftuie. Klap 3 van JS1C se 21 m-vlerk was die gekose ontwerpprobleem.

Die aeroelastiese pasmaak van die klap is gedoen deur die deurlopende analise van die opleggings terwyl die opleghoeke van die laminaatlae verander is, totdat die grootste verbetering in werkverrigting verkry is by twee vluggevalle, naamlik togsnelheid (wat vir tot 70% van die totale vlugtyd geskied) en klimsnelheid.

Die toerusting om strukture van saamgestelde materiaal te analiseer het as uitkoms die verkryging van resultate tydens die aanvanklike ontwerp. Om hierdie rede is die navorsing gerig na ‘n metode wat ‘n volledige 3-dimensionele struktuur nougeset afbreek tot ‘n stelsel van 2-dimensionele dwarssnitte geprojekteer op ‘n klassieke 1-dimensionele balk. Hierdie en ander metodes is deur breedvoerige gepubliseerde literatuur soos Hodges gestaaf.

Die gekose analiseprogram bestaan uit drie afsonderlike kodes, en is nie juis gebruikersvriendelik nie. Daarom is ‘n Matlab kode geskep om as ‘n intervlak te dien om die drie kodes saam te bedryf. Die proses van aeroelastiese doelontwerp geskied deur sistematies die bekende veranderlikes en ontwerpuitkomste, wat as insette tot die kode gegee is, te verwerk. Daarna word die buig-wringkoppeldata grafies weergegee teenoor die opleghoek van die struktuurmateriaal, waaruit die mees geskikte opleghoek gekies kan word.

Die noukeurigheid van die analisekode is gestaaf aan die hand van resultate verkry van handberekeninge en eindige elementanalise met behulp van *SolidWorks Simulation*, wat uitgevoer is op ‘n welbekende kantelbalk. Bogenoemde resultate is vervolgens ook vergelyk met dunwand-

wringteorie.

Die gekose gereedskapstuk is verder bevestig/gevalideer deur die analise van JS1C se klap 3, wat tydens ‘n eksperiment onderwerp is aan ‘n wringlas op die vry ent. Die lasgeval is ook gemodelleer en die twee stelle resultate is vergelyk. Die korrekte materiaaleienskappe, en veral die korrekte inskakeling van die deursnitmaas, is verseker tydens die vergelykende toets.

Ná die bevestiging van die aeroelastiese analisekode is dieselfde kode gebruik om die werkverrigting van die JS1C 21 m klap 3 te verbeter. Die verbeterde verrigting is moontlik gemaak deur die vermoë om die meganiese eienskappe van saamgestelde laminate sodanig te beheer dat selfs buig-wringkoppeling in die struktuur kan ontstaan wat die normale verwringing kan teëwerk.

‘n Toetsmonster is voorberei om die pasmaking te bekragtig. Die toetsmonster is basies die eerste 1 m van Klap 3 vanaf die binneboord, maar met die laminaat opgelê volgens die analiseresultate ten einde die voorgeskrewe buig-wringkoppeling te besit. Die toetsmonster is voorberei volgens die werkstandaard van Jonker Sailplanes, en is opgestel met dieselfde aangewende buigverplasing as vir die analise. Die berekende en eksperimentele resultate toon goeie ooreenkoms, met weglaatbare verskille by klein verplasings en slankheidsverhoudings groter as 13; hierdeur is bevestig dat, deur die gebruik van die *PreVABS/VABS/GEBT*-kodestel, aeroelastiese doelontwerp met welslae aangewend kan word om die aerodinamiese verrigting van die 21 m JS1C te verbeter.

Hoewel die wringgedrag van JS1C Klap 3 verbeter is deur die ontwerpte buig-wringkoppeling, sou dit nietemin steeds nodig blyk om die oorblywende wringing weens aerodinamiese kragte aan te spreek met behulp van ‘n permanente aanvanklike wringhoek.

ACKNOWLEDGMENTS

- Dr. Attie Jonker for his help, encouragement, and never wavering advice on keeping a high standard for a master's report.
- Prof. Leon Liebenberg for his help in locating literature. The advice on report writing for masters was much appreciated.
- Gerrit Grundling for his encouragement, willingness to help with the report writing and the many discussions which helped with the grasping of the difficult theoretical concepts.

DECLARATION

I, Taeke Nicolai van den Bosch, hereby declare that the work contained in this dissertation is my own work. Some of the information contained in this dissertation has been gained from various journal articles; text books, sources etc., and has been referenced accordingly.

Signature: Date: 15/09/2014

TABLE OF CONTENTS

LIST OF FIGURES XII

LIST OF TABLES XIV

KEY WORDS XV

ABBREVIATIONS XVI

ROMAN SYMBOLS XVII

GREEK SYMBOLS XVIII

DEFINITIONS XVIII

1 INTRODUCTION 1

1.1 BACKGROUND 1

1.2 PROBLEM DEFINITION 3

1.3 OBJECTIVES OF STUDY 3

1.4 LAYOUT OF DISSERTATION 4

2 LITERATURE STUDY 5

2.1 A HISTORIC OVERVIEW OF THE DEVELOPMENT OF AEROELASTIC TAILORING 5

2.2 AEROELASTIC TAILORING ANALYSIS TECHNIQUES 7

2.2.1 Experimentation 7

2.2.2 Three-dimensional finite element methods 8

2.2.3 Beam theory 9

2.2.4 Shell theory 12

2.3 COMPARISON OF ANALYSIS TECHNIQUES 13

2.4 MANUFACTURING CONSTRAINTS 14

2.5 SUMMARY OF LITERATURE STUDY 14

3 DESCRIPTION AND IMPLEMENTATION OF PREVABS, VABS AND GEBT 16

3.1 OVERVIEW OF ANALYSIS TOOLS 16

3.2 THEORY OF VABS AND GEBT 18

3.2.1 GEBT analysis tool theory 18

3.2.2 VABS analysis tool theory models for different beams cross-sections 20

3.3 REVIEW OF VABS VALIDATION 22

3.4 INTEGRATION OF ANALYSIS TOOLS INTO A SINGLE TOOL 23

3.5 SUMMARY 26

4 VALIDATION OF A FLAPERON-TYPE MODEL USING "TAILOR.M" 28

4.1 MODELLING OF FLAPERON 3 28

4.2 EXPERIMENTAL TEST OF FLAPERON 3 32

4.3 RESULTS AND DISCUSSION 32

4.4 SUMMARY 33

5 TAILORING OF FLAPERON 3 34

5.1 TAILORING REQUIREMENTS 36

5.2 SETUP AND MODELLING 40

5.3 EXPERIMENT 47

5.3.1 Test sample specification 48

5.3.2 Sample manufacture *50*

5.3.3 Experimental test *55*

5.4 EXPERIMENTAL RESULTS 59

5.5 CONCLUSION AND DISCUSSION 61

6 CONCLUSION AND RECOMMENDATIONS 62

6.1 CONCLUSION 62

6.2 RECOMMENDATIONS 63

7 REFERENCES 64

APPENDIX A - CROSS-CHECK THE OPERATION OF PREVABS, VABS AND GEBT WITH HAND CALCULATIONS AND FEM A-1

COMPARISON OF RESULTS A-8

APPENDIX B - MATLAB PROGRAM USER INTERFACE TO INTERGRATE PREVABS, VABS AND GEBT B-1

LIST OF FIGURES

FIGURE 1: JS1B 18 M IN FLIGHT WITH SELF-SUSTAINER JET SYSTEM, NOTE HOW THE WINGS DEFORM IN FLIGHT (NOMAD, 2012) 1

FIGURE 2: CARBON FIBRE WING LAID UP WITH 0°/95° FOR STRUCTURAL BENDING RIGIDITY (BENNETT, 2013) 2

FIGURE 3: JS1C FLAPERON POSITION 3

FIGURE 4: FEM WITH MILLIONS OF DOFS (YU, 2012) 9

FIGURE 5: *CLASS* $\mathcal{T}$ *BEAMS* WITH OPEN CROSS-SECTIONS 21

FIGURE 6: *CLASS* $\mathcal{S}$ *BEAMS* LONG SLENDER CROSS-SECTIONS 21

FIGURE 7: CLASS $\mathcal{R}$ BEAMS REGULAR BEAM CROSS-SECTIONS 21

FIGURE 8: HETEROGENEOUS BEAM GEOMETRICAL AND MATERIAL PROPERTIES (YU, 2012) 22

FIGURE 9: DISPLACEMENT SOLUTION RESULTS OF HETEROGENEOUS BEAM (HODGES & YU, 2007) 22

FIGURE 10: A) BEAM DISPLACEMENT ALONG THE LENGTH B) $\boldsymbol{\sigma 22}$ STRESS OVER THE CROSS-SECTION C) $\boldsymbol{\sigma 11}$ STRESS OVER THE CROSS-SECTION D) $\boldsymbol{\sigma 33}$ STRESS OVER THE CROSS-SECTION (YU, 2012) 23

FIGURE 11: PROCESS FOR CALCULATION OF CROSS-SECTIONAL PROPERTIES (CHEN & YU, 2008) 24

FIGURE 12: PROCESS FOR 3-D STRESS/STRAIN RECOVERY (CHEN & YU, 2008) 24

FIGURE 13: FLOW DIAGRAM OF THE TAILOR.M CODE 25

FIGURE 14: COORDINATE SYSTEM FOR LAYER ANGLE INPUTS, FLAPERON TIP TWIST AND FLAPERON POSITION SIGN CONVENTION 26

FIGURE 15: CIRCULAR CROSS-SECTION WITH FLAPERON 3 COMPOSITE LAYUP MESHED WITH PREVABS 29

FIGURE 16: ELLIPTICAL CROSS-SECTION WITH FLAPERON 3 COMPOSITE LAYUP MESHED WITH PREVABS 29

FIGURE 17: LARGE CIRCLE-STRAIGHT LINES-SMALL CIRCLE CROSS-SECTION WITH FLAPERON 3 COMPOSITE LAYUP MESHED WITH PREVABS 29

FIGURE 18: FLAPERON 3 CROSS-SECTIONAL MESH WITH ERRONEOUS NODAL CONNECTIONS AT THE TE 30

FIGURE 19: TE OF FLAPERON 3 WITH UPPER AND LOWER SURFACE MESH CROSSING OVER EACH WHILE NOT CONNECTING 30

FIGURE 20: ENLARGED AREA OF ERRONEOUS NODAL CONNECTIONS OF FLAPERON 3 TE MESH 30

FIGURE 21: FLAPERON 3 CROSS-SECTION CORRECTLY MESHED 31

FIGURE 22: TE OF FLAPERON 3 WITH UPPER AND LOWER SURFACE MESH MERGING CORRECTLY 31

FIGURE 23: ENLARGED AREA OF MERGING NODAL CONNECTIONS OF FLAPERON 3 TE MESH 31

FIGURE 24: FLAPERON 3 EXPERIMENTAL SETUP FOR TORQUE DEFLECTION TEST 32

FIGURE 25: AERODYNAMIC LOADS ON THE JS1C FLAPERONS DURING CRUISE 35

FIGURE 26: JS1C 21 M TIP LOADED WITH WHIFFLETREE SYSTEM AT SF 1.25 WITH A TIP DEFLECTION OF 570 MM 36

FIGURE 27: 21 M JS1C TIP DURING A 1.2 G AERODYNAMIC LOADING WITH A DEFLECTION OF A 155 MM AT THE WING TIP AND 70 MM AT THE END OF FLAPERON 3 37

FIGURE 28: CROSS-SECTION OF 21 M JS1C WING AT FLAPERON 3 DURING A THERMALLING FLAPERON SETTING OF -13.5° (DOWNWARD) AT ZERO KM/H (0° TWIST) 38

FIGURE 29: DURING THERMALLING AT 120 KM/H THE AERODYNAMIC LOADS PRODUCE A TIP TWIST OF 0.8° (UPWARD) ON THE NON-TAILORED FLAPERON 3 38

FIGURE 30: CROSS-SECTION OF 21 M JS1C WING AT FLAPERON 3 DURING A CRUISE FLAPERON SETTING OF 3° (UPWARD) AT ZERO KM/H (0° TWIST) 38

FIGURE 31: DURING CRUISE AT 220 KM/H THE AERODYNAMIC LOADS PRODUCE A TIP TWIST OF -4.7° (DOWNWARD) ON THE NON-TAILORED FLAPERON 3 39

FIGURE 32: BEND-TWIST COUPLE ANGLE VS LAYER LAYUP ANGLE AT A 70 MM DEFLECTION AND A 58 MM DEFLECTION 40

FIGURE 33: DURING THERMALLING AT 120 KM/H THE AERODYNAMIC LOADS AND TAILORED COUPLE PRODUCE A TIP TWIST OF -0.9° (DOWNWARD) ON THE TAILORED FLAPERON 3 41

FIGURE 34: DURING CRUISE AT 220 KM/H THE AERODYNAMIC LOADS AND TAILORED COUPLE PRODUCE A TIP TWIST OF -6.2° (DOWNWARD) ON THE TAILORED FLAPERON 3 41

FIGURE 35: BEND-TWIST COUPLE ANGLE VS LAYER ANGLE FOR DIFFERENT LAYER TAILORING AT 70 MM FLAPERON BENDING DEFLECTION 42

FIGURE 36: FLAPERON 3 TIP TWIST EFFECTS DURING THERMALLING 43

FIGURE 37: FLAPERON 3 TIP TWIST EFFECTS DURING CRUISE 44

FIGURE 38: PRE-TWIST OPTIMIZATION OF NON-TAILORED FLAPERON 3 FOR THERMALLING AND CRUISE 44

FIGURE 39: PRE-TWIST OPTIMIZATION OF TAILORED FLAPERON 3 FOR THERMALLING AND CRUISE 45

FIGURE 40: TAILORING OPTIMIZATION FOR FLAPERON 3 DURING THERMALLING AND CRUISE 47

FIGURE 41: BEND-TWIST COUPLE ANGLE VS LAYER LAYUP ANGLE FOR 1 M TEST SAMPLE WITH A BENT DEFLECTION OF 32 AND 150 MM 49

FIGURE 42: LAYUP DRAWING FOR FLAPERON 3 TEST SAMPLE AT A TAILORED LAYUP OF 16°. 49

FIGURE 43: 3D MODEL FOR TEST SAMPLE 50

FIGURE 44: TEST SAMPLE MOULD CNC CUT FROM NECURON 651 51

FIGURE 45: 16° LAYUP ANGLE ACCORDING TO MOULD SCRIBE LINES 52

FIGURE 46: TWO MOULD HALVES READY TO BE PREPARED FOR MOULD CLOSING 54

FIGURE 47: EXPERIMENTAL SETUP OF FLAPERON 3 TEST SAMPLE 55

FIGURE 48: INCLINOMETER METER ZEROED AT ZERO DEFLECTION 56

FIGURE 49: THE 32 MM DISPLACEMENTS ON THE TEST SAMPLE'S TE(A) AND LE(B) 57

FIGURE 50: THE 150 MM DISPLACEMENTS ON THE TEST SAMPLE'S TE(A) AND LE(B) 58

FIGURE 51: DISPLACEMENT OF 32 MM APPLIED AT THE TORSIONAL CENTROID AT 19 MM FROM THE TIP LE 59

FIGURE 52: SOLIDWORKS SIMULATION CONSTRAINTS AND LOADS A-3

FIGURE 53: SOLIDWORKS SIMULATION CURVATURE BASED MESH A-3

FIGURE 54: SOLIDWORKS SIMULATION VON MISES PLOT A-4

FIGURE 55: SOLIDWORKS SIMULATION DISPLACEMENT PLOT A-4

FIGURE 56: MESH PROCESSING PLOTS A-6

FIGURE 57: DIRECTION COSINE CALCULATOR A-7

LIST OF TABLES

TABLE 1: TAILOR.M AND THIN WALL TUBE THEORY UNDER LOAD DISTRIBUTION TORQUE 29

TABLE 2: TORQUE TWIST DEFLECTION COMPARISONS WITH EXPERIMENTAL, TAILOR.M, AND THIN WALLED TUBE THEORY 32

TABLE 3: JS1C CHARACTERISTICS WITH THE NON-TAILORED FLAPERON 3 39

TABLE 4: FLAPERON 3 TIP TWIST AT VARIOUS CONDITIONS 46

TABLE 5: COMPARISON OF EXPERIMENTAL AND TAILOR.M BEND-TWIST COUPLE RESULTS 60

TABLE 6: HAND CALCULATIONS COMPARED TO TAILOR.M AND SOLIDWORKS FEM SIMULATION A-10

KEY WORDS

Aeroelastic Tailoring

High aspect-ratio composite

Wings

PreVABS

VABS

GEBT

Gliders

1D Beams

2D cross-sections

Beam Theory

Flaps

Flaperons

Ailerons

Variational Asymptotic Beam

Experimental setup

Bend-twist couple

Matlab

NOMENCLATURE

ABBREVIATIONS

1D	One-dimensional
2D	Two-dimensional
3D	Three-dimensional
BID	Bi-directional composite fibre strand directions usually crossing at 90°
CFD	Computational Fluid Dynamics
CNC	Computer Numerically Controlled
DCM	Direction cosine matrix
DOF	Degree of Freedom
FEA	Finite Element Analysis
FEM	Finite Element Method
G	Gravitational Force acting on the object due to gravity
GEBT	Geometrically exact beam theory
JS	Jonker Sailplanes cc
PreVABS	Prepare cross-sectional geometry, material properties and layup orientation for VABS
TE	Trailing Edge of wing relative to air flow
VABS	Variational Asymptotic Beam Sectional Analysis
VAM	Variational-asymptotic method

ROMAN SYMBOLS

A	Cross-sectional area	m^2
C	Stiffness matrix	
c_l	Lift coefficient, the dynamic lift characteristics of a 2D foil section	
dx	Elemental length along the x-axis	m
E	Modulus of elasticity	Pa
E_i	Modulus of elasticity	Pa
F	Force	N
G	Shear modulus	Pa
G_i	Shear modulus of elasticity	Pa
I	Moment of area	m^4
J	Polar second moment of area	m^4
L	Length of beam	m
M	Moment	$N.m$
p	Beam loading distribution	N.m
r	Inner cross-sectional radius	m
R	Outer cross-sectional radius	m
S_y	Yield stress	Pa
S_t	Ultimate tensile stress	Pa
t	Wall thickness	m
T	Matrix transpose	

v	Beam deflection/vertical displacement	m
x	Beam axis coordinate system along the length	
xy	x-y plane	
xz	x-z plane	
y_n	Neutral axis to beam surface distance	m
y	Beam axis coordinate system along the width	
z	Beam axis coordinate system along the height	

GREEK SYMBOLS

ϵ	1D displacement vector	
κ	Twist and bending strain	
γ	Extensional and transverse shear strain	
ρ	Density	kg/m^3
ν	Poisson's Ratio	
v	Beam deflection	m
v_{max}	Maximum beam deflection	m
θ_{max}	Maximum beam slope angle	rad
σ_{max}	Maximum Stress	Pa

DEFINITIONS

Aeroelasticity – is the study of the effect of aerodynamic forces on elastic bodies (Fung, 1993). It is the term used to denote the field of study concerned with the interaction between the deformation of an elastic structure in an airstream and the resulting aerodynamic force. This study interacts with the disciplines of aerodynamics, elasticity, and dynamics. (Hodges & Pierce, 2002)

Aeroelastic tailoring – is the embodiment of directional stiffness into an aircraft structural design to control aeroelastic deformation, static or dynamic, in such a fashion as to affect the aerodynamic and structural performance of the aircraft in a beneficial way (Cheung, 2002).

Anisotropic material – The material properties of an anisotropic material at a point vary with direction. At a point an anisotropic material can have either no material planes of symmetry, or anything up to three material planes of symmetry. (Daniel & Ishai, 1994)

Composite materials – A composite material is a materials system composed of a mixture or combination of two or more micro- or macro-constituents that differ in form and chemical composition and which are essentially insoluble in each other (Smith, 1990). In the context of this report, a composite material is a multiphase material that is artificially made. Each phase is chemically dissimilar and is separated by a distinct interface. These materials are created to improve combinations of mechanical characteristics such as stiffness, toughness, and ambient and high-temperature strength. In this context these composite materials are made of a polymer epoxy matrix reinforced with a dispersed phase of continuous and aligned fibres. These fibres are mostly glass, carbon or aramids strands. (Callister, 2007)

Composite structure – In the context of this report, the structures are made up of laminar composites that are composed of two-dimensional sheets that have preferred high-strength directions. These layers are stacked together, such that the orientations of high-strength fibre directions give the structure strength in the areas that are needed to carry the load. (Callister, 2007)

Isotropic material – The material properties of these materials are the same in all directions and thus are independent of an orientation of reference axes. The material properties such as stiffness, strength, thermal expansion, and thermal conductivity are the same in all directions. This means that this material has an infinite number of planes of symmetry for its material properties. (Daniel & Ishai, 1994)

Thermalling – In order to maintain or gain altitude in a glider, rather than slowly gliding downwards, a soaring flight needs to be achieved - one method is by thermalling. This is done by locating and utilizing thermals. Successful thermalling requires the ability to locate the thermal, enter the thermal, centre in the thermal, and finally leave the thermal. Thermals come in unique sizes, shapes and strengths. (Federal Aviation Administration, 2007)

1 INTRODUCTION

1.1 BACKGROUND

Modern high-performance gliders are characterized by long, slender wings and fuselage structures. This is the result of refined aerodynamics, which aims to reduce drag and increase lift in order to produce the best possible performance. The JS1B 18 m is a modern high-performance glider shown during flight in Figure 1.

Figure 1: JS1B 18 m in flight with self-sustainer jet system, note how the wings deform in flight (NOMAD, 2012)

While aerodynamically efficient, the long slender shape introduces structural challenges to the design. Though it is possible to design the slender structures with sufficient strength, the small cross-sections produce inadequate stiffness. Such a structure will therefore deform under the flight loads, deviating from its optimum aerodynamic shape and causing the associated reduction in performance.

This phenomenon manifests in the newly developed JS1C glider's 21 m wing tips. The 21 m wing tip Flaperon has a length of 2.2 m with a thin aerofoil cross-section, which is therefore relatively soft in torsion. As this Flaperon is only driven from the root side it can twist in torsion along its length during high-speed flight. This results in a change in flaperon deflection along the span with the resultant profile drag penalty in high-speed flight.

The JS1C is mostly manufactured from composite materials. These composite materials are characterised by being anisotropic, giving it different rigidity in different directions. This is due to the high-strength fibres being more rigid in the axial direction than in the transverse direction. By laying the composite fibres at a 0° and 90° as depicted in Figure 2, the structure has more rigidity in bending. If the fibres are placed -45° and 45° the structure will have more rigidity in torsion. If the fibres are place at angles other than mentioned, couples are introduced for example bend-twist couples. These couples can be used by aeroelastically tailoring for sought-after coupling effects.

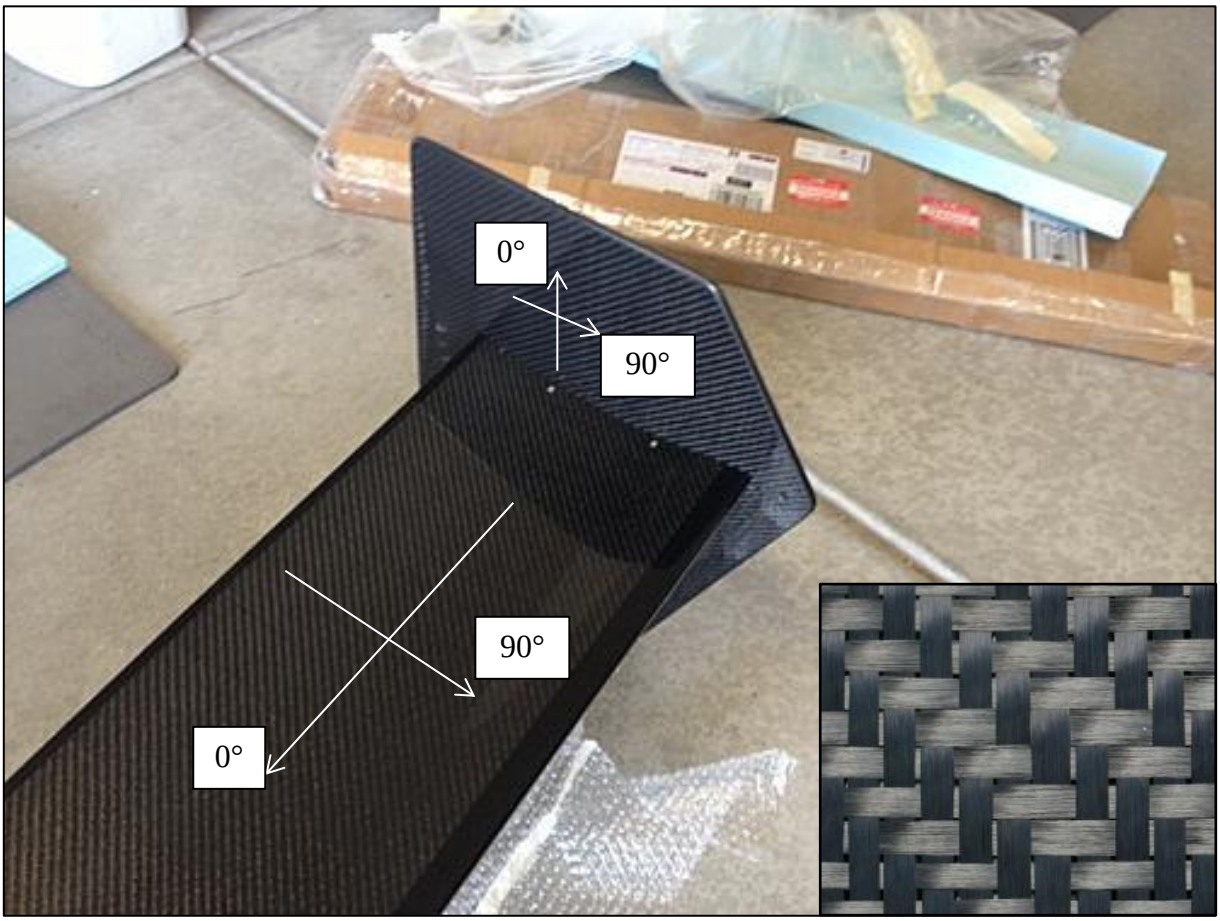

Figure 2: Carbon Fibre wing laid up with 0°/95° for structural bending rigidity (Bennett, 2013)

This provides an option to rectify the flaperon twist phenomenon through the use of aeroelastic tailoring. This method allows the design of the flaperon composite structure in such a way that there is a coupling between different deformation modes. The wing bending, for example, can be used to counteract the effect of flaperon twist and therefore reduce the profile drag.

Tailored composite aerostructures, while meeting the original design requirements, should still be tested and corrected for potentially destructive phenomena, such as flutter and divergence. However, doing so falls beyond the scope of this project.

1.2 PROBLEM DEFINITION

The purpose of this study is therefore to use an aeroelastic tailoring method to redesign the JS1C Flaperon 3 to reduce or prevent the flaperon twist problem. The JS1 Flaperon 3 is shown in Figure 3.

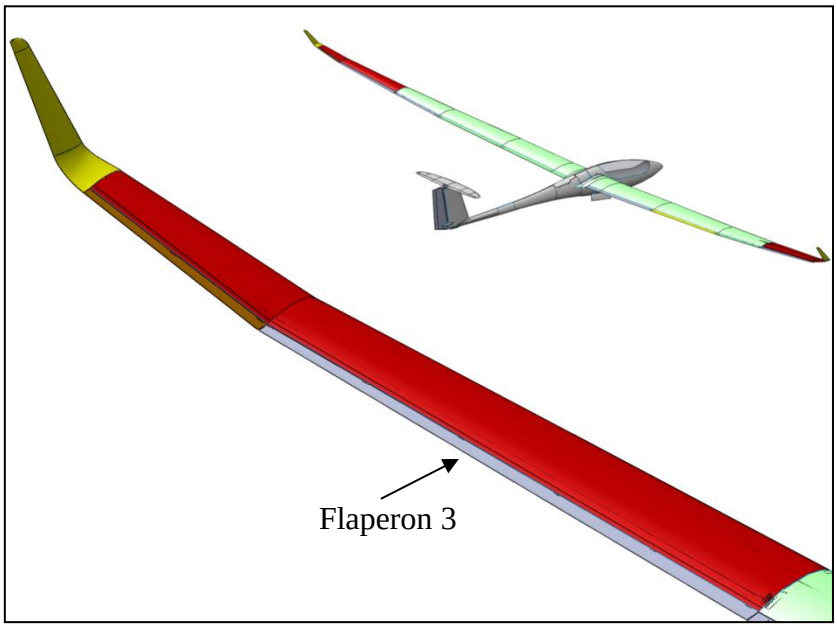

Figure 3: JS1C Flaperon position

1.3 OBJECTIVES OF STUDY

The objectives of this study are therefore:

- Review the literature for the most suitable aeroelastic tailoring methods.
- Select an analysis method and verify this against published data.
- Use preparation code for variational asymptotic beam sectional analysis (PreVABS), variational asymptotic beam sectional analysis code(VABS), and geometrically exact beam theory code (GEBT) with a coded Matlab user interface to analyse the JS1 21 m Flaperon 3 for an aeroelastic tailored design point to improve the torsional twist characteristics during flight.
- Design and manufacture a flaperon test specimen.
- Test the flaperon specimen and compare the results with calculated values.

1.4 LAYOUT OF DISSERTATION

Chapter 2 introduces the progress and development of aeroelastic tailoring, the analytical methods used to calculate composite fibre orientations for aeroelastic tailoring, and the advantages and disadvantages of the different tailoring methods on manufacturing.

Chapter 3 presents a brief overview of the selected aeroelastic tailoring analysis tools PreVABS/VABS/GEBT, including some mathematical formulations. The complexity of these programs gave a need to develop a Matlab program known as “Tailor.m” that combines these programs into a single aeroelastic tailoring analysis tool with a practical user interface. This Matlab program’s results were verified with published data.

In Chapter 4, Tailor.m will be used to model the JS1 Flaperon 3 in its original form to validate the modelling of flaperon-type structures including comparing the computed results with experimental data.

Chapter 5 includes the tailoring of Flaperon 3 and the validation with a test sample and the manufacture thereof. The test sample’s results are interpreted and compared with the composite structural analysis tool’s results.

Chapter 6 consolidates the work by providing a conclusion and recommendations.

References provides the cited references.

2 LITERATURE STUDY

2.1 A HISTORIC OVERVIEW OF THE DEVELOPMENT OF AEROELASTIC TAILORING

When advanced composites became available around 1937 (Strong, 1999), many new design possibilities were introduced. New design techniques needed to be developed, as most engineering analysis previously consisted of isotropic theory (Hibbeler, 2005) while composite fibres are fundamentally anisotropic (Hodges & Pierce, 2002).

While traditional structures are manufactured by the removal or shaping of material, composite structures are manufactured by the addition of stacked layers of fibre. The properties of the final structure depend on the properties of each layer, as well as the layers' interaction with each other. Combined with the increased cost of composite fibres over traditional materials, the need to meet the design requirements with the lowest possible cost has prompted the need to consider the effect of fibre orientation, material selection, material blending and ply stacking sequence – a process now known as elastic tailoring (Cheung, 2002; Rehfield, 1985).

Aviation has taken particular interest in composite materials, despite its increased cost, mostly because they offer high strength and low mass. In addition, composite structures can be laid up in geometrically complex, but aerodynamically efficient, shapes (Cheung, 2002; Rehfield, 1985). Incorporating the methods of elastic tailoring combined with the knowledge of aerodynamic loads on aircraft brings about aeroelastic tailoring, which is to provide directional stiffness in an aircraft structural design to control aeroelastic deformation, static or dynamic, in order to maximise the aerodynamic and structural performance of the aircraft (Shirk et al., 1986).

The phrase "aeroelastic tailoring" came into use at General Dynamics in 1969. Waddoups and his co-workers McCullers and Naberhaus (as quoted by Attaran et al., 2011) used advanced composites to investigate possible design improvements. They demonstrated that the directional properties of composites could be used to provide a significant level of anisotropy to create a coupling between bending and twisting deformation effects (Attaran et al., 2011).

Aeroelastic tailoring was used in the 1980's during the development of forward swept wings to prevent wing divergence during flight (Hodges & Pierce, 2002).

Weisshaar (Attaran et al., 2011) discussed the different effects of the laminate lay-up and fibre orientation on aeroelastic divergence, wing load redistribution, and lateral control effectiveness of swept-back and forward-swept wings. He modelled the wing as a laminate box beam, to obtain beam bending stiffness, torsional rigidity, and the bend-torsion coupling parameters. He drew an important conclusion on aeroelastic tailoring: using a bending-torsion coupling is effective for both high-aspect ratio wings and low-aspect ratio wings (Attaran et al., 2011).

Around the same time, Sherrer et al (Attaran et al., 2011) showed through low-speed wind tunnel tests, that the divergence speed of a forward-swept wing could be increased by aeroelastic tailoring with advanced composite materials (Attaran et al., 2011). Their work helped further forward-swept wing technology by introducing methods to increase the divergence speed and tailor the composite materials for advantageous bend-twist coupling characteristics (Attaran et al., 2011).

Rogers et al investigated the effect of aeroelastic tailoring on transonic drag (Attaran et al., 2011). They prepared tailored wing models (wash-out – upward bending/nose down twist; wash-in – upward bending/nose up twist – models) and one non-tailored wing model. These models were tested and compared with a rigid wing. Wind tunnel tests of these models revealed that there was a significant reduction of transonic drag versus lift for the tailored wash-out wings compared to the non-tailored and rigid wings; it was also found that the lift-curve slope increased for a wash-in wing (Attaran et al., 2011).

Work done by Isogai showed that, in addition to eliminating divergence phenomena, the transonic flutter characteristics of a transport-type high-aspect-ratio forward-swept wing could be improved by 60–80% compared to the non-tailored wing (Attaran et al., 2011).

Although sailplanes fly far below transonic speeds, their long, slender wings and thin cross sections can result in divergence. Tailoring the wings and airframe is crucial to eliminating such undesirable phenomena as divergence and flutter (Eskandary et al., 2012). The ability to analyse the wing thoroughly yet at the lowest possible cost has led to the need to develop an analysis tool that can be implemented on ordinary computers while offering aeroelastic tailoring capability during the design phase.

Several different analysis techniques have been developed for aeroelastic analysis and design. The next section will examine some of these analysis techniques for analysing high aspect-ratio composite structures with the effects of aeroelastic tailoring.

2.2 AEROELASTIC TAILORING ANALYSIS TECHNIQUES

There are several methods that are currently employed to perform aeroelastic tailoring on high aspect-ratio composite structures. These methods include the following:

- Experimentation
- Three-dimensional finite element methods
- Beam Theory
  - Classical Beam Theory
  - Engineering Beam Theory
  - Director Beam Theory
  - Asymptotic Beam Theory
  - Variation-asymptotic method of Berdichevski (VAM)
  - Variational Asymptotic Beam Section analysis (VABS)
- Shell Theory

2.2.1 Experimentation

Experimentation can be used to obtain the correct aeroelastic tailoring that is needed for a certain aerodynamic performance enhancement. Such experiments could be performed in three ways: building the actual part and testing it in the actual environment; building a scale model for testing in a simulated environment; or testing samples of the structure to analyse its coupling properties. Such methods are normally time-consuming and costly, while much iteration may be required to obtain a satisfactory design using the trial and error approach.

By contrast, it would require far fewer experiments if the behaviour of structures could be predicted or even optimised during the design phase. Experimentation could be reduced to a single validation process.

A great deal of effort has been spent on developing numerical codes for analysing composite laminate structures on digital computers. Such codes should also be simple to use, accurate and

have a quick analysis time. These codes are designed around at least one, but sometimes several, of the methods described in the next section.

2.2.2 Three-dimensional finite element methods

Numerical techniques to simulate the aeroelastic properties of a structure like finite element method (FEM) can be used to analyse a structure. When a structure is analysed with three-dimensional (3D) finite element method (FEM) approach, it takes a 3D model of the structure and uses a finite element method to subdivide the geometric shape into a mesh of finite-sized elements of a simple shape, in order to analyse the structure (Benham et al., 1996). The variation of displacement within each element is determined by simple polynomial shape functions and nodal displacements. The unknown nodal displacements are calculated through a matrix of stress and strain equations. These equations have unknowns which are solved once the boundary conditions and known values are introduced. In the matrix an equal number of unknowns and setup equations must be solved simultaneously to get a solution.

Because composite structures consist of layers of anisotropic materials, setting up the model for analysis by 3D FEM is tedious and time consuming. Since FEM tools are computer processing intensive by using millions or billions of DOF's (see Figure 4) (Wan et al., 2005), it also requires a long time to run. The large amount of time it takes to setup and solve these models result in engineers wasting time waiting instead of optimizing the structure (Yu, 2012); this renders aeroelastic design by means of FEM unfeasible (Brett & Rehfield, 2004). Thus FEM is usually employed at the end of the design to check the aeroelastic tailoring characteristics (Brett & Rehfield, 2004). This drawback of a full 3D FEM analysis has prompted a search for computationally inexpensive, more rapid analysis methods (Rehfield, 2004).

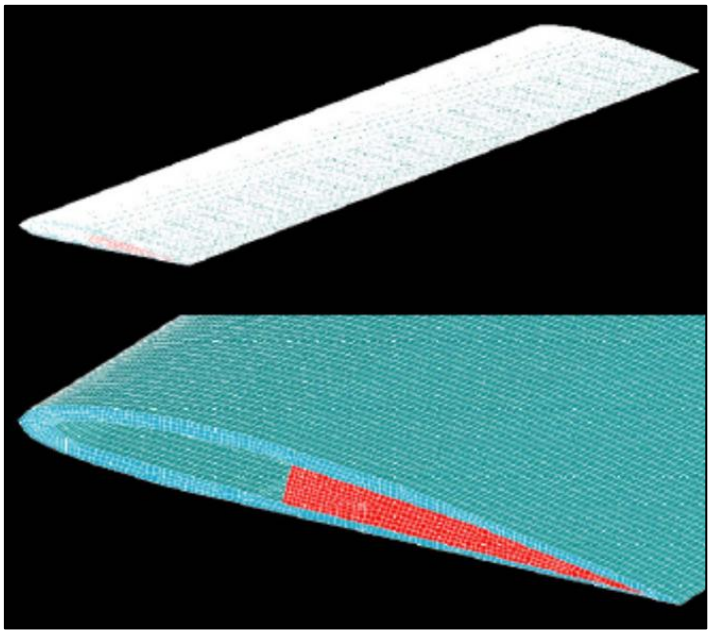

Figure 4: FEM with millions of DOFs (Yu, 2012)

As an alternative to full spatially discretised FEM, a long slender structure can be idealised as a 1D beam with cross-sectional stiffness properties. These stiffness properties are stored in a matrix, typically a 6x6 matrix that captures out-of-plane warping of the section implicitly, or a 7x7 matrix that captures the out-of-plane warping explicitly (Lemanski & Weaver, 2005). These methods are known as beam theory and were originally developed from classical beam theory.

2.2.3 Beam theory

The beginning of the major research toward nonlinear composite beam theories was motivated by the need to design better helicopter blades (Hodges, 2006). Starting in the early 1970's, Hodges and Dowell (1974) published an article that captured the nonlinear torsion coupling of combined bending in two directions (Hodges & Dowell, 1974).

From the 1940's to the 1980's the development of these beam theories covered theories that were regarded as engineering or technical theories, which include the simpler theories with *ad hoc* corrections or additions (Hodges, 2006). These theories would include methods that use the established linear theory of Houbolt and Brooks (1958 cited in Hodges, 2006) with added enhancements as explained by Bielawa (1976 cited in Hodges, 2006). Unfortunately, this theory is most likely to only model limited configurations, for example the box beam, with the drawback of the user being uncertain of its limitations and if the additional theories have been added (Hodges, 2006).

In the early days of aeroelastic tailoring with the introduction of composites, a box beam model was used to simplify calculations and create a preliminary design technique. This model was based on Bernoulli-Euler bending assumption and using Rehfield's theory of thin walled composite beams (Cheung, 2002). With warping effects and transverse shear neglected, the box beam model was used to approximate tailoring bend-twist coupling effects on wing spars. However, this method limited elastic tailoring to box beams and similar approximations.

This box beam model consisted of the following simple inputs; width, height, elastic properties of the materials, limit strain, axial loading due to bending and torsion, configuration of the ply layups, orientation for the ply layup for webs, fraction of wall thickness for front and rear spar web. The outputs of the program are: the bend-twist coupling parameter, thickness of the covers, rate of twist, bending curvature, camber curvature, global stiffness and relative weight, which are compared to a balanced benchmark reference of 0° and 45° plies (Cheung, 2002). This type of method can also be compared with the anisotropic beam model of Giovotto (Hodges et al., 1992).

Currently, newer codes for aeroelastic tailoring are still validated against literature of the anisotropic single cell box beam with the NABSA code, which is a two-dimensional (2D) finite element analysis (FEA) code based on the *ad hoc* anisotropic beam model of Giovotto. This is still the most accurate application of the Saint Venant theory with the outer solution dealing with the boundary conditions, and the inner solution dealing with the transverse shear (Willaert et al., 2010).

These engineering beam theories are based on truncation schemes, which rely on ordering parameters. Because these types of formulations may require revision when configuration parameters take on extreme values, they do not hold much promise for general-purpose analysis; neither do these theories provide any means of analysing the warp displacement field for beams made of anisotropic material (Hodges, 2006).

Engineering beam theories constructed on a small-strain approximation have simpler criteria with the ordering of terms compared to engineering beam theories constructed on truncation schemes (Hodges, 2006). These *geometrically exact theories* are compact, but they cannot calculate the warping displacement field for beams built out of anisotropic materials or those having a complex internal structure (Hodges, 2006).

Director beam theories are another type of method to solve complex beams. Such theories are geometrically exact and highly mathematical, based on the concept of a desired continuum.

However, they only treat the beam as a one-dimensional continuum without any direct linkage to three-dimensional material properties or the three-dimensional strain distribution over a cross-section (Hodges, 2006).

Asymptotic and projection beam theories is another mathematical beam theory. The full 3D beam is rigorously reduced to a system of 2D cross-sections and a 1D beam. Asymptotic Beam Theory has an extensive history of development. This theory efficiently calculates high aspect-ratio composite structures specifically used by competition gliders. Such low- and high-order theories use either projections of three-dimensional elasticity on function spaces or asymptotic expansions in a slenderness parameter, and typically result in an elegant hierarchical set of theories where the lowest-order equations may correspond to "classical" theories that treat extension, twist and bending only; the higher-order equations model phenomena that are beyond the reach of classical theory. This type of theory includes a means by which the one- and three-dimensional representations can be connected. However, a way must be found to put it into a simpler form if applications-oriented engineers are to grow comfortable in using such a theory (Hodges, 2006).

From *circa* 1985, the challenges faced with the formulation of suitable one-dimensional constitutive laws in terms of the known three-dimensional elastic constants was solved by using closed form or finite element methods (Hodges, 2006). This technique does not have restrictions on material type or the geometry of the cross-section (Hodges, 2006).

The abstract tensor analysis, which was difficult to work with for applications-oriented engineers, was improved using a minimal amount of tensor analysis in a derivation which does not affect the application (Hodges, 2006).

The three-dimensional beam model was rigorously reduced to a system of a 1D beam having 2D cross-sectional properties. By developing a kinematic description which would allow the 3D strain field to be expressed in terms of the intrinsic 1D measures for initially twisted and curved beams, expressions for the 3D strain could be obtained that involved no tensor analysis at all; this could facilitate the incorporation of nonlinear effects with no significant increase in complexity (Hodges & Yu, 2007).

This Asymptotic Beam theory was then further developed into the variation-asymptotic method (VAM) of Berdichevski (Berdichevsky, 1979). When using anisotropic material, the energy functional is coupled with various modes of deformation, which are represented by differential

equations (Hodges et al., 1992). This method solves the differential equations simultaneously by expanding them asymptotically (Willaert et al., 2010).

By using the theory of Popescu and Hodges with VAM the problem is split into a nonlinear 1D problem and a linear 2D problem while using prismatic beam elements (Willaert et al., 2010). From this theory Cesnik and Hodges developed a finite element code, known today as "VABS" (the Variational Asymptotic Beam Section analysis) (Hodges & Yu, 2007).

Recently VABS theory has been improved to incorporate smart beams giving results comparable to a 3D multiphysics simulation in ANSYS (Roy et al., 2007). During the development of this tool for efficient high-fidelity design and analysis of multibody systems, it has been shown that a geometrically exact beam model constructed using the variational asymptotic method (represented by the VABS software) is fully compatible with the geometrically nonlinear beam elements (Han et al., 2007).

To reduce computational calculations, Volovoi and Hodges improved VAM to allow for thin - walled beams (Yu & Hodges, 2005). The shell kinematics theory was used to affect the shell on the displacement field of a thin - walled beam. This theory can have open or closed cross – sections which give correct results. These results are used for the Euler stiffness matrix (Willaert et al., 2010).

2.2.4 Shell theory

Shell theory is used with the Timoshenko beam stiffness matrix derivation that is computationally efficient to create a continuous cross-sectional modeller (Willaert et al., 2010).

Work is currently underway at Delft University to extend the theory of Volovoi and Hodges with transverse shear (Yu et al., 2005). This can be done by modifying VAM to calculate thin-walled aircraft wings or rotor blades more efficiently. The advantage of using kinematics is that it does not have to calculate the elements in the thickness direction, which reduces the number of degrees of freedom. Delft is also challenged to derive the Timoshenko beam stiffness matrix in a straightforward way. With this improvement the code will have reduced sensitivities making the code work better for aeroelastic computations and optimization purposes (Willaert et al., 2010).

2.3 COMPARISON OF ANALYSIS TECHNIQUES

During the design of the Concordia, Dillinger attempted to use NASTRAN to tailor the long, slender wings; however, in addition to being resource intensive, time consuming and tedious to operate, NASTRAN offers the user almost no control over, nor insight into, the loads calculated (Dillinger, 2007).

By contrast, MORPHEUS - a predecessor of GEBT, developed by the Chair of Aerospace Structures, Delft University of Technology - allows the user to specify, review and revise the beam loads and constraints. It has also proven to have a good tailoring application range (Dillinger, 2007).

Boston et al. (2011) mentioned that GEBT can benefit joined-wing aircraft optimization during design, as unique bend-twist deformations require non-linear analyses. FEM packages usually take more time to solve non-linear problems than they do for linear problems, to which they are ideally suited. Analytical tools like GEBT can reduce the solution time for optimization by using higher order beam theory (Boston et al., 2011). Hodges claims that VABS has been benchmarked in validation studies to show that it has accuracy and analysis flexibility comparable to more costly, general purpose three-dimensional finite element analyses codes, yet it can reduce computational effort by about three orders of magnitude compared to FEM. (Hodges, 2006)

An article by Chen et al. (2010), stated that VABS is proven technology in the helicopter industry. When combined with the dedicated pre-processor PreVABS, accurate modelling of wind turbine blades requires no more human interaction effort than the earlier codes PreComp, FAROB, or CROSTAB. This indicates that VABS may also be used for slender composite wing structures due to the similarity with helicopter blades and wind turbine blades (Chen et al., 2010).

Because it treats a wing as a higher order beam with known cross-section properties, VABS has the ability to rapidly calculate bending-torsion couples in composites structures. Dillinger utilised this capability in the design of the Concordia's wing skins to yield the least possible twist for the desired flight condition, although Dillinger used MASProT[i], a program similar to PreVABS, to calculate the wing skin section properties. (Dillinger, 2007)

Chen has proposed a design strategy, using PreVABS, VABS and GEBT in the preliminary design stages to perform aeroelastic tailoring on composite structures, which can then be verified and possibly refined by means of conventional 3D FEM analysis (Yu & Blair, 2012). With recent

advancements in computational software and hardware, a FEM model of the final design can be coupled with a CFD model (Chen et al., 2010). This would give the most accurate prediction if done correctly, yet is still a costly and time consuming method (Chen et al., 2010).

It therefore appears that beam theory provides the most time effective method for calculating the elastic couplings in long, slender structures made from anisotropic material – an essential requirement when attempting aeroelastic tailoring. PreVABS, VABS and GEBT are three commercial codes based on this theory. It was shown that these codes have been thoroughly validated and will therefore be used in this study.

2.4 MANUFACTURING CONSTRAINTS

In order to create a bend-twist couple, stiffness is created that is not aligned with the axis of the composite structure (Cheung, 2002). This is accomplished by either placing off-axis plies giving an unbalanced layup of angle ply rotation, or by rotating the entire laminate layup (Cheung, 2002). Using a balanced laminate layup for rotating off-axis is better for manufacturing, since this avoids or minimizes warping (Cheung, 2002). Although angle ply rotation can be used to tailor some complex coupling effects, the unbalanced laminate's warping may adversely affect manufacturing.

2.5 SUMMARY OF LITERATURE STUDY

The introduction of advanced engineering composites has brought about the need for new design techniques, owing to the anisotropic nature of the materials. Traditional engineering methods relied on isotropic behaviour and a single material or averaged aggregate.

Advances in computer technology have allowed even large complex structures to be analysed by discrete elements without the need for experimentation. This can be done using 3D FEM. Since 3D FEM modelling is time consuming and complex to set up (Friedmann et al., 2009), simplified methods are sometimes preferred.

Slender structures can be reduced to a higher order classical beam with known cross sections, which allows these structures to be solved with a high degree of accuracy with a greatly reduced computational effort (Hodges & Pierce, 2002). The mathematical beam theory as implemented in

the computer programs VABS, GEBT and PreVABS and will be used in this study as the primary analysis tools.

The anisotropic nature of composite laminates, combined with the ability to rapidly and accurately analyse such structures, have allowed engineers to incorporate new and unusual behaviour into composite structures, such as bend-twist couples (Hodges & Pierce, 2002). This is accomplished by the rotation of some of the layers in the laminate, or by the rotation of the entire laminate, relative to the structure's orientation.

3 DESCRIPTION AND IMPLEMENTATION OF PREVABS, VABS AND GEBT

The literature study has given insight into the development of aeroelastic tailoring and the analysis methods used. It was shown that the preferred analysis tools for this study is a higher order beam theory as implemented in the programs PreVABS, VABS, and GEBT. This chapter will give a brief overview of these composite analysis tools, including the mathematical formulations.

The selected analysis tools PreVABS, VABS and GEBT consist of separate programs that each analyse different aspects of the composite structure. The use of these programs requires a lot of manual preparation and manipulation and is prone to user induced errors. In an attempt to refine this process, a Matlab program was developed that integrates these programs into a single aeroelastic tailoring tool with a simplified user interface. This tool is presented in this chapter.

3.1 OVERVIEW OF ANALYSIS TOOLS

The analysis of slender structures is accomplished through the use of three different codes PreVABS, VABS and GEBT. Each of these is concerned with the solution of a different aspect of the full 3D structure. A brief description of each of these programs is presented here:

- PreVABS is a pre-processing computer program for VABS, which effectively generates high resolution finite elements. The elements are created by directly using design parameters from the geometric coordinate inputs; these include both the span-wisely and chord-wisely varying composite laminate lay-up schema of the aircraft wing cross-sections. PreVABS takes the composite wing's material and geometrical properties and automatically models the complex cross-sectional composite layers with mixed quadrilateral and triangular meshes. This is based upon a few design parameters including airfoil geometry, web positions, titling angles, and chord-wisely varying composite laminate lay-up schema. The finite element modelling process meshes the cross-section with elements which are fine enough to mesh each individual composite layer. The ply orientation, fibre orientation and ply thickness are solved for each element (Chen & Yu, 2008).

- The VABS computer program is then used to analyse the PreVABS compiled input data to

- Obtain multiple sectional properties along the span. VABS calculates the following structural properties:
  - Position of the neutral axis
  - centroid, elastic axis/shear centre
  - shear correction factors
  - extensional/torsional/bending/shearing stiffness
  - principal bending axes pitch angle
  - modulus-weighted radius of gyration

  The following inertial properties are also calculated:

  - centre of mass
  - mass per unit span
  - mass moments of inertia
  - principal inertia axes pitch angle
  - mass-weighted radius of gyration

  The processed VABS results contain distributed span-wise inertial and stiffness data. This data, combined with aerodynamic loads and boundary conditions, are used as the input to GEBT (Yu, 2011a).

- GEBT (Geometrically Exact Beam Theory) is a code for implementing the mixed variation formulation of the geometrically exact intrinsic beam theory developed by Hodges at the Georgia Institute of Technology. This code captures all the geometrical nonlinearities obtained in a beam model, which it calculates without numerical integration by using the lowest order shape functions and the element matrices. The variables are then calculated directly by using mixed variation formulation. In a static analysis example, the variables used include three displacements, three rotations, three forces, and three moments. GEBT has the advantage of treating an arbitrary assembly of beams made of arbitrary material and oriented arbitrarily in 3D space with little computational effort (Yu, 2011b). With this GEBT has the capability of handling static, dynamic as well as transient systems (Yu & Blair, 2012).

- The 1D beam results of GEBT can be analysed by VABS to obtain: (Yu, 2011a)

- 3D stress/strain fields, which produce a 3D representation of the 2D cross-sections positioned at each 1D beam point.
- 3D point wise displacement fields, which shows each 2D cross-sectional point positioned at each 1D beam point and its 3D displacement.

3.2 THEORY OF VABS AND GEBT

3.2.1 GEBT analysis tool theory

The formulation of GEBT 1D beam theory uses the application of the Euler-Bernoulli beam theory with a 4x4 stiffness matrix that takes into consideration the slope and displacement at the 1D beam's two end nodes, albeit with the assumption that the planar cross-sectional surfaces remain in plane and normal to the axis and thus neglecting shear deformation. The material stiffness uses the generalized Hooke's law for stress-strain relations of linear elastic materials (Chandrupatla & Belegundu, 2002). Timoshenko expands on the Euler-Bernoulli beam theory, keeping the planar surfaces in plane but without restricting the planes to remain normal to the beam axis. This assumption introduces two shear angles, which expands the 4x4 stiffness matrix to a 6x6 stiffness matrix. (Green, 2009)

The Euler-Bernoulli beam theory has the following governing equations (Chandrupatla & Belegundu, 2002):

$$\frac{d^2}{dx^2}\left(EI\frac{d^2v}{dx^2}\right) - p = 0 \quad (3.1)$$

Where dx is the elemental length along the x-axis, with v being the beam deflection and p as the beam loading distribution. The modulus of elasticity being E, and I is the moment of inertia.

From the generalized Hooke's law the one dimensional case gives (Chandrupatla & Belegundu, 2002):

$$\sigma = E\epsilon \quad (3.2)$$

With σ the normal stress and ϵ being the normal strain.

Hodges furthered beam theory for long slender structures by omitting several assumptions that are normally required with beam theories. Danielson and Hodges improved the theory with the polar decomposition theorem, which has the advantage of giving an accurate yet compact expression for the strain in the beam for large deflections (as quoted by Green, 2009). They also addressed the global kinematics of deformed beams by using Cartesian tensors and matrix notation, which reduce the size of the equations required. (Green, 2009)

Parker introduced asymptotic analysis, which uses the 2D cross-sectional stiffness in a 1D nonlinear beam. Atilgan and Hodges incorporated this method to determine the appropriate stiffness for a 1D nonlinear beam. (Green, 2009)

With the use of the Atilgan and Hodges variation approach combined with Hamilton's principle, the geometrically exact beam theory (GEBT) was formulated. This theory has the advantage of a compact matrix form despite the absence of any approximations in the geometry of the deformed elements along the beam axis. There is no requirement of numerical quadrature over the elements since discontinuities in field variables are possible between elements. The 1x1 quadrature is calculated at the centre of each element to obtain an approximate stiffness, mass, etc. (Green, 2009)

The Timoshenko approach also makes the assumption of small strains, yet does not restrict displacements and rotational variables. This can be shown by the derivation of the theory using geometrically nonlinear, three dimensional elasticity theory(Benham et al., 1996). This theory is expressed in energy variables which are compatible with large global displacements and rotations

The stiffness matrix for a prismatic isotropic material for GEBT is (Green, 2009) :

$$C = \begin{pmatrix} EA & 0 & 0 & 0 & 0 & 0 \\ 0 & GA_x & 0 & 0 & 0 & 0 \\ 0 & 0 & GA_z & 0 & 0 & 0 \\ 0 & 0 & 0 & GJ & 0 & 0 \\ 0 & 0 & 0 & 0 & EI_x & 0 \\ 0 & 0 & 0 & 0 & 0 & EI_z \end{pmatrix} \quad (3.3)$$

As stated by Green, EA is the axial stiffness, EI_x is the bending stiffness about the global X-axis, EI_z is the bending stiffness about the global Z-axis, GJ is the torsional stiffness, GA_x is the shear stiffness about the global x-direction, and GA_Z is the shear stiffness in the global z-direction. The 1D displacement vector ϵ is defined as (Green, 2009) :

$$\epsilon = \lfloor \gamma_x 2\gamma_{xy} 2\gamma_{xz} \kappa_x \kappa_y \kappa_z \rfloor^T \quad (3.4)$$

As stated by Green, γ_x is the extensional strain of the reference line, $2\gamma_{xy}$ and $2\gamma_{xy}$ are the transverse shear strain measures, and $\kappa_i$are the twist and bending generalized strain measures. The force vector applied to the beam is (Green, 2009) :

$$F = \lfloor F_x F_y F_z M_x M_y M_z \rfloor^T \quad (3.5)$$

As stated by Green, F is the force in the x, y, or z direction and M is the moment about the x, y, or z-axis. From the mixed formulation in GEBT, the 1D constitutive relations for isotropic materials are (Green, 2009) :

$$\begin{Bmatrix} F_x \\ F_y \\ F_z \\ M_x \\ M_y \\ M_z \end{Bmatrix} = \begin{bmatrix} EA & 0 & 0 & 0 & 0 & 0 \\ 0 & GA_x & 0 & 0 & 0 & 0 \\ 0 & 0 & GA_z & 0 & 0 & 0 \\ 0 & 0 & 0 & GJ & 0 & 0 \\ 0 & 0 & 0 & 0 & EI_x & 0 \\ 0 & 0 & 0 & 0 & 0 & EI_z \end{bmatrix} \begin{Bmatrix} \gamma_x \\ 2\gamma_{xy} \\ 2\gamma_{xz} \\ \kappa_x \\ \kappa_y \\ \kappa_z \end{Bmatrix} \quad (3.6)$$

This explains the mathematical formulation of GEBT used to solve isotropic 1D beams. This method is extended to solve an anisotropic composite beam by using a 6x6 Timoshenko flexibility matrix. For anisotropic materials, the resultant 6x6 matrix will have non-zero values away from the diagonal (Hodges, 2006).

GEBT requires the cross-sectional elastic constants, EI, GJ, etc. as inputs. These are calculated by VABS and are given in the form of a 6x6 Timoshenko flexibility matrix (Hodges, 2006). This approach can be used to solve complex beam structures.

3.2.2 VABS analysis tool theory models for different beams cross-sections

VABS is based on the Timoshenko theory, and calculates the flexibility properties of the cross-sections along the beam from the geometric and material properties received from PreVABS. Although the application of VABS is restricted to beams, it can effectively use the cross-sectional stiffness matrix to solve many beam problems with varying boundary conditions, loading, and motion. (Yu et al., 2012)

VABS uses different models to solve for different beam cross sections that include classical Euler beam theory, generalized Timoshenko theory and generalised Vlasov theory (Hodges, 2006). VABS also includes a trapeze effect to account for a centripetal force (Hodges, 2006). The beam cross-section are categorised into different classes in order to allow simpler models to be selected:

- *Class $\mathcal{T}$ beams* have open cross-sections and thin-walls (Figure 5) in which the VABS models – classic Euler, Vlasov and Timoshenko - and trapeze effect model may be used (Hodges, 2006).

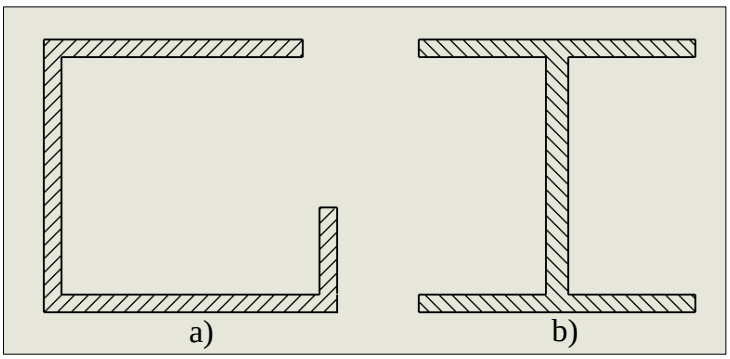

Figure 5: *Class $\mathcal{T}$ beams* with open cross-sections

- *Class $\mathcal{S}$ beams* have long slender cross sections (Figure 6) in which all models except the generalized Vlasov model may be used. (Hodges, 2006).

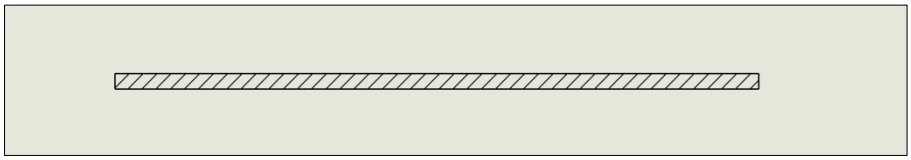

Figure 6: *Class $\mathcal{S}$ beams* long slender cross-sections

- *Class $\mathcal{R}$ beams* are called regular beams, which also including the wing cross-sections (Figure 7) in which all models except the generalized Vlasov model and Trapeze affect model may be used (Hodges, 2006).

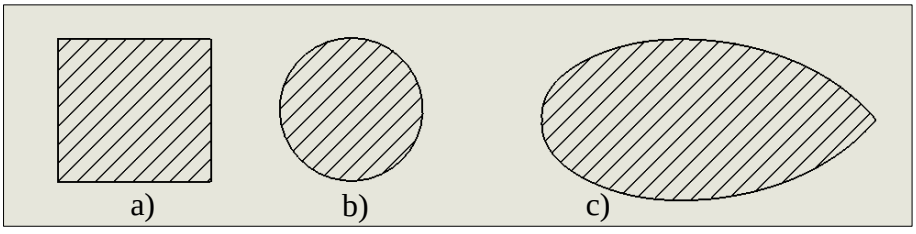

Figure 7: Class $\mathcal{R}$ beams regular beam cross-sections

3.3 REVIEW OF VABS VALIDATION

The VABS analysis tool and its theory have been validated and the results compared with the results of other 3D finite element software and programs such as NABSA and ABAQUS (Yu et al., 2002(a)). Literature recounts a comparison between VABS and ANSYS in the analysis of a heterogeneous beam, shown in Figure 8 (Yong hui & Hai-yan, 2005). Notably, the runtime of VABS was 35 minutes versus the 11 hours for ANSYS, as shown in Figure 9. According to Yu (2012), the short runtime of VABS will thus benefit engineers by allowing rapid tailoring throughout the design process. The published results showed a good comparison between VABS and ANSYS as shown in Figure 10 (Yu, 2012).

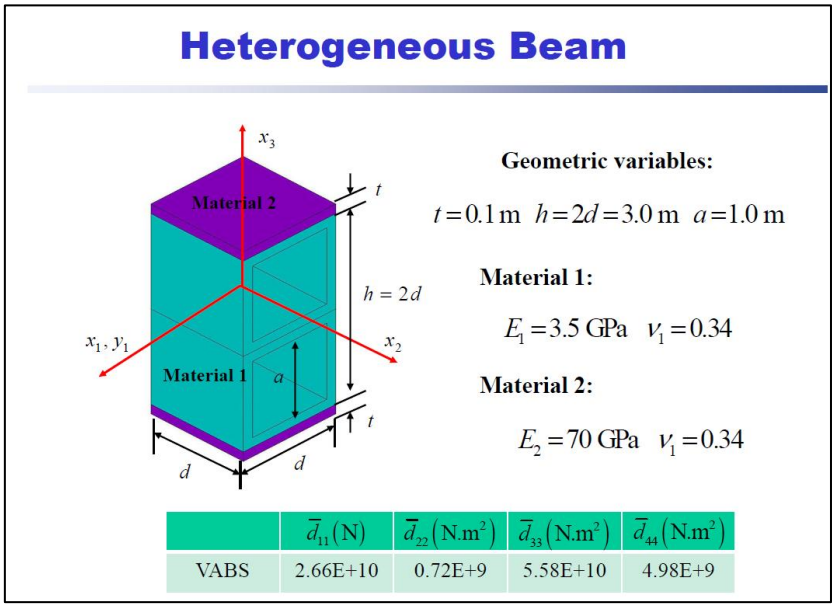

	$\bar{d}_{11}$ (N)	$\bar{d}_{22}$ (N.m^2)	$\bar{d}_{33}$ (N.m^2)	$\bar{d}_{44}$ (N.m^2)
VABS	2.66E+10	0.72E+9	5.58E+10	4.98E+9

Figure 8: Heterogeneous beam geometrical and material properties (Yu, 2012)

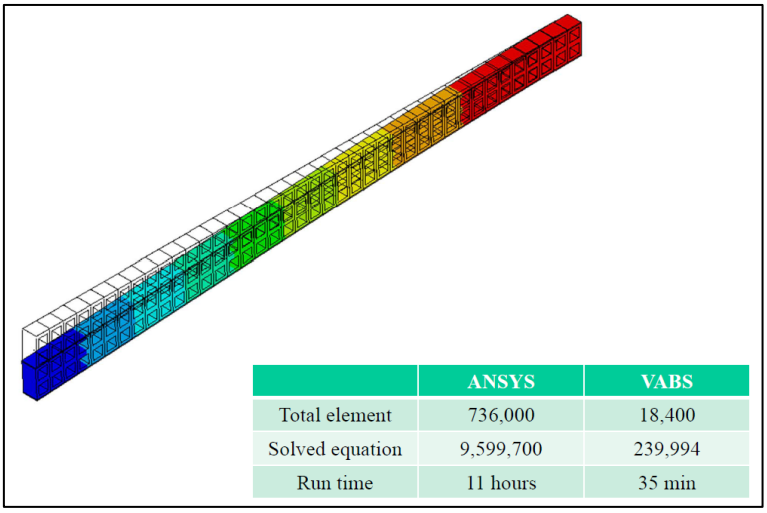

	ANSYS	VABS
Total element	736,000	18,400
Solved equation	9,599,700	239,994
Run time	11 hours	35 min

Figure 9: Displacement solution results of heterogeneous beam (Hodges & Yu, 2007)

Figure 10 shows that there is a good correlation between the predicted results of ANSYS and VABS. The maximum difference between the displacements is in the vicinity of 1% while the maximum difference in the stress prediction is approximately 2% (Yu & Hodges, 2004).

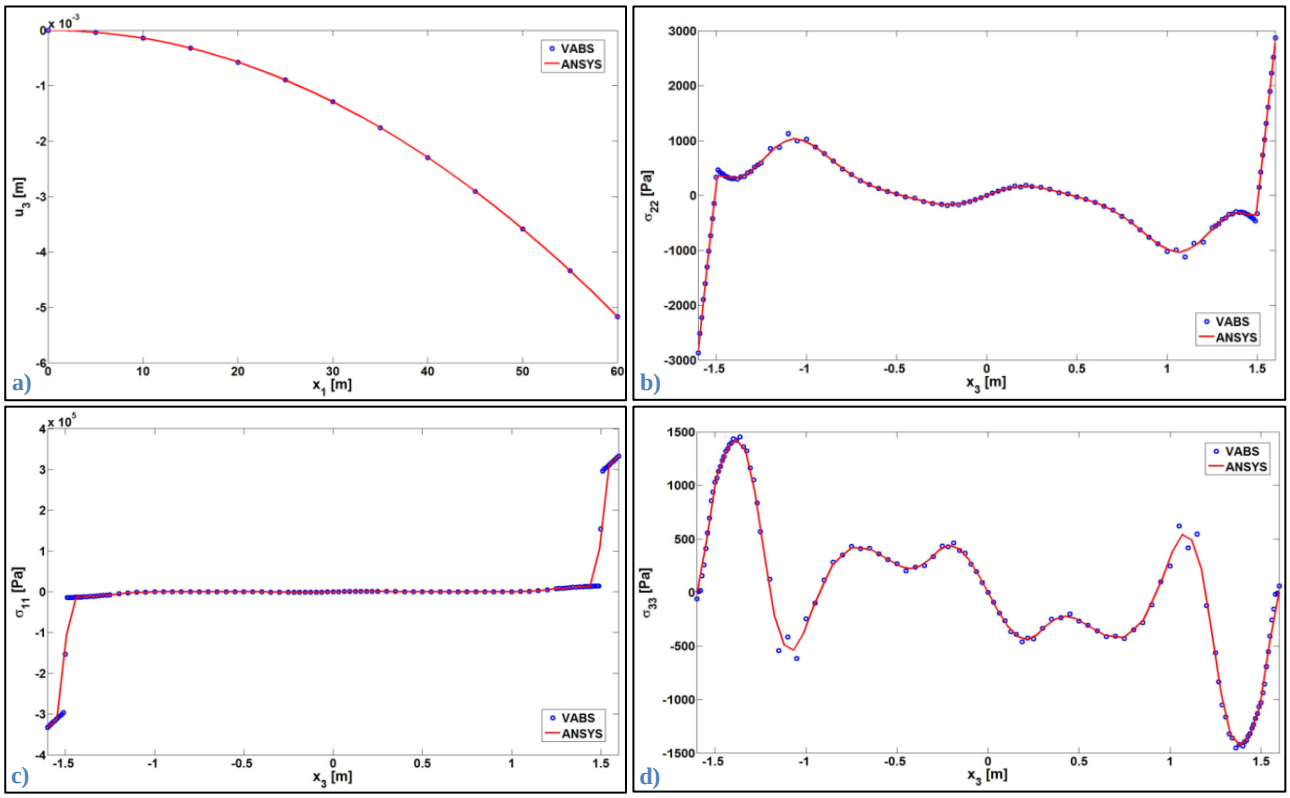

Figure 10: a) Beam displacement along the length b) σ_{22} Stress over the cross-section c) σ_{11} Stress over the cross-section d) σ_{33} Stress over the cross-section (Yu, 2012)

This shows that VABS gives results with an adequate accuracy for this project (Yu, 2012).

3.4 INTEGRATION OF ANALYSIS TOOLS INTO A SINGLE TOOL

PreVABS is an executable program that takes text files as input (Chen & Yu, 2008). These text files contain the geometries, material properties and composite layups of a selected cross-section. PreVABS calculates a mesh and prepares an output text file for VABS (Yu, 2011a). VABS uses this text file to calculate the flexibility and stiffness matrixes, which is written to a text file. This flexibility matrix is extracted and inserted in the input text file required by GEBT. This input file among others gives 1D beam coordinates, prescribed conditions. The GEBT program outputs twist bend deflections as well as resultant forces and moments. These results can be used as is, or

recalculated in VABS with a cosine direction matrix (DCM) to give 3D stress, strain and deflections. The process is depicted in Figure 11 and Figure 12.

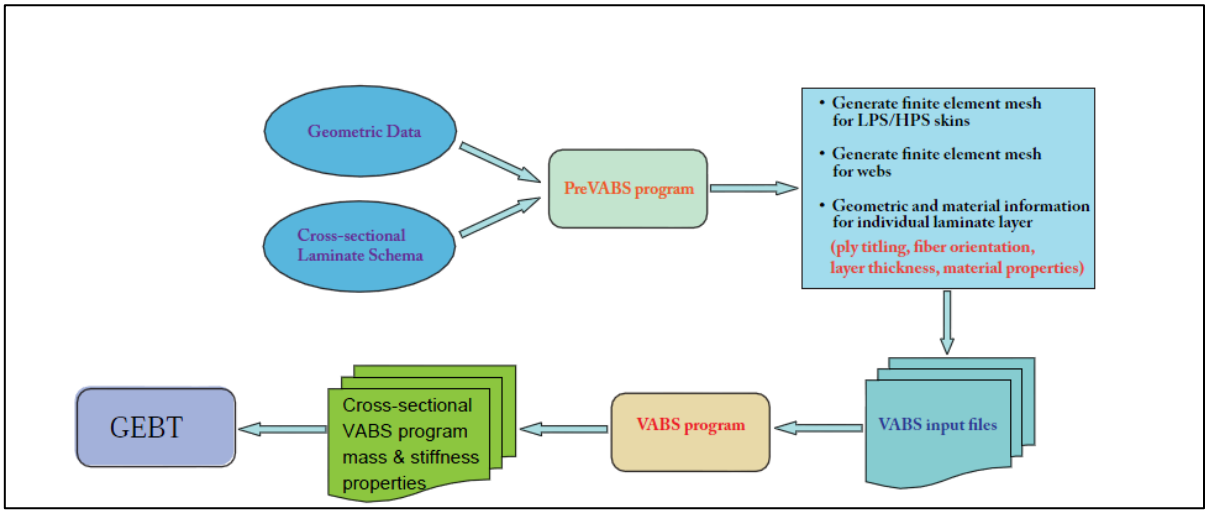

Figure 11: Process for calculation of cross-sectional properties (Chen & Yu, 2008)

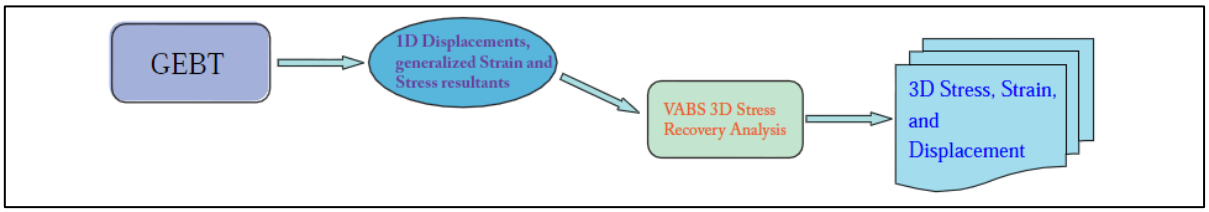

Figure 12: Process for 3-D Stress/Strain Recovery (Chen & Yu, 2008)

As this process is too complicated and time consuming to perform manually, it was decided to develop a Matlab program that controls the analysis process (Torenbeek, 2013). The program contains all the input variables and run PreVABS/VABS/GEBT sequentially to obtain the analysis results see Figure 13. The analysis process runs iteratively for different composite layup angles, and compiles a graph with the tailoring deflection couples versus layup angles. The basic Matlab program consists of the following components (The program code is available in Appendix C):

- A tailor.m code which takes full control of every process and creates plots of the output results.
- A function controlfilesec1.m which creates the input files and then runs PreVABS.
- A function VABS.m which runs VABS with its input file created from PreVABS.
- A function GEBTprep.m which extracts data from the VABS output files and creates an input file for GEBT, then finally running GEBT.
- A function GEBTresults.m that extracts the data from the GEBT output file into a Matlab cell matrix.

- A function Recover.m updates VABS input file with recovery results from GEBT, and the DCM needed for a 3D recovery of stress, strain, and deflections of the 2D cross-sectional points.
- A function VABSrecover.m to re-run VABS with the updated recovery data in the input file.
- A function Recoveryresults.m that extracts all the 3D results of stress, strain and deflection in a Matlab cell matrix.

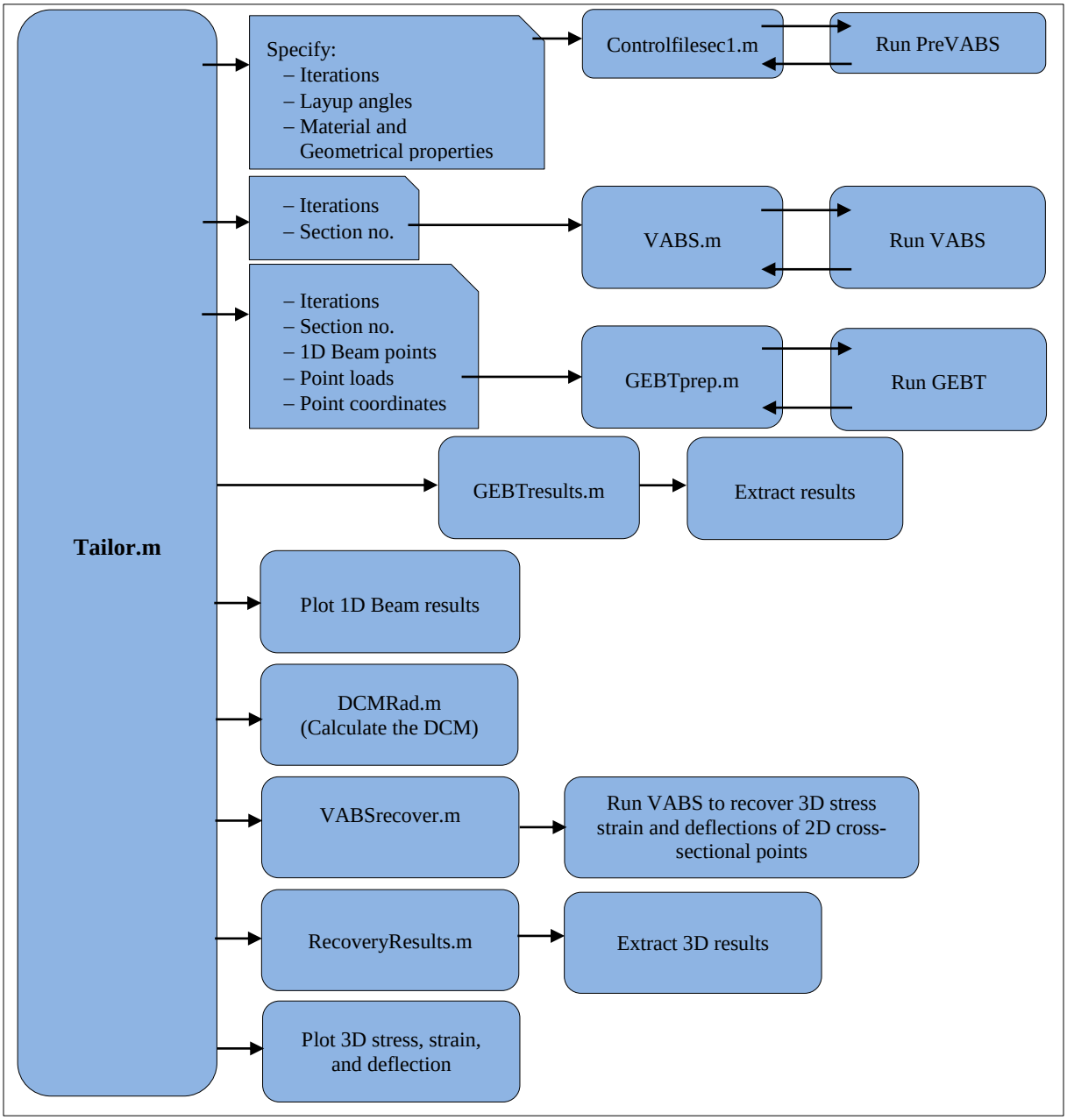

Figure 13: Flow diagram of the Tailor.m code

The tailor.m code gives the user the option of selecting which function to run, and which data to plot. The user specifies in tailor.m the number of calculations, number of cross-sections, chord lengths, total length, layer angles, pre-twist angles, last cross-sectional outer node on the TE, and varying values including varying material property values. The code can be set to plot bend-twist couples versus layup angle, forces versus deflections, 3D deflection plot, 3D strain plot and 3D stress plot. The defined composite layer angles and the twist sign convention is defined from this coordinate system as shown in Figure 14. This sign convention will also be applied to the Flaperon, as if it were an independent wing.

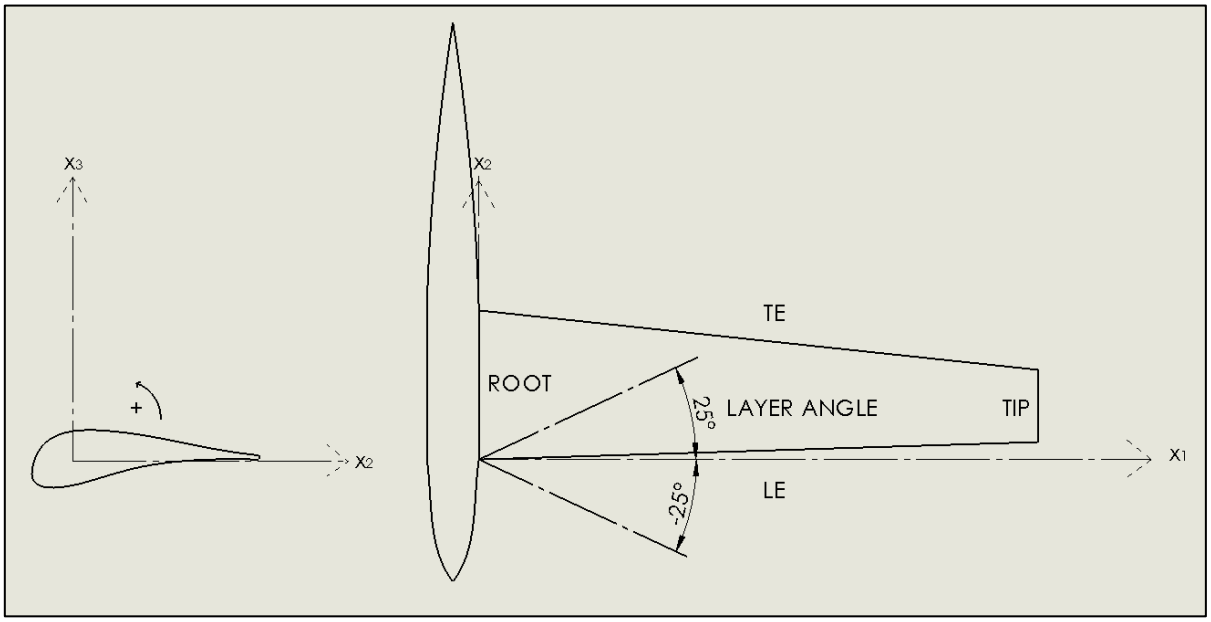

Figure 14: Coordinate system for layer angle inputs, flaperon tip twist and flaperon position sign convention

The Matlab program was run, and the results were compared with the manual results of PreVABS, VABS and GEBT to check if the program was coded correctly. This verified that the Matlab program also ran PreVABS/VABS/GEBT correctly. (Refer to Appendix A and B for a comparison of Tailor.m with hand calculations, FEM and manual analysis results of PreVABS, VABS and GEBT)

3.5 SUMMARY

A short discussion on the workings of PreVABS, VABS and GEBT showed the capabilities of this analysis software.

The theory of PreVABS and VABS is well published in literature. Types of beams were identified and classified, and the solution methods applicable to each class of beam were discussed. A mathematical formulation of GEBT showed the advantage of its compact matrix form, with the absence of any approximations in the geometry of the deformed elements along the beam axis, as well as the Timoshenko approach with its compatibility to large global displacements and rotations.

The verification through published data showed the comparison between VABS's and ANSYS's analysis results of a heterogeneous bream. The comparable accuracy of VABS, combined by its much reduced runtime compared to ANSYS, makes it a powerful and effective tool in composite wing design.

A Matlab program, called "Tailor.m", was developed to take control of the tailoring process by running PreVABS, VABS and GEBT automatically to ease user effort. The operation of "Tailor.m" was verified against PreVABS/VABS/GEBT run manually. It will now be attempted to utilise this tool in the tailoring of flaperon-type composite structures; however, before that can happen, "Tailor.m" will be used to model the JS1 Flaperon 3 in its original form to validate modelling of flaperon-type structures.

4 VALIDATION OF A FLAPERON-TYPE MODEL USING "TAILOR.M"

In this section a flaperon-type structure will be modelled with the program Tailor.m. This will be a final validation step to ensure that the flaperon structure can be accurately modelled. The calculated result will be compared with thin wall tube theory as well as with experimental results.

4.1 MODELLING OF FLAPERON 3

With PreVABS/VABS/GEBT incorporated into the user interface of tailor.m, a closed walled composite structure can be modelled iteratively to give results for many different composite fibre layup angles. The most simplified form of a closed walled structure is circular in shape. The flaperon shape has a typical round leading edge with a sharp trailing edge (TE) as shown in Figure 18. The sharp shape of the TE can introduce modelling meshing problems with the resultant loss in accuracy.

For this validation it was decided to use the JS1 Flaperon 3 geometry due to the availability of a physical specimen for experimental investigations. The normalised coordinates of the root and tip cross-sections of Flaperon 3 were set up in the Matlab file "controlfilesec1.m". The composite layup and material properties, obtained from *a priori* calculations by Jonker Sailplanes Pty, were also specified.

The JS1 control surfaces, including Flaperon 3, were designed using thin-walled tube theory and the design data was made available to the author. A simple load case was set up with the flaperon fixed at one end, and a single torque applied to the other end. A torque value of T = 4.2 N.m was applied. The simple thin tube theory predicted a twist angle of 18°, while Tailor.m predicted an angle of 9.8°. This large disparity in results called for a further investigation.

The meshing of the flap structure was investigated first by comparing the meshing of cross-sections with structures of simple shapes such as circles, ellipses and a large circle LE with straight edges, connected at the TE by means of a small circle as shown in Figure 15, Figure 16, and Figure 17 respectively. From this it can be seen that the mesh is properly developed with all the mesh points correctly linked to neighbouring points.

When subjecting these simple shapes to a distribution torque, the results between tailor.m and thin wall theory was in close agreement as shown in Table 1. When the Flaperon 3 was subjected to the same torque loading, a twist angle of 400° was seen at the tip. A further inspection of the Flaperon 3 mesh showed erroneous nodal connections in the vicinity of the trailing edge. The two sheets of the upper and lower skin do not connect at the trailing edge, which allows the surfaces to slide over each other, rather than behave like a single solid as shown in Figure 18, Figure 19, and Figure 20 respectively.

Table 1: Tailor.m and Thin wall tube theory under load distribution torque

	Thin wall theory	**Tailor.m**	**Percentage difference**
Tip twist angle	4.6°	5°	10%

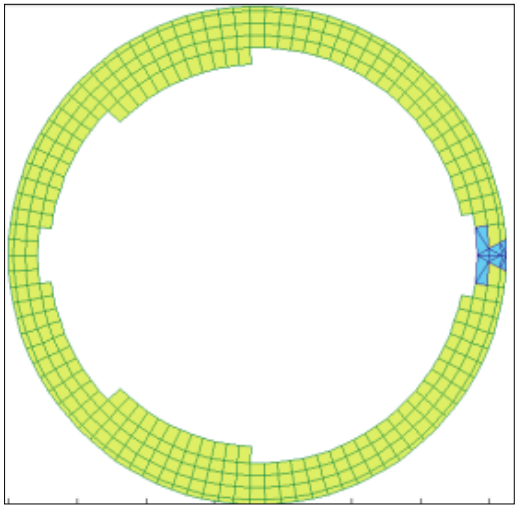

Figure 15: Circular cross-section with Flaperon 3 composite layup meshed with PreVABS

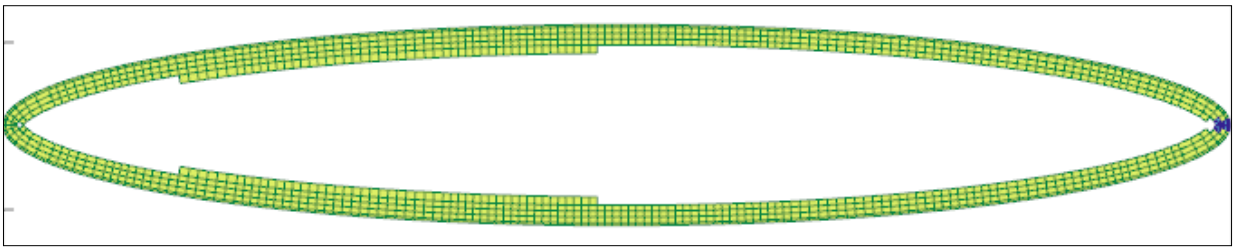

Figure 16: Elliptical cross-section with Flaperon 3 composite layup meshed with PreVABS

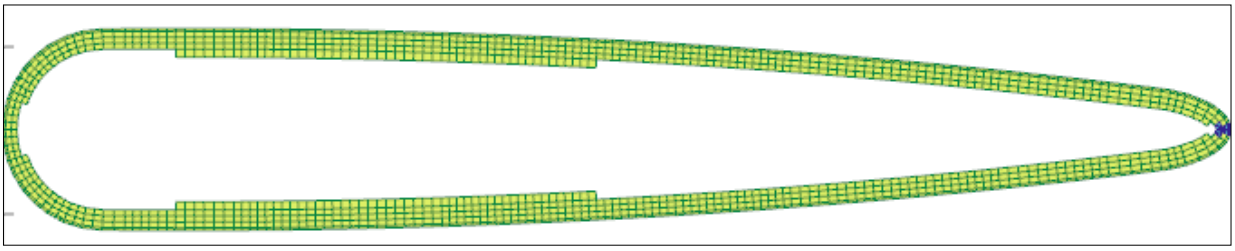

Figure 17: Large circle-straight lines-small circle cross-section with Flaperon 3 composite layup meshed with PreVABS

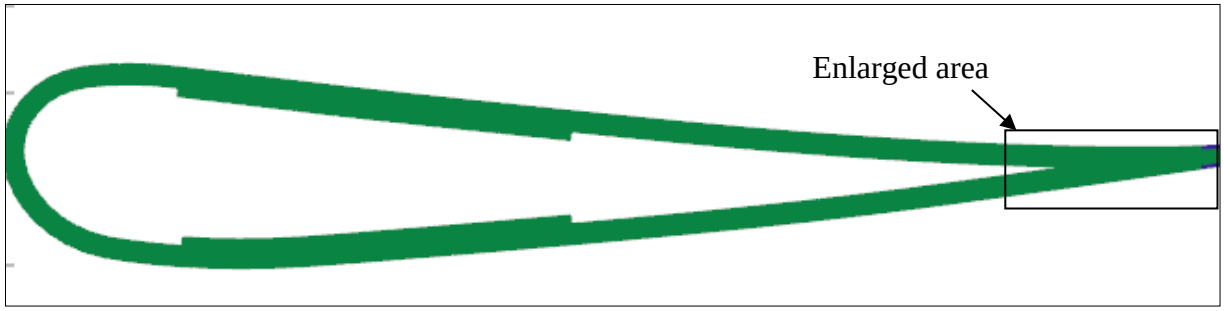

Figure 18: Flaperon 3 cross-sectional mesh with erroneous nodal connections at the TE

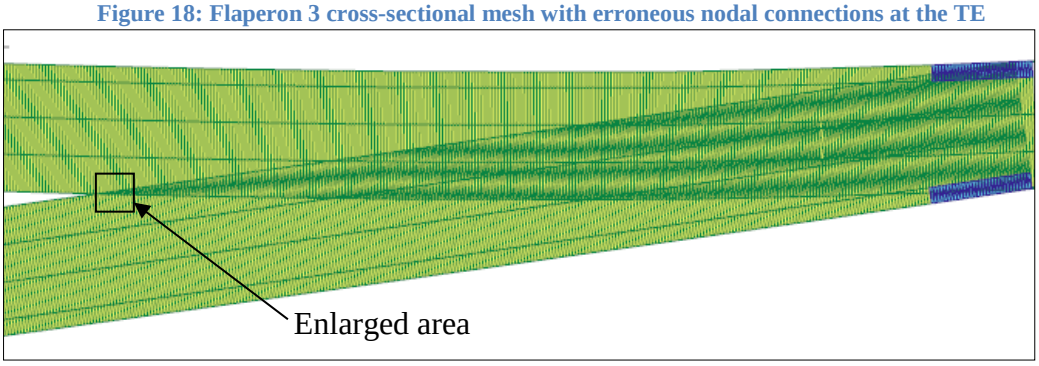

Figure 19: TE of Flaperon 3 with upper and lower surface mesh crossing over each while not connecting

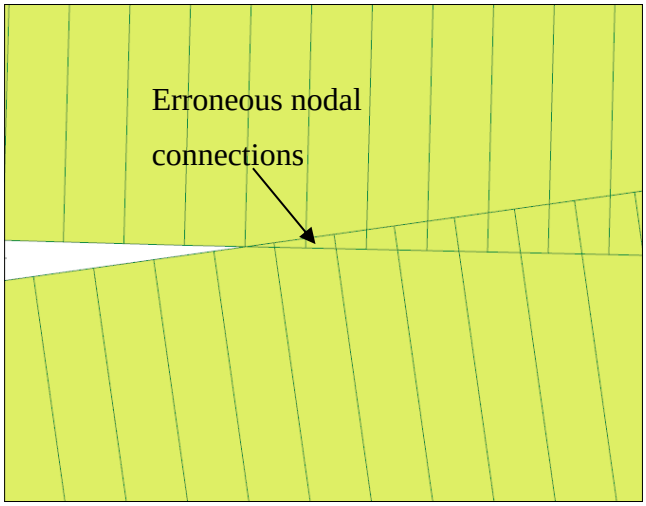

Figure 20: Enlarged area of erroneous nodal connections of Flaperon 3 TE mesh

The problem was resolved by reducing the number of forced nodal points on the upper and lower skin at the TE and re-meshing until the vertex of the inner skin surface connected directly to the vertex of the outer skin surface as shown in Figure 21, Figure 22, and Figure 23 respectively. These forced nodal points on the outer skin surface define the outer cross-sectional shape as well as the skin position for certain meshing nodal points. This showed that PreVABS mesh results can converge easier if fewer points at the TE skin are forced.

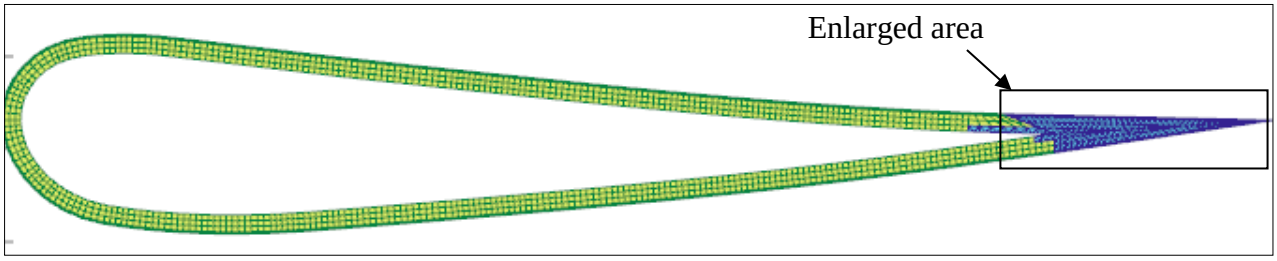

Figure 21: Flaperon 3 cross-section correctly meshed

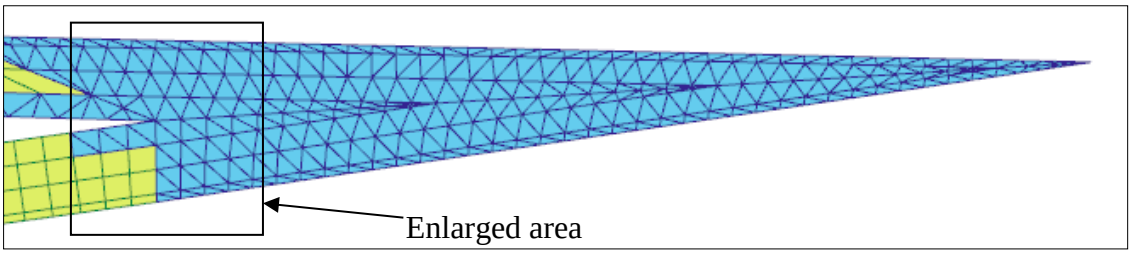

Figure 22: TE of Flaperon 3 with upper and lower surface mesh merging correctly

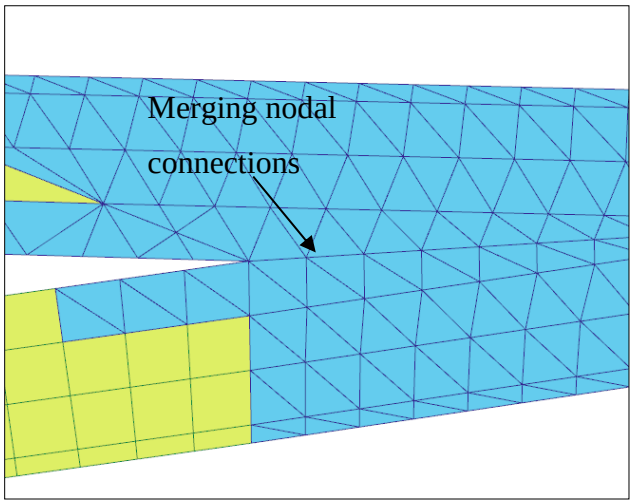

Figure 23: Enlarged area of merging nodal connections of Flaperon 3 TE mesh

Repeating the simulation with the rectified mesh yielded 38° of tip twist, which is a much improved result. The twist angle was still much larger than predicted by both the simpler geometries and the thin-walled tube calculations as seen in Table 1. The problem was traced to incorrectly specified material properties. It was found that the material properties of the carbon fibre layers must be given with E_z, and G_{yz} equal to zero for Tailor.m to give better results. This makes physical sense since the through thickness properties of composite materials are thin. After this correction the discrepancy between the tip twist angles of the thin wall tube theory and tailor.m was about 0.4° or 10% as seen in Table 1.

4.2 EXPERIMENTAL TEST OF FLAPERON 3

To confirm the modelling process, values predicted by tailor.m compared with the experimental results where the JS1 Flaperon 3 was physically loaded in torque. For this test a production sample of the JS1 Flaperon 3 was tested. The flaperon was supported at the hinge points and the inboard end was fixed. A torque of T = 4.2 N.m was applied at the other end. The experimental setup is shown in Figure 24.

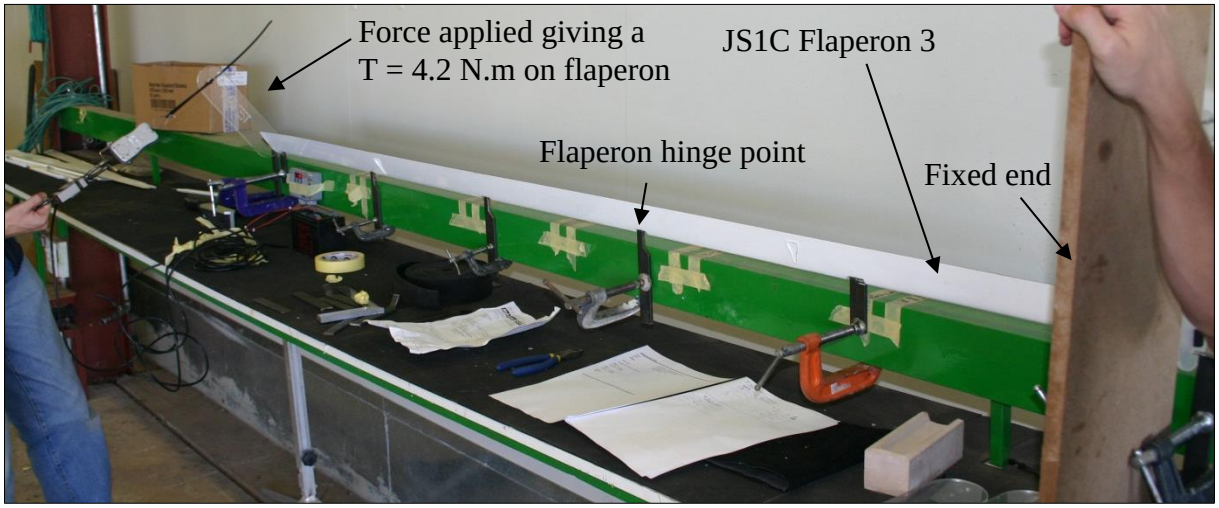

Figure 24: Flaperon 3 experimental setup for torque deflection test

4.3 RESULTS AND DISCUSSION

The experimental results were compared with the calculated results from tailor.m as well as with the results of a thin wall theory calculation. A summary of the results are shown in Table 2.

Table 2: Torque twist deflection comparisons with experimental, Tailor.m, and thin walled tube theory

Torque applied	Experimental results of Flaperon 3	Tailor.m	Thin walled tube torsion theory	Percentage difference to experimental results
$T_{4.2\ N.m\ at\ tip}$	-11.39°	-9.8°	-18°	14% to Tailor 38% to Thin walled tube theory

The single torque load produced a twist of 11.39° experimentally, while tailor.m predicted a twist of 9.8° and the thin wall theory predicted a twist of 18°. The tailor.m results therefore differ by 14%

from the measured deflection. The calculated twist angle was 1.59° less than that obtained in the experiment; this may be because PreVABS/VABS/GEBT assumes small strains for calculations (Yu et al., 2002(a)) while this test subjected the flap to an 11.4° twist deflection which is a large twist deflection. A small strains assumption would be a twist deflection less than 5.7°. The thin wall calculation differed from tailor.m by 45%. It is therefore clear that tailor.m twist deflection results are more accurate than that of thin wall theory. It would have been interesting to have checked tailor.m versus the experimental setup for smaller torques as well, but the experimental data did not cover smaller torques, because the experiment was for structural limit testing.

4.4 SUMMARY

This Chapter has validated that tailor.m can model Flaperon 3 correctly. This was shown by loading the flaperon with a torque at one end and comparing it with thin walled tube theory and experimental results.

During the verification it was found that the meshing of the thin TE of the flaperon was not satisfactory. Thus by comparing the meshing with simpler cross-sectional shapes like circles and ellipses, it showed that the flaperon TE had erroneous nodal connections. By giving fewer forced outer skin nodal points in the area of the flaperon TE gave better results, by allowing the upper and lower skins mesh to converge.

It is important to specify the material properties correctly as making the wrong assumptions can lead to inaccurate results.

Having validated that the Flaperon 3 was modelled correctly in Tailor.m, Flaperon 3 was ready for aeroelastic tailoring.

5 TAILORING OF FLAPERON 3

During cross-country flight, gliders fly long distances by alternately climbing in thermals (colloquially referred to as “thermalling”) and cruising, transferring the altitude into distance. The glider is therefore designed to climb well, but also to cruise efficiently. This is accomplished in the case of the JS1C by the use of flaps. During slow turning flight in thermals, the glider uses positive flap deflections to increase the airfoil maximum lift; during cruising, negative flap settings with lower lift and drag is used.

The slenderness of the JS1C Flaperon 3 allows it to twist under load, away from the optimum flap setting as is required for climbing or cruising. Aeroelastic tailoring might provide a solution to reduce undesirable torsional twist characteristics. The higher wing bending during thermalling might be used to induce a coupling in the flaperon, which might in turn attempt to counter the twist characteristics.

It has been stated that Flaperon 3 of the JS1C is at its optimum aerodynamic shape if it has no twist deflections. However, because of its aerofoil-shaped cross-sections, aerodynamic forces and moments will cause the flaperon to bend around its hinge line in chord wise bending (which is negligibly small due to the relatively small chord to thickness ratio). This means that counter-deflections are required to reverse the effects of the aerodynamic loads at the selected flight conditions.

A classical solution is to design the flaperon with a pre-twist to counter the aerodynamic torque loads on the flaperon. The largest performance penalty comes from the flaperon deflection at high speed (known as cruise), in which 70% of modern gliding flight is conducted. Countering the flap twist under these conditions will therefore yield the best performance gain. The aerodynamic load during flight will then tend to untwist the flaperon to the required optimum shape, shown as the optimum high speed flaperon position in Figure 25.

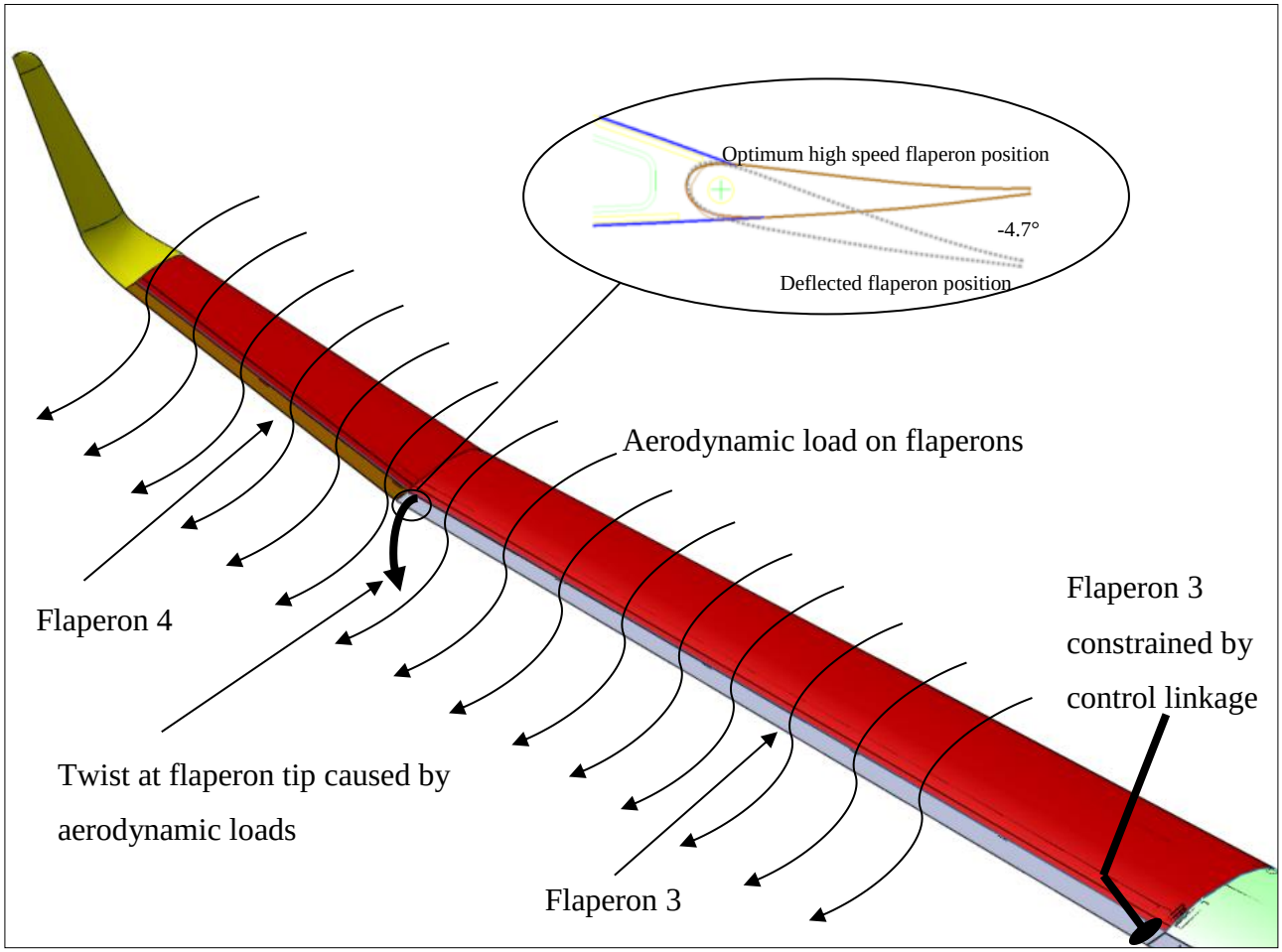

Figure 25: Aerodynamic loads on the JS1C flaperons during cruise

This however means that the flaperon will also have a pre-twisted shape in the low speed condition.

Alternatively, a composite structure could be aeroelastically tailored to introduce a bend-twist coupling. If a bend-twist coupling could be introduced to the flaperon, bending of the main wing due to the aerodynamic load can be used to affect a sufficient amount of counter-twist in the flaperon. The aerodynamic forces acting upon the flaperon will again untwist the flaperon.

It is possible that not all the twist can be removed using the bend-twist coupling. If that be case, classical pre-twist could be added as well. But this is of little consequence as the negative twist on the outer flaperons will result in an effective wing washout, which may improve handling and reduce tip stalling tendencies.

This tailoring approach will be modelled in the following sections.

5.1 TAILORING REQUIREMENTS

It is hoped to improve the flight performance of JS1 by incorporating aeroelastic tailoring into its Flaperon 3. To perform the tailoring, it is necessary to know the deflections of Flaperon 3 at its most prevalent flight conditions, namely cruising, and climbing (McCormick, 1995).

JS1 Flaperon 3 was designed using an Excel spreadsheet, "Wing structural _JS1_21_V1.xlsx" created by A.S. Jonker (2011), which is based on thin-walled tube theory. The 21m wing tip was also tested for structural design verification. The results from both the calculations and the experiment, performed by Jonker Sailplanes, were used to determine the maximum flexural deflections of Flaperon 3.

Figure 26: JS1C 21 m tip loaded with whiffletree system at SF 1.25 with a tip deflection of 570 mm

Flight recorders fitted to JS1 have shown that the loads experienced during climbing average 1.2 G, while the cruising load is necessarily 1.0 G as the glider is only flying in a straight line. Obtaining the deflections of Flaperon 3 under these two flight conditions were done by interpolation from the experimental and calculated maximum load deflections.

During experimental testing, the 21 m tip of the JS1C was loaded on the ground with a whiffle tree system as shown in Figure 26. A load of 260 kg was applied to the tip, which corresponds to a safety factor of 1.25. At this load the tip deflection was measured to be 570 mm. Calculations for the wing were performed for loads up to 5.5G, when the safety factor is exactly 1.

Linearly interpolated data gives the 1.2 G deflection at the wing tip as 155 mm. The measured point of deflection is 3 m from the wing tip junction. The end of Flaperon 3 is 2.2 m from the wing tip junction. Interpolation gives a deflection of 114 mm at the end of Flaperon 3; however, to account for the flexural curvature, the displacement was estimated to be 70 mm as shown in Figure 27.

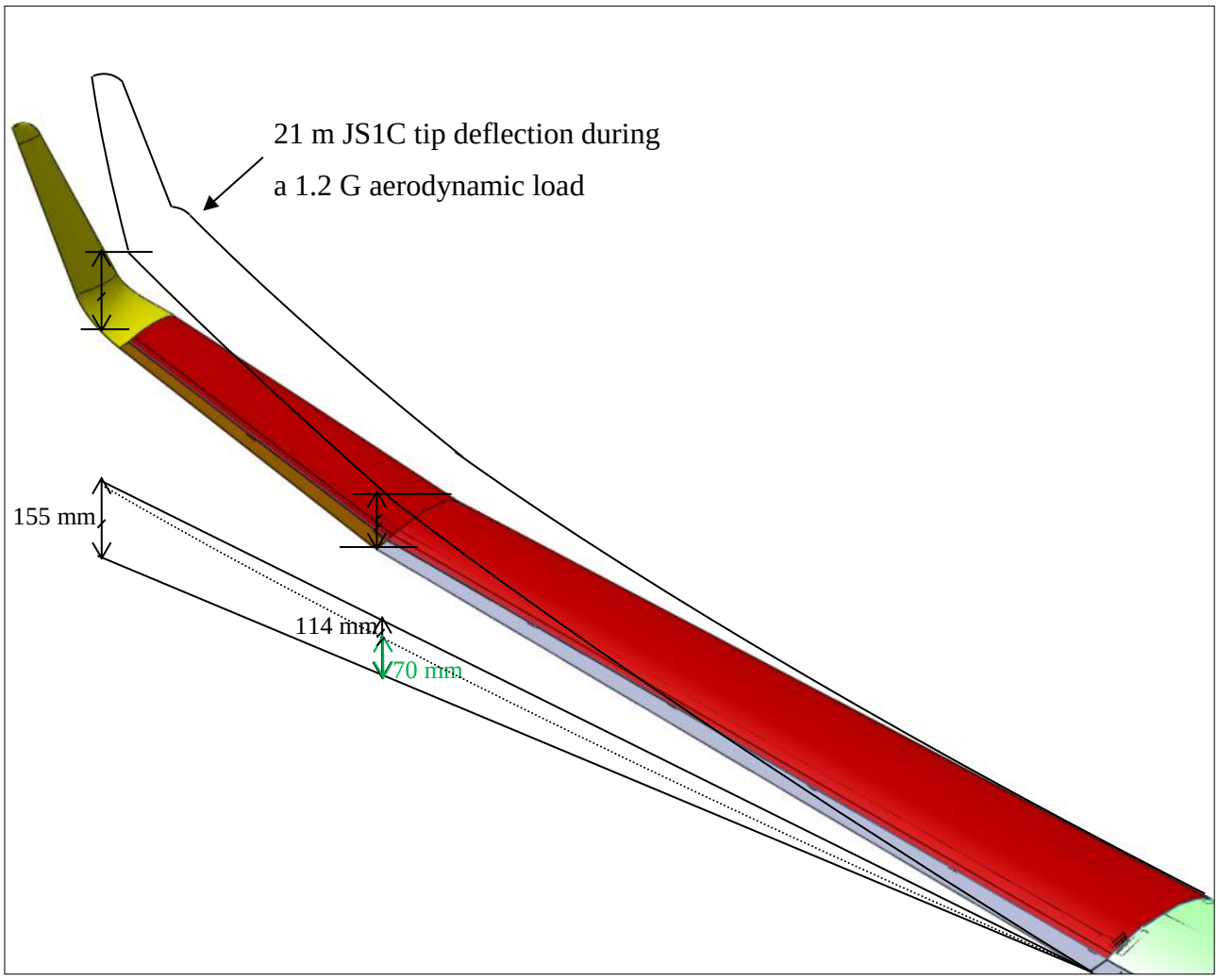

Figure 27: 21 m JS1C tip during a 1.2 G aerodynamic loading with a deflection of a 155 mm at the wing tip and 70 mm at the end of Flaperon 3

Because the difference between the cruise load and thermalling(climbing flight) load is much smaller than the difference between the thermalling(climbing flight) load and the tested load, Flaperon 3's deflection at 1.0 G was obtained by interpolating from the estimated deflection at 1.2 G, yielding 58 mm.

These values are used as inputs to the code "Tailor.m" as bending deflections for Flaperon 3, from this the bend-twist couple can be calculated.

The Excel spreadsheet “Wing structural _JS1_21_V1.xlsx” (Jonker, 2011) uses flight speed rather than loading to calculate the forces, moments and deformations. It also gives the recommended flap setting for the flight speed, which is then made available in the JS1 Flight Manual. These flap settings are shown for climbing in Figure 28 and for cruise in Figure 30. The non-tailored Flaperon 3 tip twist angles during climbing and at cruise were calculated by this code as 0.8° and -4.7° respectively, as depicted in Figure 29 and Figure 31 and summarized in Table 3. The coordinate system for the flaperon position setting and tip twist angle is shown in Figure 14. The coordinate system for the flaperon setting and the pilot’s flight terms are opposite as shown in Table 3. All the flight condition data collected with the non-tailored and no pre-twist Flaperon 3’s installed is summarized in Table 3.

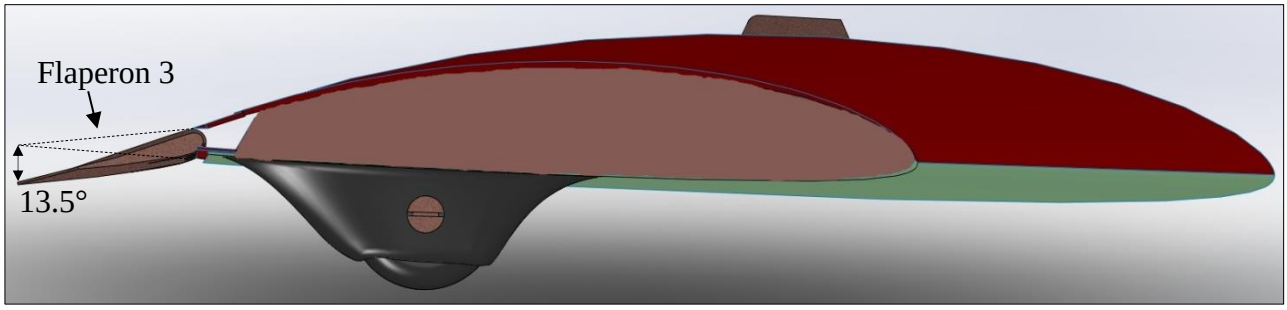

Figure 28: Cross-section of 21 m JS1C wing at Flaperon 3 during a thermalling flaperon setting of -13.5° (downward) at zero km/h (0° twist)

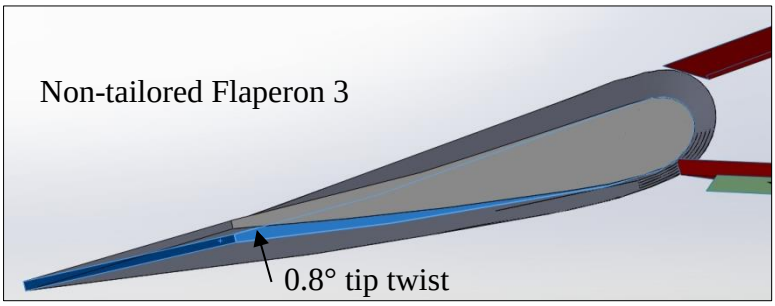

Figure 29: During thermalling at 120 km/h the aerodynamic loads produce a tip twist of 0.8° (upward) on the non-tailored Flaperon 3

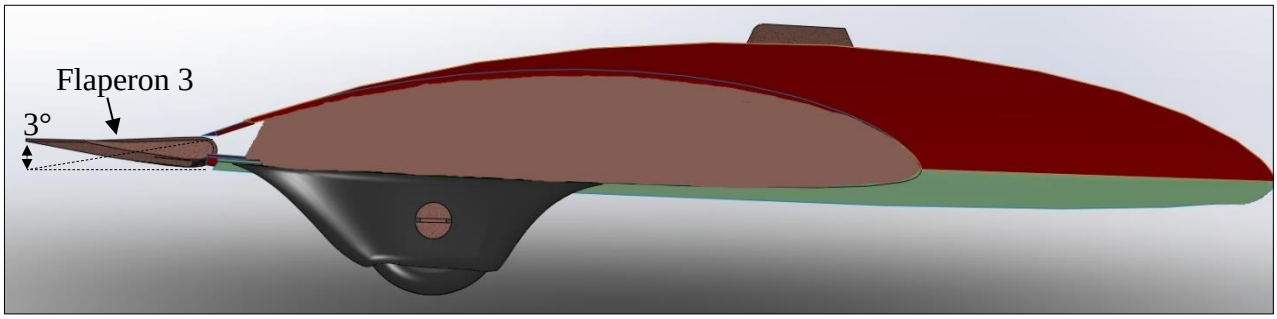

Figure 30: Cross-section of 21 m JS1C wing at Flaperon 3 during a cruise flaperon setting of 3° (upward) at zero km/h (0° twist)

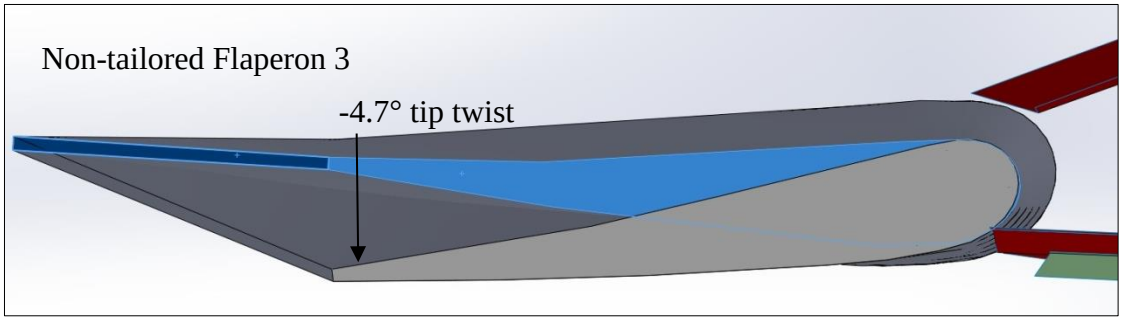

Figure 31: During cruise at 220 km/h the aerodynamic loads produce a tip twist of -4.7° (downward) on the non-tailored Flaperon 3

Table 3: JS1C characteristics with the non-tailored Flaperon 3

Flight data during thermalling(climbing flight)		
	Airspeed	120 km/h
	Average Bank angle	33°
	Load factor	1.2 G
	Flaperon setting	-13.5°(downward) (known as a positive flap setting)
	Flaperon loaded deflection at tip due to wing bending	70 mm bending deflection
	Flaperon tip twist under aerodynamic forces	0.8°
Flight data during cruise		
	Airspeed	220 km/h
	Bank angle	0°
	Load factor	1.0 G
	Flaperon setting	+3°(upward) (known as a negative flap setting)
	Flaperon loaded deflection at tip due to bending	58 mm bending deflection
	Flaperon tip twist under aerodynamic forces	-4.7°

5.2 SETUP AND MODELLING

The desired outcomes for the tailoring have been obtained from results calculated earlier: the bend-twist couple to be introduced to Flaperon 3 would have to counteract a downward (-) twist angle of 4.7° at cruise (Figure 31) and an (+) upward 0.8° twist angle during climbing (Figure 29). However, the lift distribution over the wing is also restricted to a total reduction in lift not exceeding $c_l = 0.1$ in order to maintain the optimal elliptical lift distribution (Jonker, 2013). Since the twist effect of Flaperon 3 will be most prominent near the its tip, a reduction in lift at the wing tip of the JS1 will effectively create a reduced wing span without a similar reduction in drag.

The first attempt at tailoring Flaperon 3 was performed using the thermalling(climbing flight) deflection as the input to Tailor.m. Tailor.m then incrementally rotated the layup angle of the laminate iteratively between 0°/90° and 45°/-45°, the period of a bi-directional layer. The graph should be rotationally symmetric around 0° or 45°. As seen in Figure 32 the lines do not seem to converge on zero at 45°. This was not expected, but could be due to the cross-sectional shape of the Flaperon 3 airfoil. From this analysis, the relationship between the resultant bend-twist angle and the layup angle was obtained. The cruise deflection was given as the input for the second run. Tailor.m returned the results in the graph shown in Figure 32.

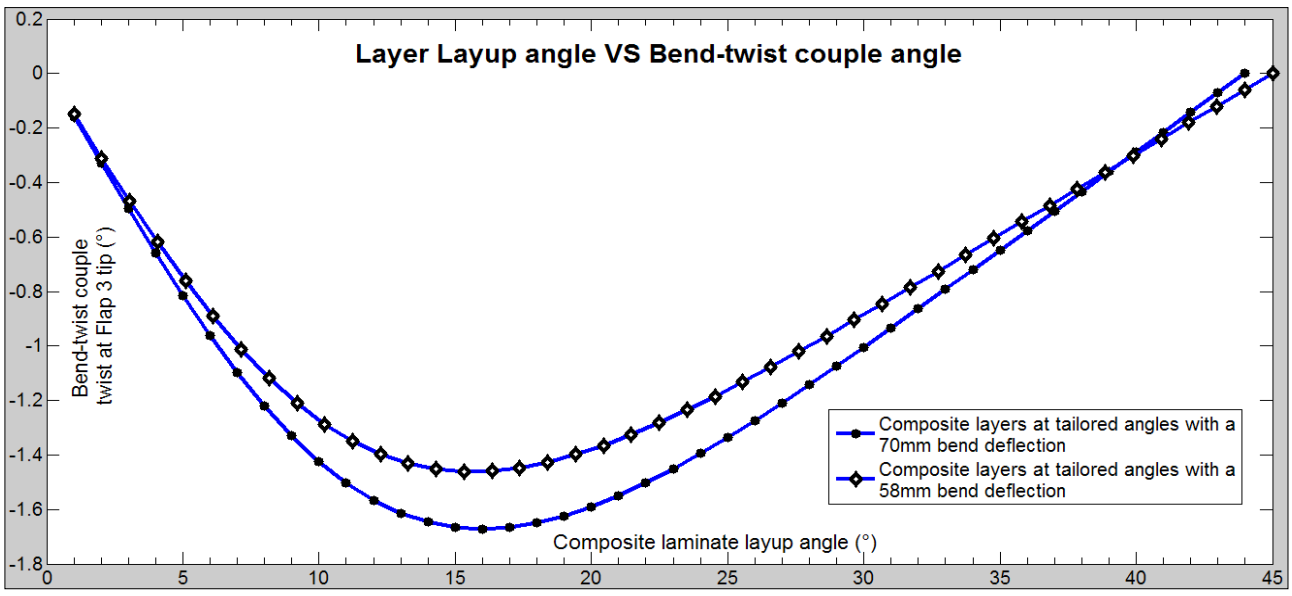

Figure 32: Bend-twist couple angle VS layer layup angle at a 70 mm deflection and a 58 mm deflection

It can be seen from the results in Figure 32 that, although slightly different, in both cases the maximum twist will be obtained if the layup angle is changed to approximately 16°. The bend-twist

couple will cause a maximum of ±1.5° twist downwards if Flaperon 3 is deflected by 58 mm, and almost ±1.7° downward twist if deflected by 70 mm.

Rotating the layup through 16° seems to favour thermalling(climbing flight) – in fact, it introduces too much "untwisting", resulting in Flaperon 3 twisting to 0.9° downwards (Figure 33). It would appear that a layup angle change by either 6° or 33° would cure the twist during thermalling.

However, this would not solve anything during cruise as the -6.2° tip twist from the tailored couple in Figure 34 would make the Flaperon aerodynamically worse. At -6.2° tip twist the most manufactured pre-twist of 4° will still fail to return Flaperon 3 to its optimum shape during cruise. Certainly, rotating the layup angle to 74° would reduce the tip twist to -3.2° during cruise as the bend twist couple would introduce a Δ1.5° counter twist to the tip, but this would also increase the upward twist during thermalling to 2.5°, reducing the lift over the tip. This will introduce washout which, while benefitting the handling characteristics, may also lead to a loss in lift and a disruption in the elliptical lift profile.

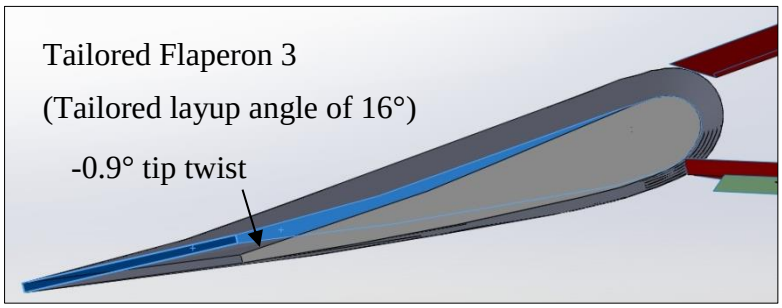

Figure 33: During thermalling at 120 km/h the aerodynamic loads and tailored couple produce a tip twist of -0.9° (downward) on the tailored Flaperon 3

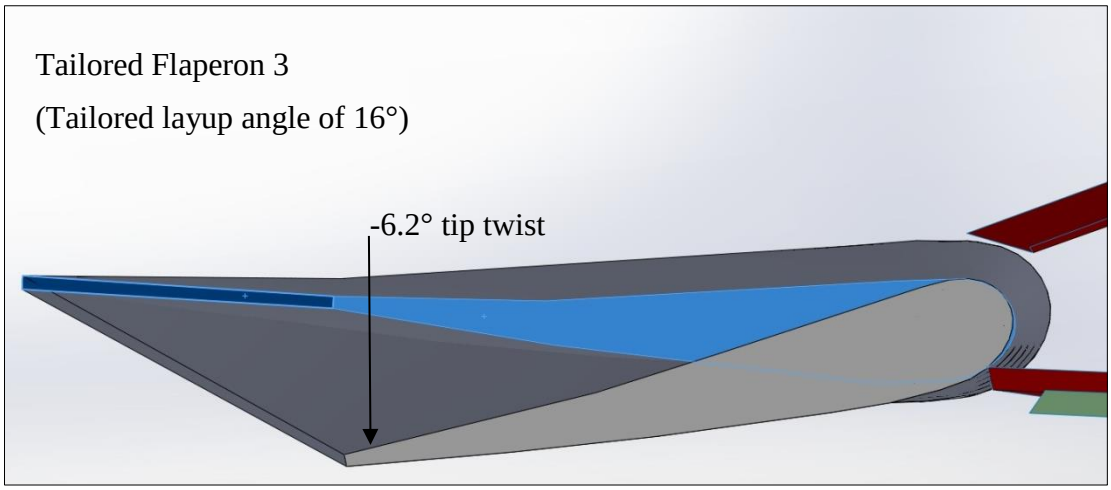

Figure 34: During cruise at 220 km/h the aerodynamic loads and tailored couple produce a tip twist of -6.2° (downward) on the tailored Flaperon 3

It was then attempted to tailor the layup by rotating selective layers instead of the entire laminate.

First, one layer was chosen to be rotated by Tailor.m and the deflection of Flaperon 3 during thermalling was selected as the input. Next, two layers were allowed to be rotated for the thermalling input. The results are shown in Figure 35.

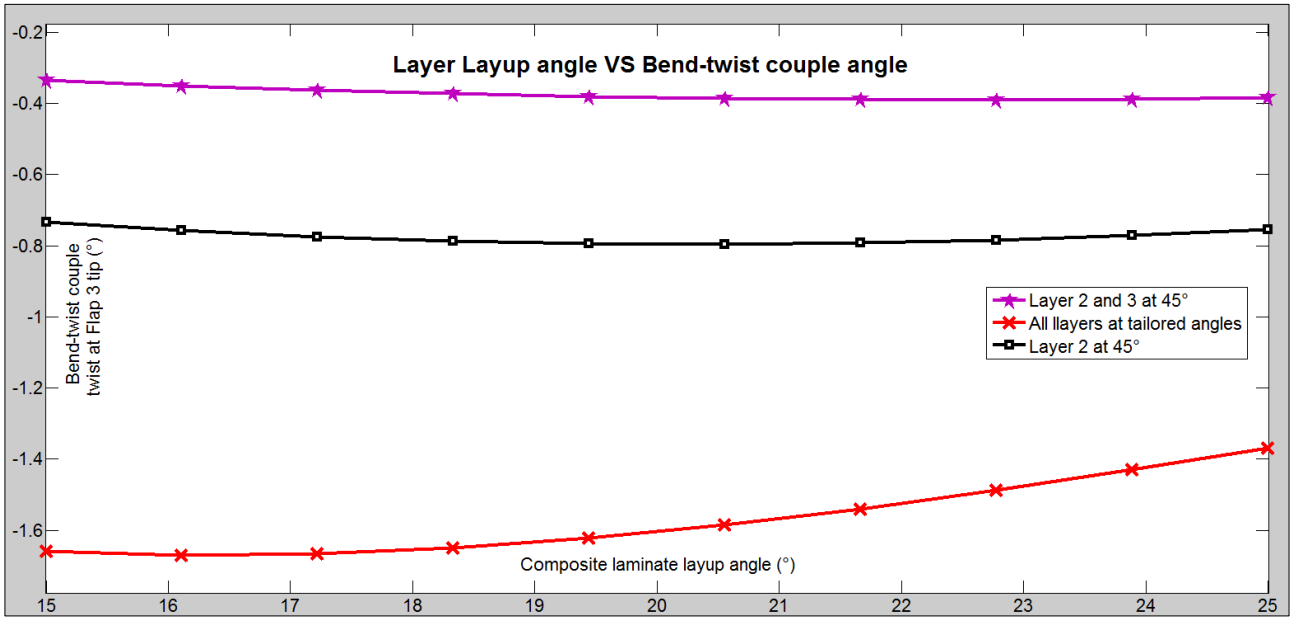

Figure 35: Bend-twist couple angle VS layer angle for different layer tailoring at 70 mm flaperon bending deflection

It is clearly seen from Figure 35 that rotating only some of the layers have a reduced effect compared to rotating the entire laminate. There appears to be no further need to pursue this option.

So far, using only aeroelastic tailoring has failed to completely address the twist in Flaperon 3 during both cruise and thermalling(climbing flight). Therefore it is time to investigate the effect of also introducing pre-twist.

The amounts of pre-twist required for thermalling and for cruising differ in both magnitude and direction: to improve cruising performance requires an upward pre-twist, while a much smaller downward pre-twist would be necessary to improve thermalling performance. It is now required to determine which aspect of the JS1's performance to optimise for.

Flight data obtained from the onboard flight computers of several JS1's have indicated that cruising makes up approximately 70% of the flight time, while only about 30% of the time is spent climbing. This indicates that the most performance can be gained by improving the cruise behaviour of Flaperon 3.

To allow for optimum zero twist in Flaperon 3 during cruise, the non-tailored flaperon would have to be manufactured with an upward pre-twist of 4.7° (Figure 37, countering the effect shown in Figure 31). From this assume that a washout of 5.5° is introduced in Flaperon 3 at its tip during thermalling, as seen in Figure 36.

Washout would have the advantage of reducing tip stall tendencies, but it is now required to check that this effect does not cause a skewing of the elliptical lift profile by causing a loss of lift of more than 0.1 in c_l. From JS1 data, a change in flaperon settings from -13.5° to -10.5° would give a 0.073 loss in c_l. This means that a washout of more than 4° would skew the sought-after elliptical lift profile.

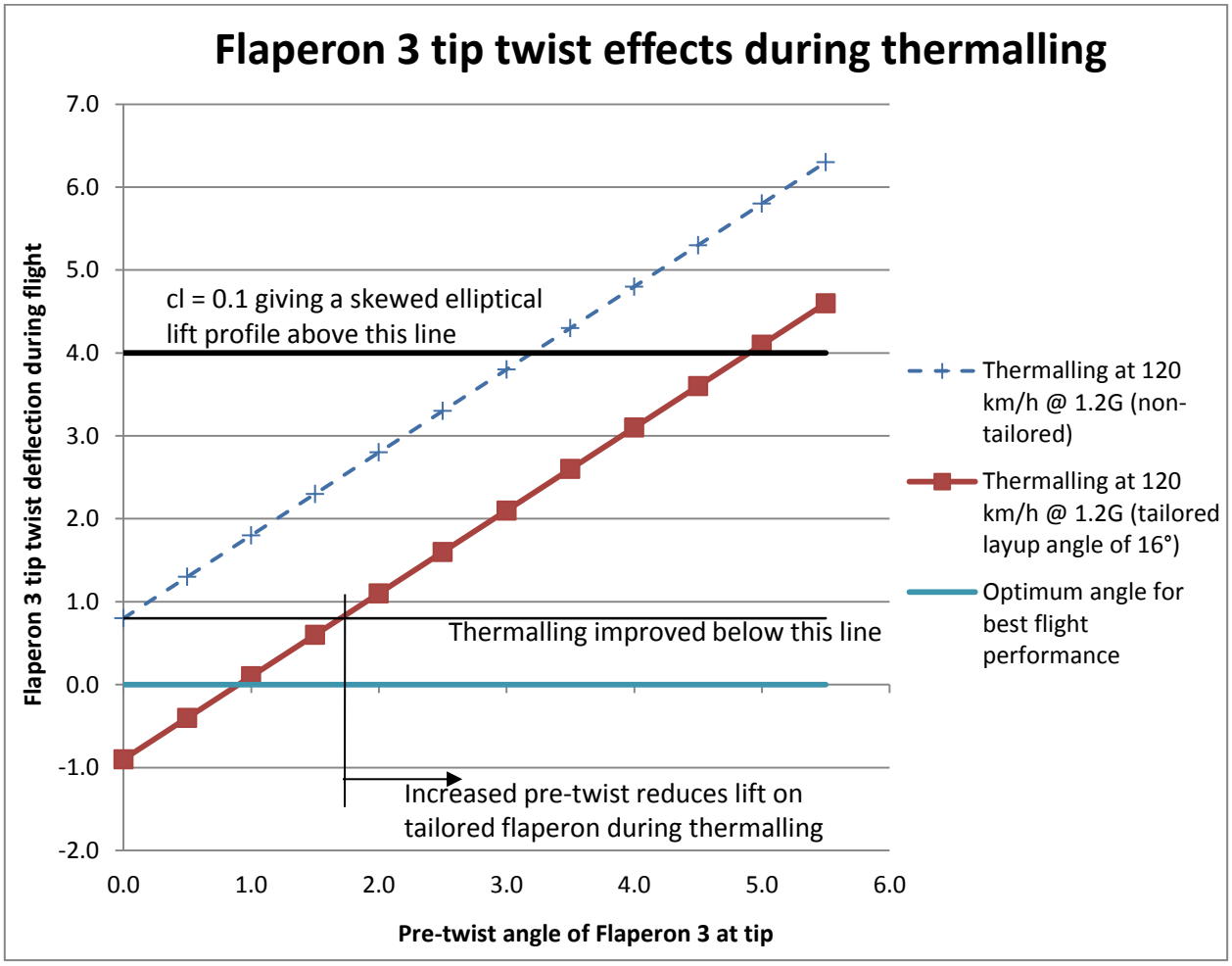

Figure 36: Flaperon 3 tip twist effects during thermalling

For this reason, the manufactured pre-twist of the non-tailored Flaperon 3 would have to be reduced to no more than 3.2° according to Figure 36, for the washout twist limit during thermalling to remain below 4°. This would produce a downward deflected Flaperon 3 tip twist of 1.5° as seen in Figure 38.

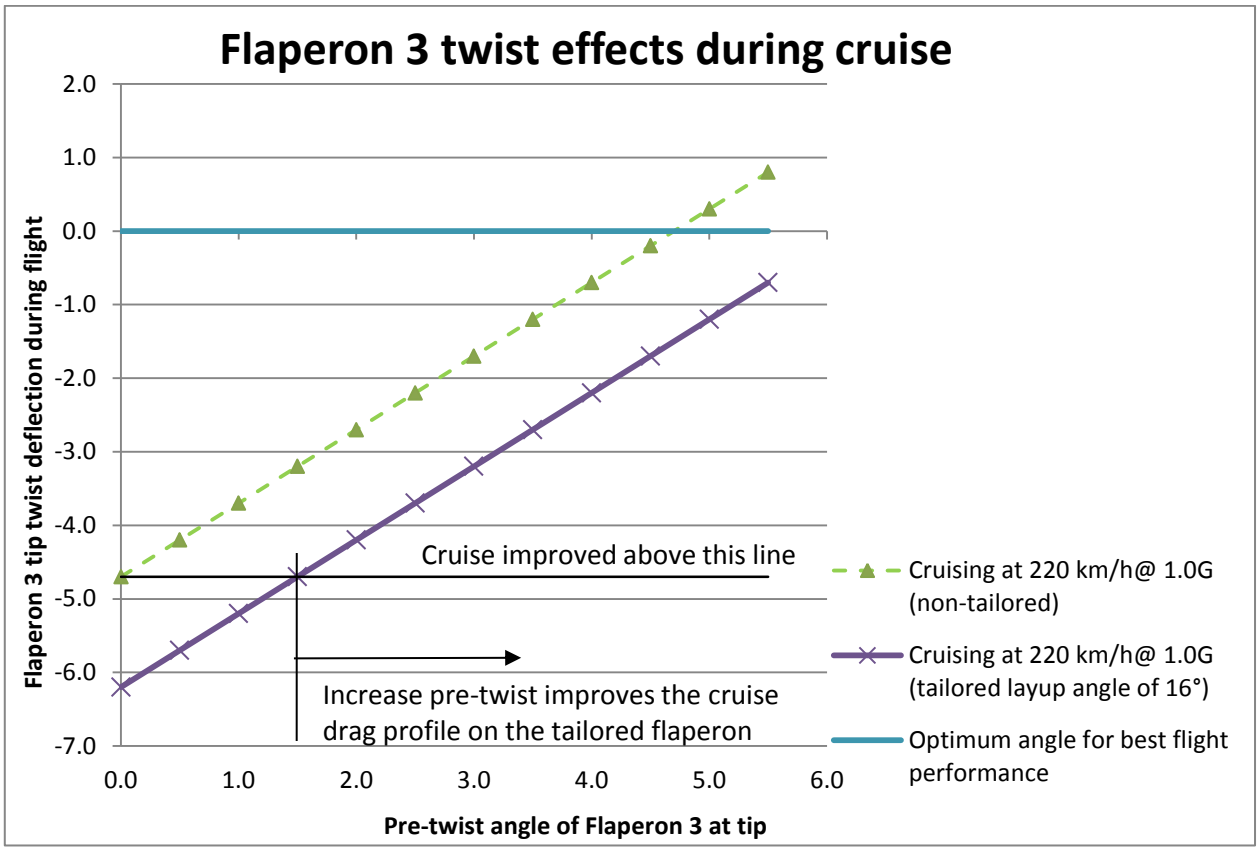

Figure 37: Flaperon 3 tip twist effects during cruise

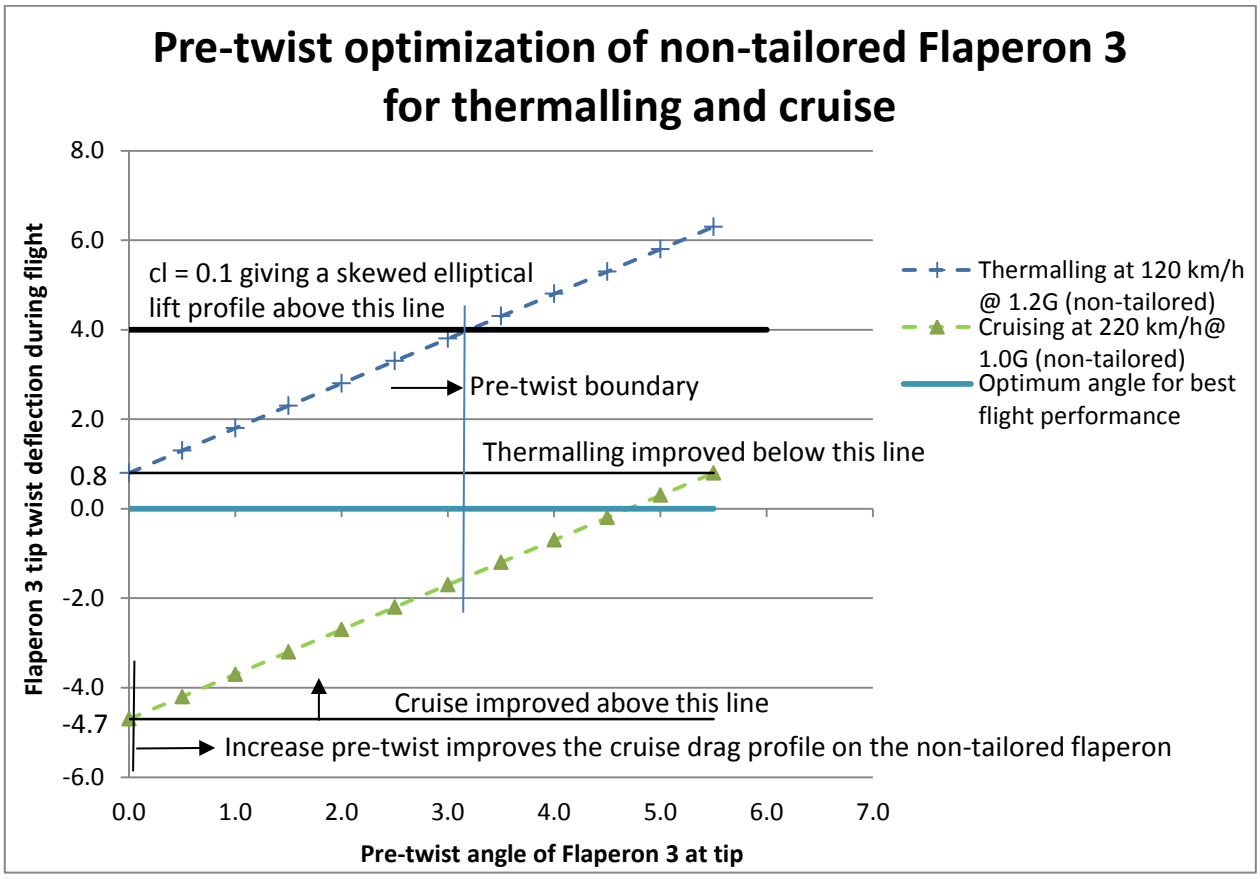

Figure 38: Pre-twist optimization of non-tailored Flaperon 3 for thermalling and cruise

By combining pre-twist with an aeroelastically tailored bend-twist couple resulting from the laminate layup angle of 16° on Flaperon 3, Figure 36 indicates that the thermalling washout limit can be maintained below 4° by changing the pre-twist to 4.9°, giving Flaperon 3 a downward tip twist angle of 1.3° during cruise (Figure 39). The combination of the pre-twist and bend-twist couple changes the original Flaperon 3 downward deflected tip twist from 4.7° to 1.3°, giving a total of 3.4° twist improvement. Pre-twist contributes an improvement of 3.2°, with the aeroelastic tailoring contributing only 0.2°.

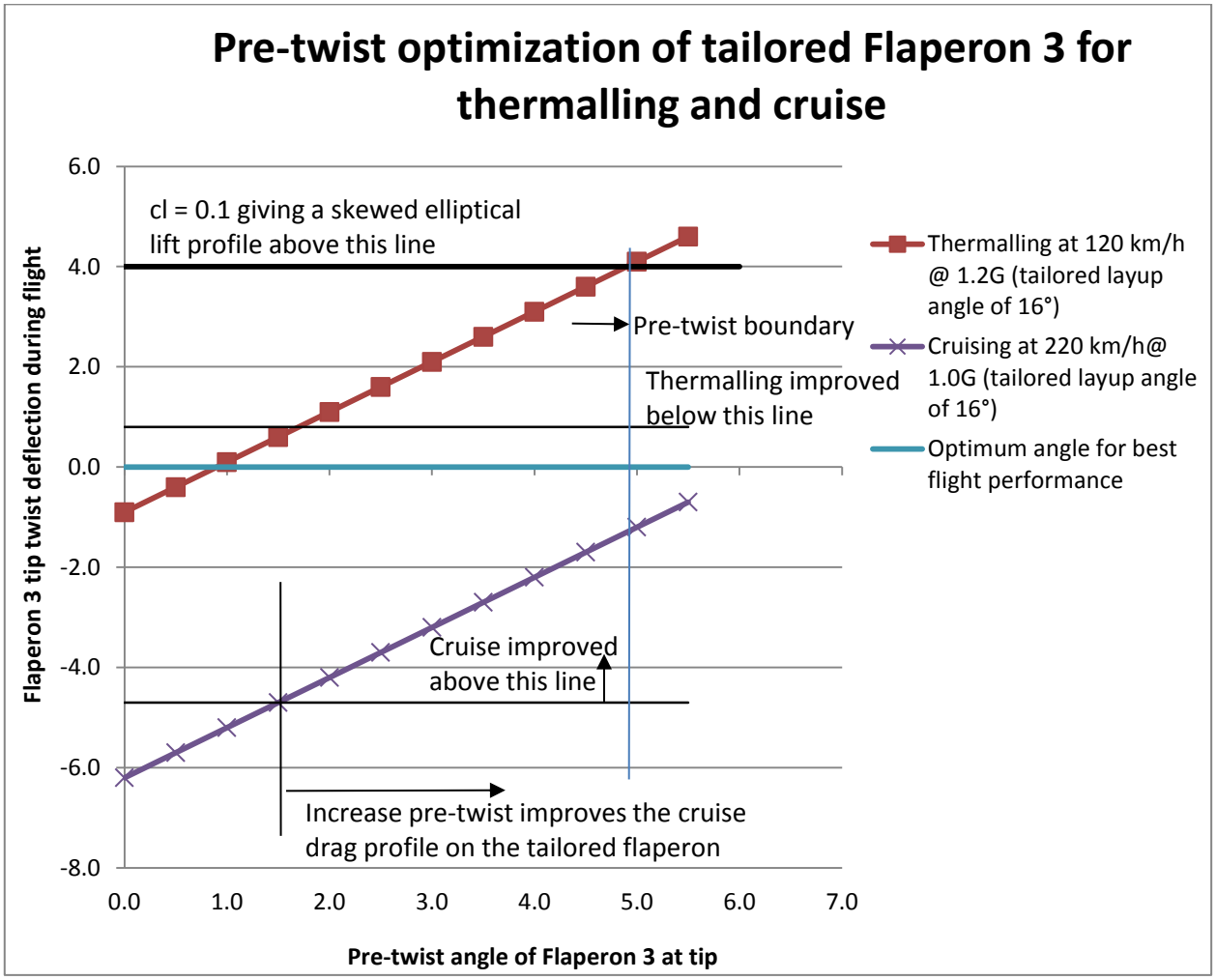

Figure 39: Pre-twist optimization of tailored Flaperon 3 for thermalling and cruise

Table 4 and Figure 40 summarize the combined effects of tailoring and pre-twist on both cruise and thermalling. The first column of angles in Table 4 describes Flaperon 3 manufactured with 0° pre-twist. This column is shown in a set of figures as follows:

- The glider on the ground at zero km/h with the thermalling flaperon setting in Figure 28 and with the cruise flaperon setting in Figure 30.
- The glider thermalling at 120 km/h under a flight load of 1.2 G's with a non-tailored Flaperon 3 in Figure 29.
- The glider thermalling at 120 km/h under a flight load of 1.2 G's with Flaperon 3 tailored at a 16° layup angle in Figure 33.
- The glider cruising at 220 km/h under a flight load of 1.0 G's with a non-tailored Flaperon 3 in Figure 31.
- The glider cruising at 220 km/h under a flight load of 1.0 G's with Flaperon 3 tailored at a 16° layup angle in Figure 34.

Table 4: Flaperon 3 tip twist at various conditions

	Flaperon 3 tip twist with 0° being the design point							
Pre-twist on ground at zero km/h (manufactured twist)	0°	1°	1.5°	2°	2.5°	3°	3.5°	4°
Thermalling at 120 km/h @ 1.2 G (non-tailored)	0.8°	1.8°	2.3°	2.8°	3.3°	3.8°	4.3°	4.8°
Thermalling at 120 km/h @ 1.2 G (tailored layup angle of 16°)	-0.9	0.1°	0.6°	1.1°	1.6°	2.1°	2.6°	3.1°
Cruising at 220 km/h @ 1.0 G (non-tailored)	-4.7°	-3.7°	-3.2°	-2.7°	-2.2°	-1.7°	-1.2°	-0.7°
Cruising at 220 km/h @ 1.0 G (tailored layup angle of 16°)	-6.2°	-5.2°	-4.7°	-4.2°	-3.7°	-3.2°	-2.7°	-2.2°

From Table 4 it can be seen that a flaperon with pre-twist of 4° would be optimal for cruise, but a pretwist of 1° would be optimal for thermalling for the Flaperon 3 with a 16° tailored layup angle.

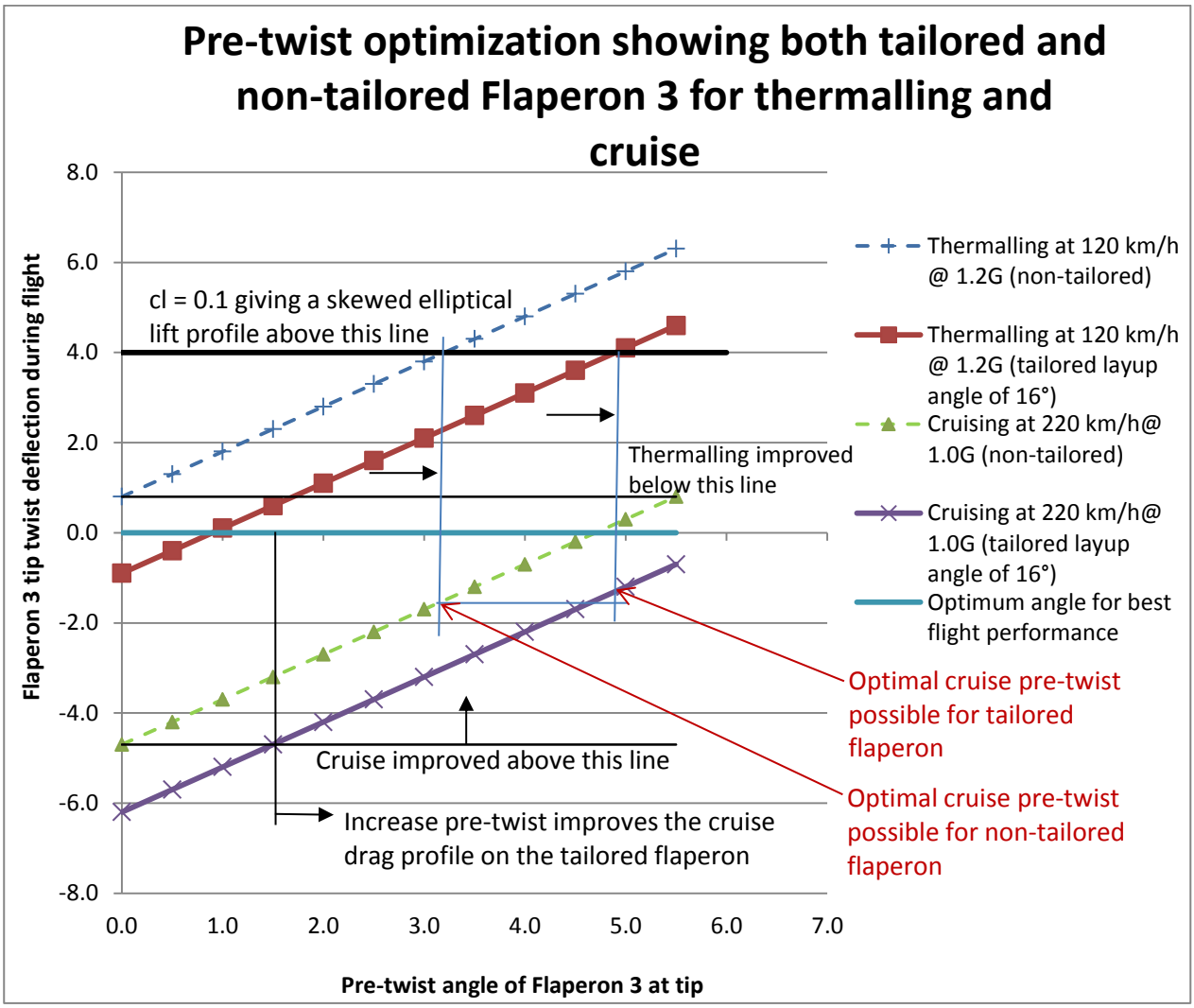

Figure 40: Tailoring optimization for Flaperon 3 during thermalling and cruise

As an aside, rotating the laminate layup angle by 61° might have proven to be the best possible option if no pre-twist were to be added. But this would allow for very little further correction by adding pre-twist, of which only 0.5° could still be added before skewing the elliptical lift distribution.

5.3 EXPERIMENT

For the validation of the aeroelastic tailoring, it was decided to design a simple structure which makes use of the aeroelastic tailoring, and to test and compare the results with the calculated results.

As the required problem of this project is to design a tailored flaperon for the JS1, it was decided to use a very similar structure for the test geometry. The specific aerodynamic shape and functionality

of the JS1 flaperon is not important for the test sample, but the geometry must be similar in shape and easy to manufacture.

5.3.1 Test sample specification

The test sample had the following characteristics:

- The test sample used the root and tip cross-sections of Flaperon 3, with coordinates taken directly from the Tailor.m cross-section properties.
- The length of the test sample was reduced to 1 m, as 2.2 m length of the moulds for the JS1C Flaperon 3 has increased complexities. The reduced length will also show if VABS/GEBT is affected by the differences in the slenderness ratios between the test sample and Flaperon 3.
- The effect of the flaperon hinge slots were assumed to be negligible, and thus not modelled in the Tailor.m flaperon model. Consequently the test sample was modelled without hinges, and portrayed the Tailor.m model coordinates.
- The test sample was manufactured with a 2° pre-twist washout, as a pre-twist would be implemented on Flaperon 3 as well.

The test sample was analysed with Tailor.m and the improved layer layup angles, as tailored per bend-twist angle, are shown below in Figure 41. It has been observed that Tailor.m shows a different tailored twist couple improved layer angle for different bending deflections.

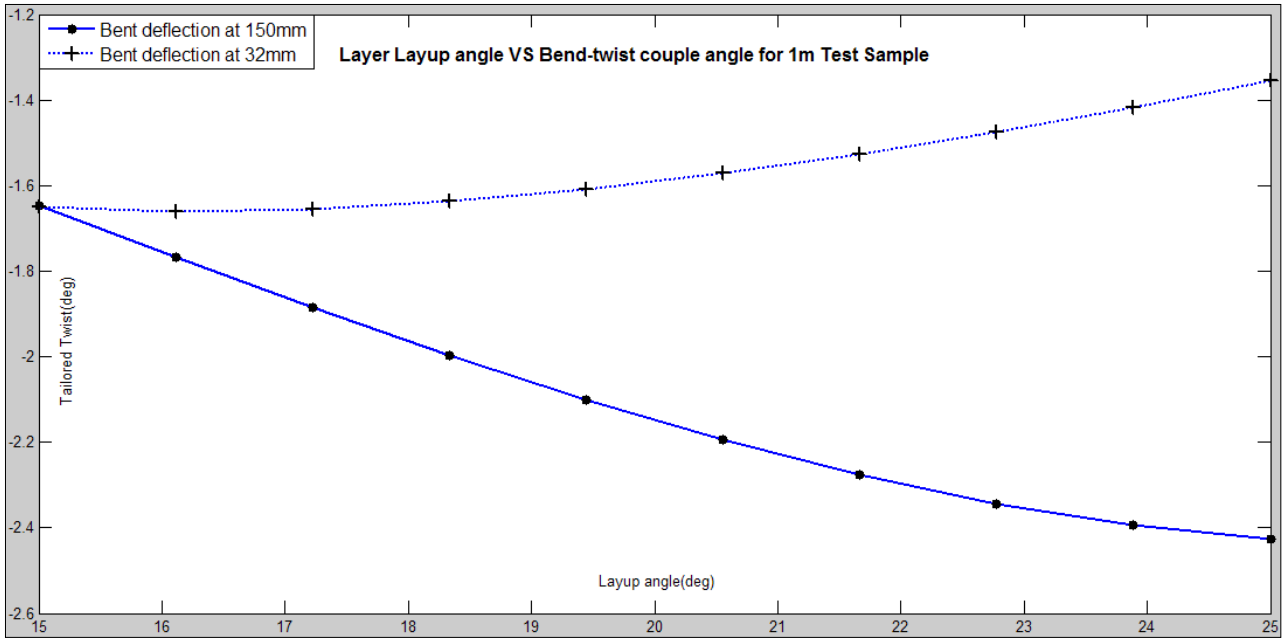

Figure 41: Bend-twist couple angle VS layer layup angle for 1 m Test Sample with a bent deflection of 32 and 150 mm

The result of the tailoring was used to produce a layup drawing for the manufacture of the tailored test sample as depicted in Figure 42.

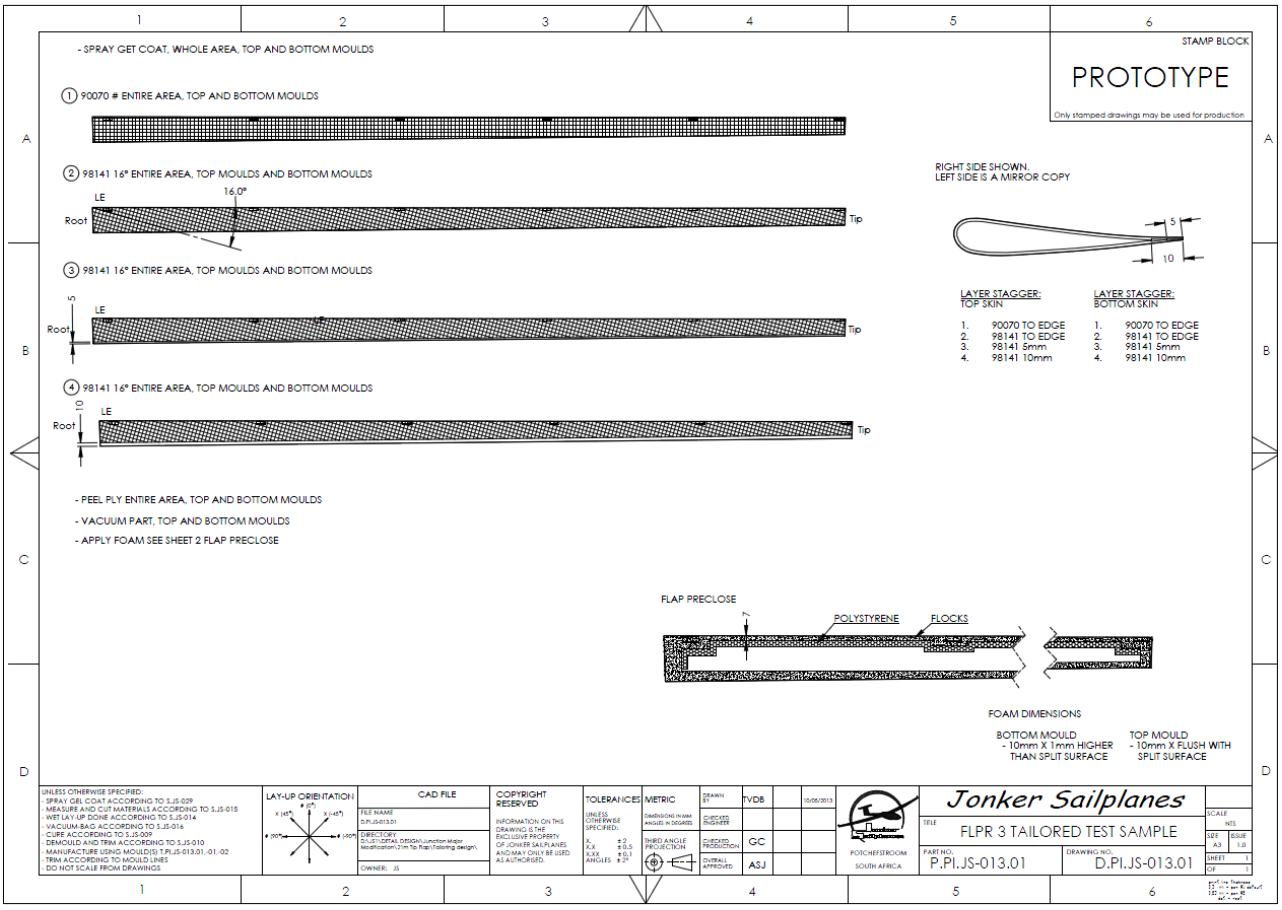

Figure 42: Layup drawing for Flaperon 3 test sample at a tailored layup of 16°.

5.3.2 Sample manufacture

5.3.2.1 MOULD DESIGN

In theory, the Tailor.m flaperon model of the flaperon test sample has an infinitely smooth surface. To achieve this, all vertical surfaces need at least a 2° positive draft angle. The smallest radius must be at least 0.5 mm larger than the ball nose radius of the smallest tool used to cut that area.

Provision was also made for resin squeeze-out, by including cavities at the leading and trailing edges. Gaps with a size of 1 mm were left at the leading and trailing edges for the composite layers to be in contact with one another during the two mould halves bonding process.

To locate the trim lines, a new method of using a change of surface angle at the trim lines would neatly mark the part with lines for trimming.

As this mould will only be used a few times, locator studs were machined into the mould. The final 3D model is shown in Figure 43.

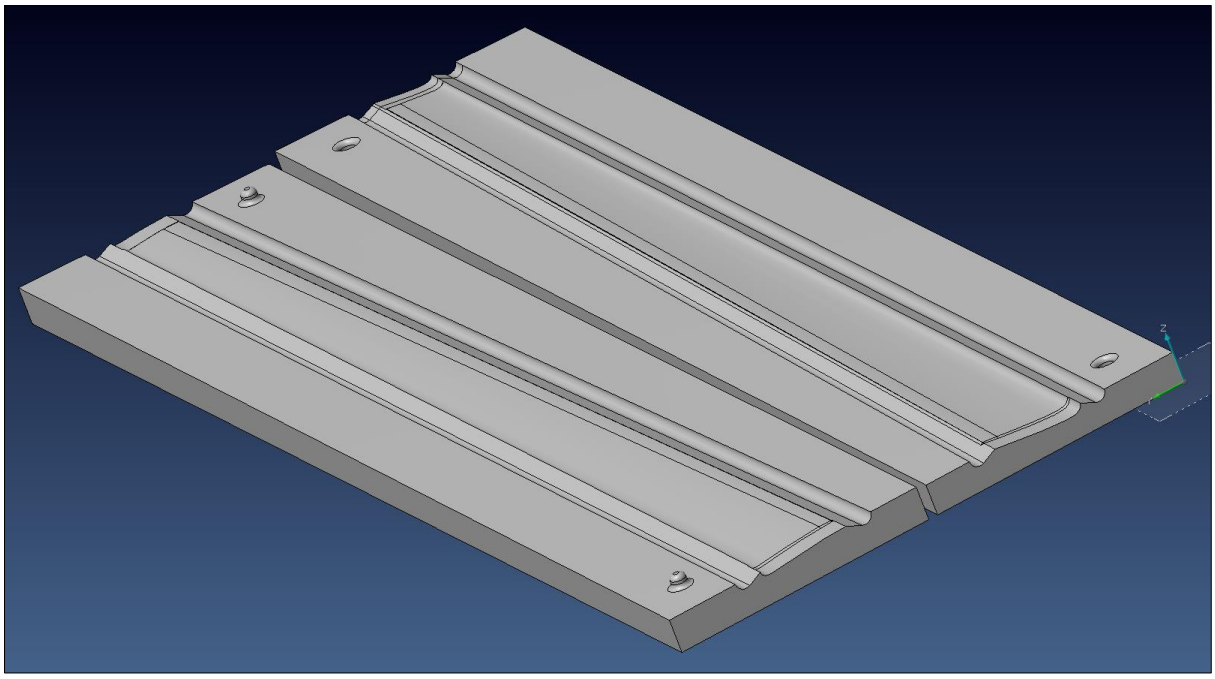

Figure 43: 3D model for Test Sample

5.3.2.2 CNC MOULD CUTTING

The CNC machine was programmed to get a Class A finish on the mould surface. A Class A finish ensures that the demoulded part has a high quality finish, with no further finishing work required before delivery. Once the roughing operations were done, the surface areas were split into boundaries. The surfaces of the mould that did not mould the part, such as the split surfaces etc. were cut with a constant step-over process.

The complete CNC cut mould is depicted in Figure 44.

Figure 44: Test sample mould CNC cut from Necuron 651

5.3.2.3 MOULD PREPARATION

Once the mould was cut on the CNC, it was finished first with P600 grit, then P800 grit sandpaper to remove the machining marks. To produce a hardened mould surface, a thin coat of Hexion® F 260/F 16 polyurethane casting resin was evenly applied over the surfaces.

The mould was then polished to ensure a proper surface finish that would allow easy demoulding of the part from the mould. A release agent was also applied to the mould surface 5 times at intervals of 30 minutes.

In order to reproduce the manufacturing techniques used at JS, the test sample was built to JS composite manufacturing standards. The test sample was built according to the "FLPR 3 TAILORED TEST SAMPLE" composite layup drawing.

5.3.2.4 PREPARING THE COMPOSITE LAYERS

All composite layers were cut and prepared before the layup in the mould. This was to ensure quick and easy wet layup before the resin had time to cure. First, the bi-directional (BID) 98141 composite fabrics were laid out on the table, making sure the strands were straight and crossing at 90° to each other. Masking tape was used to mark off layers correctly at a 16° orientation. The fabric was then cut through the masking tape. The masking tape gave the advantage of holding the strands in place for the composite layup.

5.3.2.5 WET LAYUP

The resin was prepared as per JS manufacturing standard. The first layer was BID glass 92007 placed at a 0° - 90° orientation. This first layer is a fine weave glass to give a smoother surface finish than the coarser BID carbon.

The top and bottom halves of the mould had lines scribed into the split surfaces on either side of the part. This gave a reference to align the layers' strand orientations as shown in Figure 45.

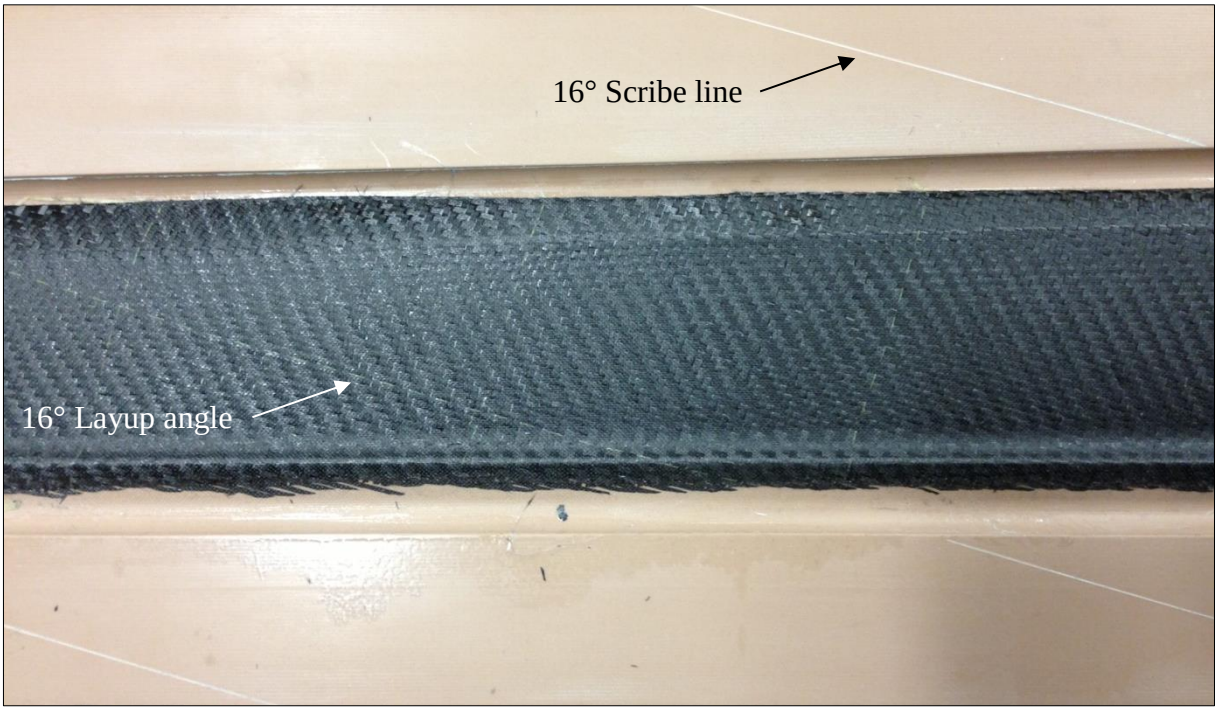

Figure 45: 16° layup angle according to mould scribe lines

All layers were wetted and pressed into the mould with a brush. Peel Ply was laid over the final layer of glass to absorb excess resin.

5.3.2.6 VACUUM BAGGING

The layers in the mould were vacuum bagged to ensure that the layers took the shape of the mould without any air pockets or excess resin during curing.

5.3.2.7 CURING

The vacuum-bagged halves of the sample, left in their moulds, were allowed to cure for 48 hours. The temperature in winter is not favourable for curing, often below 25° Celsius. To reduce the curing time, ambient temperature must be maintained at no less than 30° Celsius. JS employs a large curing oven for this purpose.

5.3.2.8 PREPARING FOR MOULD CLOSING

The vacuum bagging was removed and the bonding surfaces of the two part halves were sanded with P200 grit paper. Often the layers at the bonding areas are too thick and prevent the mould from closing. These areas were sanded down until the mould closed completely. The two part halves are shown in Figure 46.

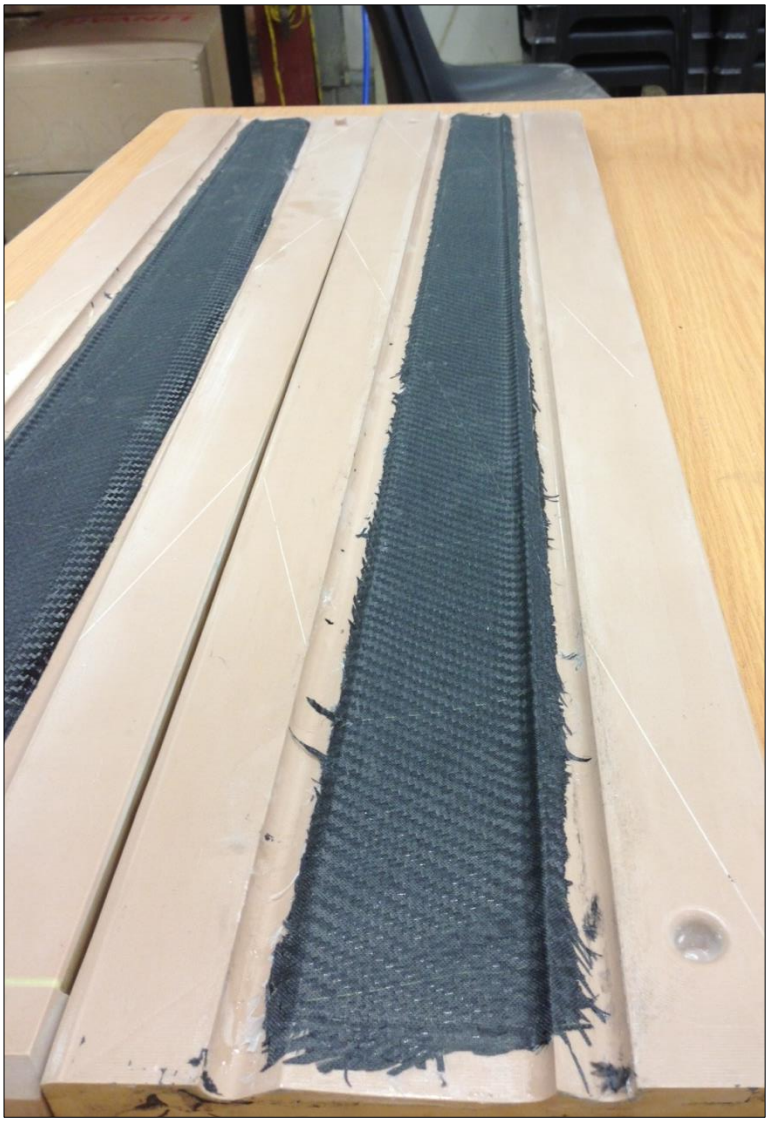

Figure 46: Two mould halves ready to be prepared for mould closing

5.3.2.9 MOULD CLOSING

Adding cotton fibres to a resin mixture increases its viscosity, allowing the mix to be applied like a paste on the two mould halves; this mix is called “cotton flox”. This cotton flox is applied on the leading and trailing edge for bonding the part together. In order to give structural strength for clamping the root end and lifting the tip end, cotton flox was applied over a 40 mm strip at the ends. The mould was closed and clamped down on a flat table.

5.3.2.10 CURING

The mould was again allowed to cure for 48 hours to ensure the part had set.

5.3.2.11 DEMOULDING

The part was demoulded easily due to good mould design and properly applied release agent. The excess layers and flox was trimmed off according to the trim lines imprinted in the part.

5.3.2.12 POST-CURING AND WARPING CHECK

The tailored layup schedule was balanced (i.e. symmetrical) to ensure that the composite part did not warp during curing. (Cheung, 2002). The Flaperon 3 test sample was placed on a flat table to check that it lay flat and the twist gap at the tip was measured as 1.5 mm. The sample was then placed in the curing oven at a temperature of 45° Celsius for 48 hours, after which the oven temperature was increased to 60° Celsius for another 48 hours.

The test sample was again placed on a flat table after post-curing to check for warping. It was observed that the twist gap still measured 1.5 mm and no warping took place. This confirmed that the balanced laminate layup discussed by Cheung is a good design methodology.

5.3.3 Experimental test

The experimental setup of the Flaperon 3 test sample was set up on a flat table. The sample was clamped to the table at its root, in a cantilever configuration. An inclinometer was fixed to the tip of the test sample. The inclinometer was a Digital Protractor Pro 3600 with a calibration Certificate T9536 (Instrument SN 11220). The tip of the test sample's LE and TE was first deflected up 32 mm and later 150 mm according to digital vernier calipers. At each deflection the reading on the inclinometer was noted. The experimental setup is shown in Figure 47.

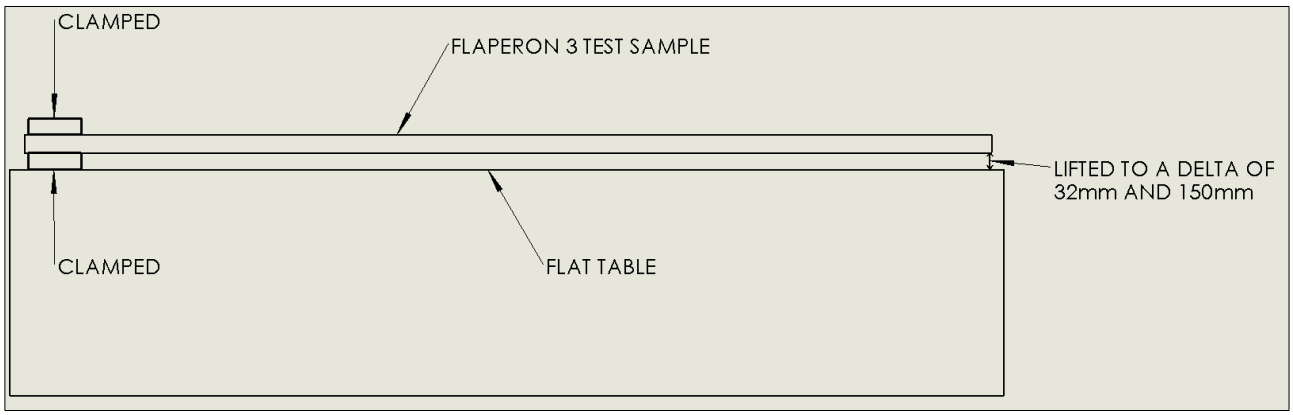

Figure 47: Experimental setup of Flaperon 3 test sample

The inclinometer was fixed to the tip of the test sample and the angle set to zero at zero deflection as shown in Figure 48.

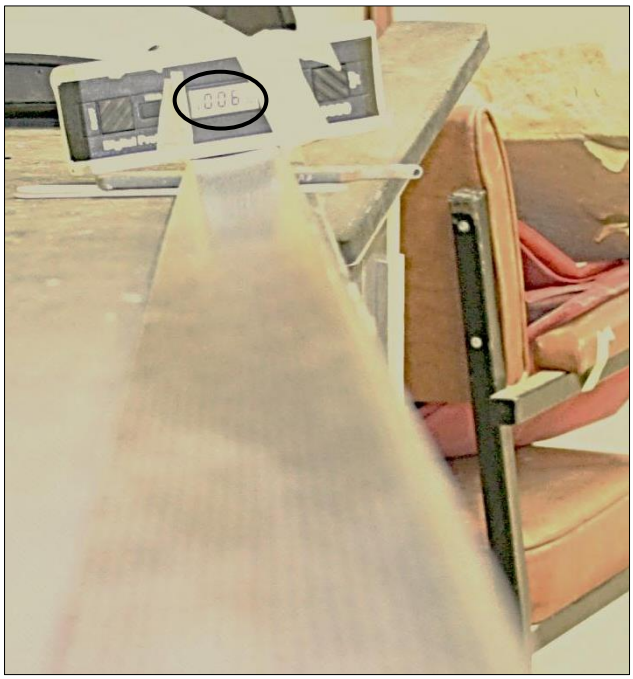

Figure 48: Inclinometer meter zeroed at zero deflection

The vernier caliper was set to 32 mm and then used to displace the test sample at the TE and LE respectively as shown in Figure 49. Note the difference in twist angle between the applications of load on the TE versus the LE.

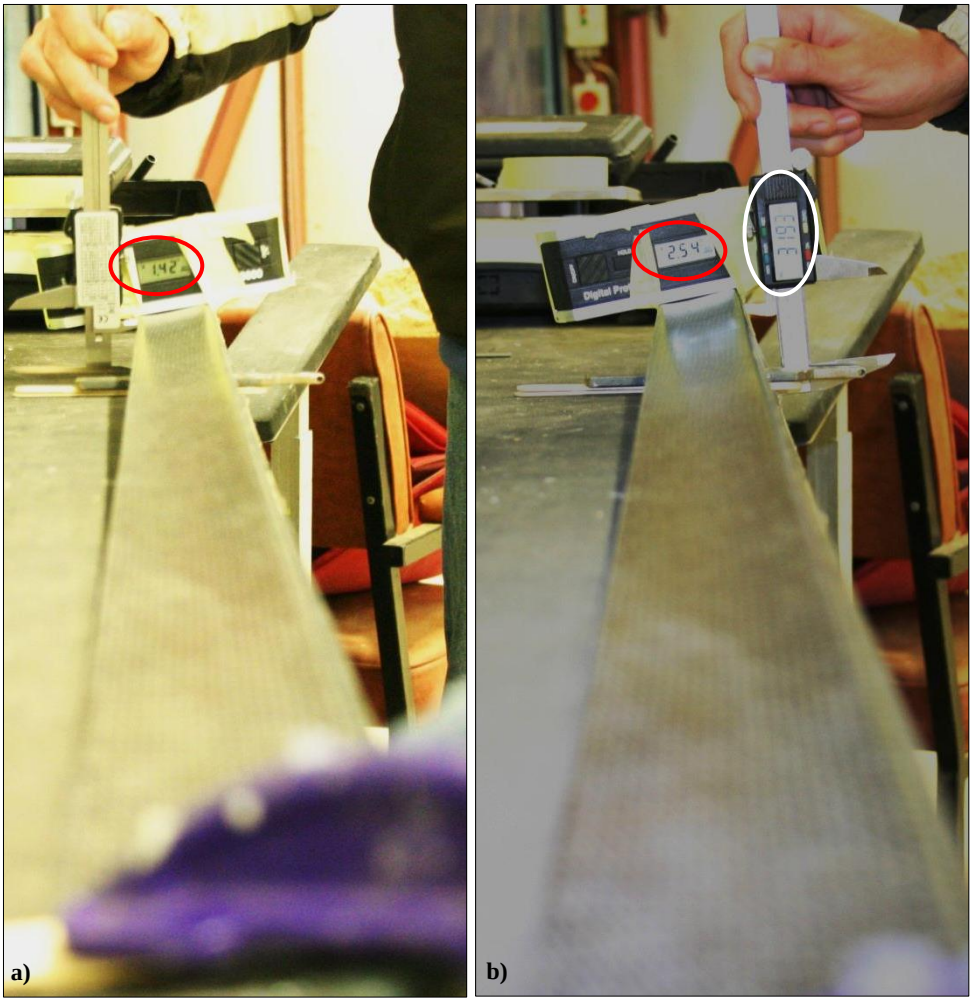

Figure 49: The 32 mm displacements on the test sample's TE(a) and LE(b)

The 150 mm deflections of the test sample as shown in Figure 50 give interesting results compared to the Tailor.m results - the bend-twist couple of the sample proved to be ±9° which much larger than the bend-twist couple predicted by Tailor.m at 1.8° as shown in Table 5.

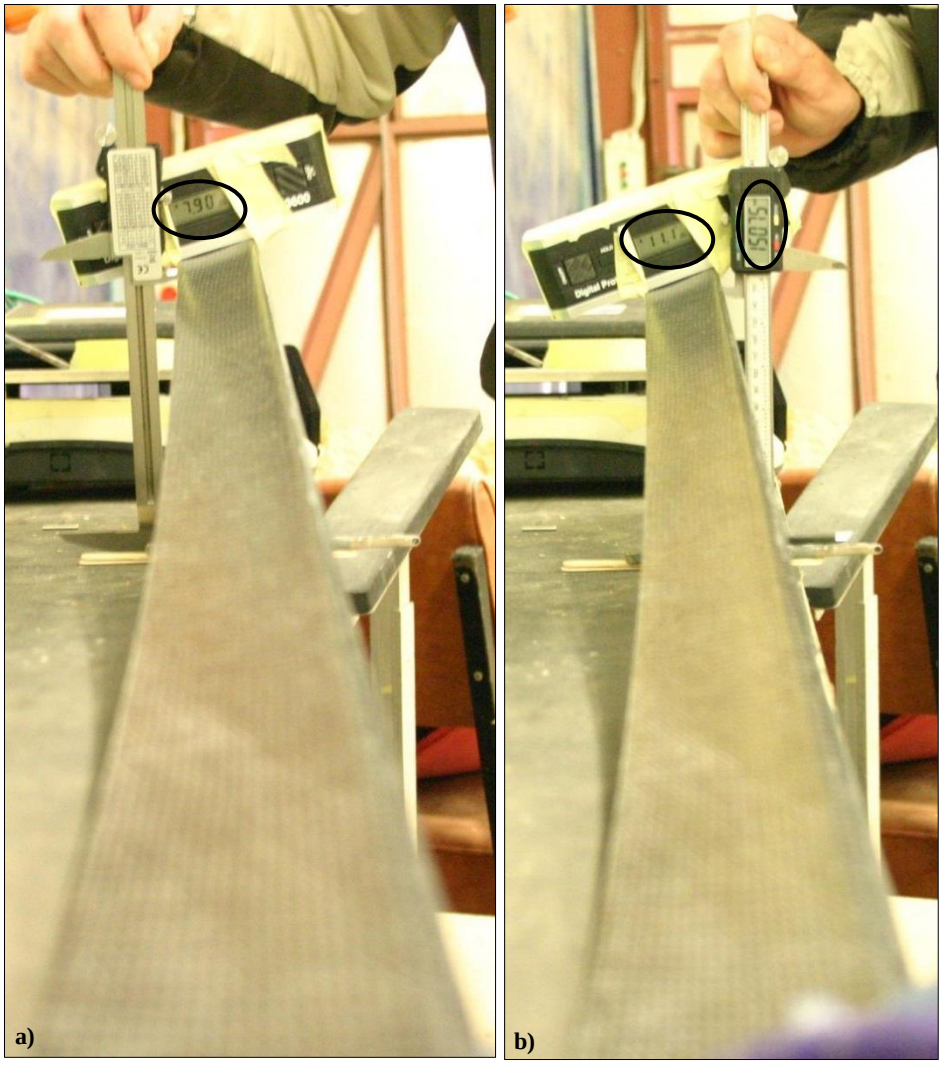

Figure 50: The 150 mm displacements on the test sample's TE(a) and LE(b)

The GEBT part of Tailor.m applies the displacement at the torsional centroid of the 1D beam. This is to prevent the presence of induced torsional loads. The torsional centroid at the tip of the test sample was calculated by the VABS part of Tailor.m as 19 mm from the LE. The displacement of 32 mm was applied at this centroid as shown in Figure 51. The 1.68° twist of the experimental test was similar to the predicted value of 1.7° as shown in Table 5.

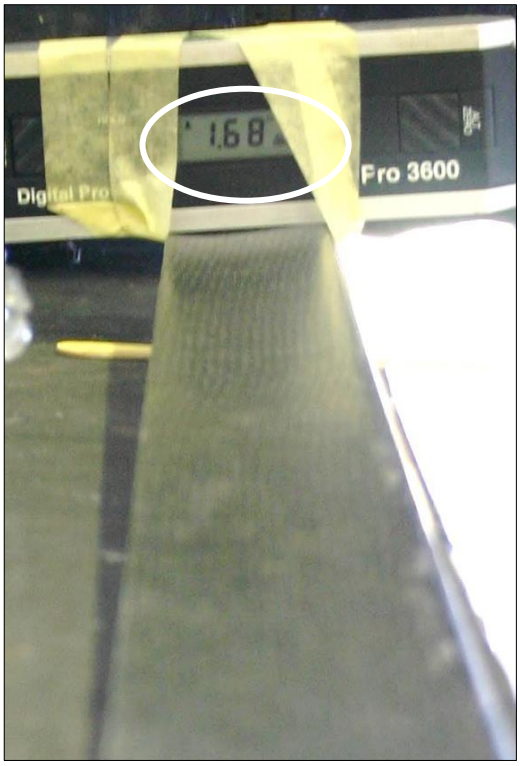

Figure 51: Displacement of 32 mm applied at the torsional centroid at 19 mm from the tip LE

5.4 EXPERIMENTAL RESULTS

The Flaperon 3 test sample has shown that it can be manufactured according to JS manufacturing standards without additional complications.

A practical experiment was set up using a tailored sample of Flaperon 3, and the tip was deflected by 32 mm. However, the test was done by applying the displacement first on the LE and then on the TE. This induced a torsional load which either acted against or together with the tailored bend-twist couple. Consequently, the test sample was seen to incur a 2.5° twist when the displacement was applied to the LE, and only a 1.4° twist when the displacement was applied to the TE. Having obtained the torsional centroid of the sample from the VABS part of Tailor.m, the experiment was repeated, but with the displacement applied at the neutral axis of the test sample.

The aeroelastically tailored sample of Flaperon 3 was given a 32 mm tip deflection in the simulation using Tailor.m. Since the VABS/GEBT part of Tailor.m uses a flexibility matrix from the 2D cross-section and calculates the displacements and couples on a 1D beam, the displacement was applied on the flexural axis.

In Table 5 the first column describes the position where vertical displacement of the flaperon test sample tip was applied at the tip. The second column gives the flaperon test samples change in twist angles when the vertical tip displacement goes from zero to the specified displacement. The third column gives the calculated torsional deflection as modelled with Tailor.m. The fourth column gives the percentage error between the calculated and experimental twist angles. The experimentally measured angles were rounded off to one decimal place to allow for the inclinometer measurement error.

Table 5: Comparison of experimental and Tailor.m bend-twist couple results

Position where vertical displacement was applied	Measured torsional deflection	Calculated torsional deflection with Tailor.m	Error (%)
$v_{at\ 32\ mm\ LE}$	2.5°	1.7°	32%
$v_{at\ 32\ mm\ TE}$	1.4°		-21%
$v_{at\ 32\ mm\ centroid}$	1.7°	1.7°	0%
$v_{at\ 150\ mm\ LE}$	11.1°	1.8°	84%
$v_{at\ 150\ mm\ TE}$	7.9°		77%

There is clear correlation between the Tailor.m results and the experimental results for the small deflection case. It must also be noted that the slenderness ratio for VABS with the Timoshenko theory may only produce a 32% accuracy for an aspect ratio of 5, which could improve to 8% accuracy for an aspect ratio of 10 (Yu et al., 2002(b). The length:root chord aspect ratio of the test sample is 13. The experimental results showed a very good comparison with the aeroelastic tailoring predictions.

VABS/GEBT assumes small strains which gives more accurate beam deflection results if the deflection is less than 10% of the beam length (Friedmann et al., 2009). A displacement of 32 mm is 3.2% of the test sample length, which lies within the small strain assumption of VABS/GEBT. The displacement of 150 mm violates the small strain assumption, with a displacement equal to 15% of the test sample length. The 150 mm displacement is too large for the VABS/GEBT small strain assumptions, thus giving an error in these results.

5.5 CONCLUSION AND DISCUSSION

The objective of this project was to improve the performance of JS1 by removing unwanted twist from Flaperon 3 using a tailored bend-twist couple. However, tailoring a bend-twist couple into Flaperon 3 failed to fully counter the twist brought about by the aerodynamic forces. For this reason it was decide to add pre-twist as well.

The formulation used to calculate the bend-twist couple has proven sufficiently accurate and reliable, provided that the deflection of the structure remains less than 10% of its span.

Far greater benefits are reaped from tailoring the entire laminate than from just rotating selected layers. These include greater bend-twist couples and a reduced chance of unwanted deformation after demoulding the composite component.

JS1 was considered for only two flight conditions, namely thermalling and cruising. The tailoring and pre-twist was performed to yield the best performance gain, which is why cruise was favoured. The addition of pre-twist to compensate the inability of the bend-twist couple to fully rectify the twisting of Flaperon 3 during flight reduced the performance gain that could be had during thermalling.

However, the effects of tailoring should also be analysed for the entire flight regime to ensure the absence of or resistance to such phenomena as flutter and divergence.

6 CONCLUSION AND RECOMMENDATIONS

6.1 CONCLUSION

The quest to improve the performance of the JS1 by removing the Flaperon 3 twist problem could be solved through a method like aeroelastic tailoring. This gave a need to model and analyse the composite flaperon structure.

A composite analysis tool was sought to predict and tailor the aeroelastic behaviour of aerodynamic structures for optimum performance, including the bend-twist relationship of slender structures. Such a tool would need to give reliable and accurate results in a short time, thus eliminating full 3D finite element method packages. Literature identified the combination of PreVABS, VABS and GEBT to best meet the requirements. There is a substantial amount of published data for the research and validation into VABS and GEBT.

As the process of iteratively analysing a structure for tailoring sequentially with PreVABS, VABS and GEBT is too complicated and time consuming to perform manually, it was decided to develop a user interface Matlab program "Tailor.m" that controls the analysis process.

Tailor.m was further checked by analysing a simple beam made from isotropic material. Hand calculations and an existing FEM package were also used to solve the beam deflections, and the results of Tailoring compared favourably. A validation of a flaperon-type model using Tailor.m was done as a pre-step before using Tailor.m in the tailoring process of Flaperon 3.

A method was devised to test the aeroelastic tailoring and the Tailor.m results, which included doing a full aeroelastic tailoring and then comparing the designed experimental sample with the calculated results.

Composite laminates are anisotropic. Care must be taken during tailoring that the layup schedule, while meeting the mechanical requirements, does not result in components susceptible to warping. The Flaperon 3 test sample was manufactured according to JS standards and checked for warping. This validated the manufacturing technique and the aeroelastic tailoring process.

Experimental results compared favourably with the Tailor.m predictions, with a negligible difference. This confirmed that the aeroelastic tailoring process, used to perform aeroelastic tailoring on Flaperon 3 of the 21 m version of JS1 Revelation, gave accurate results. This program can analyse the composite layups quickly and give good results for long slender structures

undergoing small displacements. Unfortunately, even the greatest bend-twist couple could not fully address the twist problem by itself, necessitating the addition of pre-twist.

While it has been shown that a combination of pre-twist and aeroelastic tailoring introduces desirable bend-twist couples in JS1 Flaperon 3, the extent to which it can address the problem of twist under aerodynamic loads has yet to be studied in full before it can be implemented in the production of Flaperon 3.

However, the aeroelastic tailoring tool, developed in the course of this project, may well be incorporated in the design of future JS composite structures.

6.2 RECOMMENDATIONS

Tailored composite aerostructures, while meeting the original design requirements, it is recommended that they should still be tested and corrected for potentially destructive phenomena, such as flutter and divergence.

It may be useful to investigate conventional control by elastically bending the flight surfaces using torque tubes and servo motors controlled by a programmed control system, as an alternative to aeroelastic tailoring (van Zyl, 2012).

It is also recommended that other aeroelastic tailoring programs, such as the continuous cross-sectional modeller NABSA used by Delft (De Breuker, 2012), and optimization techniques be further investigated. VABS/GEBT should also be subjected to further tests, to ascertain its usefulness and limitations for a variety of design challenges.

It is also recommended that further studies be done to investigate the accuracy of the VABS/GEBT and other such programs when analysing for large displacements, as well as finding the transition areas where they become less accurate.

7 REFERENCES

Attaran, A., Majid, D. L. & Mohd Rafie, A. S., 2011. Structural Optimization of an Aeroelastically Tailored Composite Flat Plate Made of Woven Fiberglass/epoxy. *Aerospace Science and Technology,* 15(1), pp. 393-401.

Benham, P. P., Crawford, R. J. & Armstrong, C. G., 1996. *Mechanics of Engineering Materials.* 2nd ed. Essex: Pearson Education Limited.

Bennett, J., 2013. *Performance Boats.* [Online] Available at: http://www.performanceboats.com/jet-boats/132154-*new*-carbon-fiber-wing.html [Accessed 15 May 2013].

Berdichevsky, V. L., 1979. Variational-Asymptotic Method of Constructing a Theory of Shells. *Journal of Applied Mathematics and Mechanics (Parameterized Perturbation Method),* 43(4), pp. 664-687.

Boston, J. et al., 2011. Experiments with Geometric Nonlinear Coupling for Analytical Validation. *Journal of Aircraft,* 48(4), pp. 1136-1146.

Brett, S. & Rehfield, L. W., 2004. *Linear Modeling of Aeroelastic Twist of a High Aspect Ratio Wing with Significant Taper,* Davis: University of California.

Callister, J. W. D., 2007. *Material Science and Engineering : An Introduction.* 7th ed. New York: John Wiley & Sons, Inc..

Chandrupatla, T. R. & Belegundu, A. D., 2002. *Introduction to Finite Elements in Engineering.* 3rd ed. s.l.:Prentice Hall.

Chen, H. & Yu, W., 2008. *Manual of PreVABS,* Utah: Utah State University.

Chen, H., Yu, W. & Capellaro, M., 2010. *A Critical Assessment of Computer Tools for Calculating Composite Wind Turbine Blade Properties,* Utah and Stuttgart: Utah State University and Stuttgart Univeristy.

Cheung, R. H.-Y., 2002. *Some Stratergies For Creating Bend-twist Coupling in Box Beams,* Davis: University of California,.

Daniel, I. M. & Ishai, O., 1994. *Engineering Mechanics of Composite Materials.* 1st ed. New York: Oxford University Press.

De Breuker, R., 2012. *VABS versus a new continuous cross-sectional modeller* [Interview] (Delft University of Technology, Delft 10 April 2012).

Dillinger, J., 2007. *Aerodynamic and Structural Design of the Open Class Sailplane Concordia,* Hamburg: American Institute of Aeronautics and Astronautics.

Eskandary, K., Dardel, M., Pashaei, M. H. & Moosavi, A. K., 2012. Nonlinear Aeroelastic Analysis of High Aspect-ratio Wings in Low Subsonic Flow. *Acta Astronautica,* 70(1), pp. 6-22.

Federal Aviation Administration, 2007. *Glider Flying Handbook.* illustrated ed. New York: Skyhorse Publishing, Inc..

Friedmann, P. P., Glaz, B. & Palacios, R., 2009. A Moderate Deflection Composite Helicopter Rotor Blade Model with an Improved Cross-sectional Analysis. *International Journal of Solids and Structures,* Volume 46, pp. 2186-2200.

Fung, Y. C., 1993. *An Introduction to the Theory of Aeroelasticity.* Dover edition ed. New York: Dover Publications, Inc..

Green, N. S., 2009. *Structural Optimization of Joined-wing Beam Model with Bend-twist Coupling Using Equivalent Static Loads,* Ohio: Air Force Institute of Technology.

Han, D., Yu, W. & Roy, S., 2007. A Geometrically Exact Active Beam Theory for Multibody Dynamics Simulation. *Smart Materials and Structures,* 17(4), pp. 1136-1147.

Hibbeler, R. C., 2005. *Mechanics of Materials.* 6th ed. Singapore: Prentice Hall.

Hodges, D. H., 2006. *Nonlinear Composite Beam Theory.* 1st ed. Virginia: American institute of Aeronautics and Astronautics, Inc..

Hodges, D. H., Atilgan, A. R., Cesnik, C. E. S. & Fulton, M. V., 1992. On a Simplified Strain Energy Function for Geometrically Nonlinear Behaviour of Anisotropic Beams. *Composites Engineering,* 2(5-7), pp. 513-526.

Hodges, D. H. & Dowell, E. H., 1974. *Nonlinear Equations of Motion for the Elastic Bending and Torsion of Twisted Nonuniform Rotor Blades,* Washington, D.C.: NASA Technical Note TN D-7818.

Hodges, D. H. & Pierce, G. A., 2002. *Introduction to Structural Dynamics and Aeroelasticity.* 1st ed. New York: Cambridge University.

Hodges, D. H. & Yu, W., 2007. A Rigorous, Engineering-Friendly Approach for Modeling Realistic, Composite Rotor Blades. *Wind Energy, 10(2):179{193, 2007},* 10(2), pp. 179-193.

Jonker, A. S., 2011. *Wing structural _JS1_21_V1.xlsx sheet Flap Twist.* Potchefstroom: Jonker Sailplanes.

Jonker, A. S., 2013. *Effects of washout on the elliptical lift distribution of a wing* [Interview] (20 November 2013).

Lemanski, S. & Weaver, P., 2005. Flap–torsion Coupling in Sandwich Beams and Filled Box Sections. *Thin-Walled Structures,* 43(1), pp. 923-955.

McCormick, B. W., 1995. *Aerodynamics, Aeronautics, and Flight Mechanics.* 2nd ed. s.l.:John Wiley & Sons, Inc..

NOMAD, P., 2012. *NOMAD aviation images JS1 JET.* [Art] (NOMAD Photography 2012).

Rehfield, L. W., 1985. *Design Analysis Methodology for Composite Rotor Blades.* Denver, Colorado, Proceedings of the Seventh DoD/NASA Conference on Fibrous Composites in Structural Design AFWAL-TR-85-3094, pp- (V(a)- 1)-(V(a)- 15).

Rehfield, L. W., 2004. *Modeling and Design Analysis Methodology for Tailoring of Aircraft Structures with Composites,* Davis: University of California.

Roy, S., Yu, W. & Han, D., 2007. An Asymtotically Correct Classical Model for Smart Beams. *International Journal of Solids and Structures,* 44(25-26), pp. 8424-1147.

Shirk, M. H., Hertz, T. J. & Weisshaar, T. A., 1986. Aeroelastic Tailoring - Theory, Practice, and Promise. *Journal of Aircraft,* 23(1), pp. 6-17.

Smith, W. F., 1990. *Principles of Materials Science and Engineering.* 2nd ed. Singapore: McGraw-Hill Publishing Company.

Starlino Electronics, 2011. *DCM Tutorial - An Introduction to Orientation Kinematics.* [Online] Available at: http://www.starlino.com/dcm_tutorial.html [Accessed 20 August 2012].

Strong, A. B., 1999. *History of Composite Materials*, Brigham: Brigham Young Univeristy.

Torenbeek, E., 2013. *Advanced Aircraft Design: Conceptual Design, Analysis and Optimization of Subsonic Civil Airplanes.* 1st Edition ed. s.l.:John Wiley & Sons, Ltd..

van Zyl, L., 2012. *Aeroelastic Tailoring versus Conventional Control* [Interview] (Council for Scientific and Industrial Research, DPSS Division, Pretoria 3 March 2012).

Wan, Z.-q., Yan, H., Liu, D.-g. & Yang, C., 2005. Aeroelastic Analysis and Optimization of High-aspect-ratio Composite Forward-swept Wings. *Chinese Journal of Aeronautics,* 18(4), pp. 317-325.

Willaert, M. M., Abdalla, M. M. & Gürdal, Z., 2010. *A Simple Finite Element Cross-sectional Modelling of Thin-walled Beams*, Delft: Aerospace Structures, Delft University of Technology.

Yong hui, Z. & Hai-yan, H., 2005. Structural Modeling and Aeroelastic Analysis of High Aspect-ratio Composite Wings. *Chinese Journal of Aeronautics,* 18(1), pp. 25-30.

Yu, W., 2011a. *VABS Manual for Users*, Utah: Utah State University of Technology.

Yu, W., 2011b. *Manual of GEBT*, Utah: Utah State University.

Yu, W., 2012. *VABS Presentation at Sandia National Laboratory's Wind Turbine Workshop.* [Online]
Available at: http://energy.sandia.gov/wp/wp-content/gallery/uploads/2B-D-2-Yu.pdf [Accessed 21 August 2012].

Yu, W. & Blair, M., 2012. GEBT: A General-Purpose Tool for Nonlinear Analysis of Composite Beams. *Composite Structures*, 94(1), p. 2677–2689.

Yu, W. & Hodges, D. H., 2004. Elasticity Solutions Versus Asymptotic Sectional Analysis of Homogeneous, Isotropic Prismatic Beams. *Journal of Applied Mechanics,* 71(1), pp. 15-23.

Yu, W. & Hodges, D. H., 2005. Generalized Timoshenko Theory of the Variational Asymptotic Beam Sectional Analysis. *Journal of the American Helicopter Society,* 50(1), pp. 46-55.

Yu, W., Hodges, D. H. & Ho, J. C., 2012. Variational Asymptotic Beam Sectional Analysis - An Updated Version. *International Journal of Engineering Science,* Volume 59, pp. 40-49.

Yu, W., Hodges, D. H., Volovoi, V. & Cesnik, C. E., 2002(a). On Timoshenko-like Modeling of Initially Curved and Twisted Composite Beams. *International Journal of Solids and Structures,* 39(1), pp. 5101-5121.

Yu, W., Hodges, D. H., Volovoi, V. V. & Eduardo, D. F., 2005. A Generalized Vlasov Theory of Composite Beams. *Thin-Walled Structures,* 43(9), pp. 1493-1511.

Yu, W., Volovoi, V. V., Hodges, D. H. & Hong, X., 2002(b). Validation of the Variational Asymptotic Beam Sectional Analysis. *American Institute of Aeronautics and Astronautics Journal,* 40(10), pp. 2105-2113.

APPENDIX A - CROSS-CHECK THE OPERATION OF PREVABS, VABS AND GEBT WITH HAND CALCULATIONS AND FEM

The combined operation of PreVABS, VABS and GEBT was cross-checked by setting up a problem which could be solved by hand calculations. These results were also compared with SolidWorks FEM. The results of the hand calculations would be compared with the PreVABS/VABS/GEBT results to determine whether these analysis tools where correctly used.

The beam problem was set up with the following specifications:

- Isotropic Aluminium 2024-T3 S_t = 485 MPa S_y = 345 MPa E = 72.4 GPa ν = 0.33 ρ = 2780 kg/m^3 – because anisotropic materials cannot be calculated with simple beam theory.
- Cylindrical cross section with outer radius R = 17.5 mm and inner radius r = 12.5 mm – this cross section would be a simplistic airfoil profile.
- Hollow thin-walled tube with a wall thickness of t = 5 mm – similar to a composite wing-like structure.
- Long slender tube of L = 5 m long – a good comparison to a high aspect-ratio composite structure.

The model was fixed like a cantilever beam with a point load F = 20 N at the end.

Analysis by hand calculations

The cantilevered beam slopes and deflections theory was used from (Hibbeler, 2005).

The geometric properties were calculated as follows:

$$I = \frac{1}{4}\pi R^4 - \frac{1}{4}\pi r^4$$

$$I = \frac{1}{4}\pi\{(0.0175)^4 - (0.0125)^4\}$$

$$I = 54.49 \times 10^{-9}$$

The maximum deflection was calculated as follows (Hibbeler, 2005) :

$$v_{max} = \frac{-FL^3}{3EI}$$

$$v_{max} = \frac{-(20)(5)^3}{3(72.4 \times 10^9)(54.46 \times 10^{-9})}$$

$$v_{max} = -0.211245\ m$$

The maximum slope was calculated as follows (Hibbeler, 2005):

$$\theta_{max} = \frac{-PL^2}{2EI}$$

$$\theta_{max} = \frac{-(20)(5)^2}{2(72.4 \times 10^9)(54.46 \times 10^{-9})}$$

$$\theta_{max} = -0.0634\ rad$$

The maximum stress was calculated as follows (Hibbeler, 2005) :

$$\sigma_{max} = \frac{My_n}{I}$$

$$\sigma_{max} = \frac{(20 \times 5)(0.0175)}{54.49 \times 10^{-9}}$$

$$\sigma_{max} = 32.1\ MPa$$

Analysis by SolidWorks 2012 Simulation

The SolidWorks Simulation was set up with a static study. The material of the tube was defined as 2024-T3. The tube was fixed at one end and an external load was applied to the opposite end of the tube. A force of 20 N was applied on the tube end face as depicted in Figure 52.

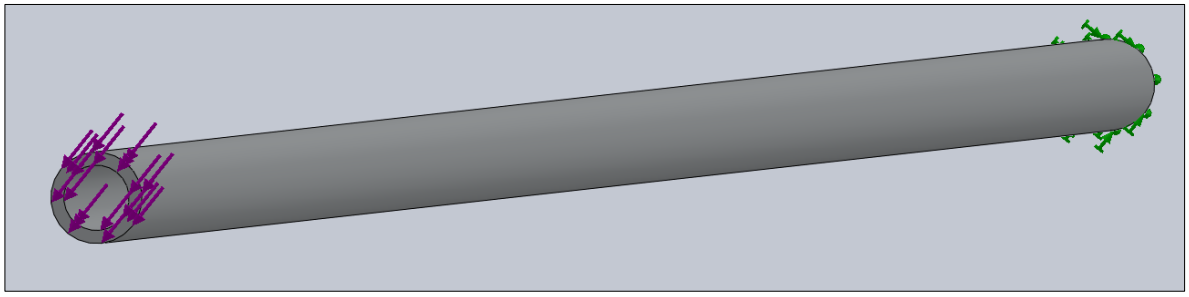

Figure 52: SolidWorks Simulation Constraints and Loads

The use of a Curvature based mesh was used to obtain quicker convergence of results as depicted in Figure 53. The simulation was solved at five mesh element size settings from max/min of 38 mm – 15 mm to a max/min of 10 mm – 3 mm. The solution difference per simulation run was 0.047% showing a good convergence of the displacement results.

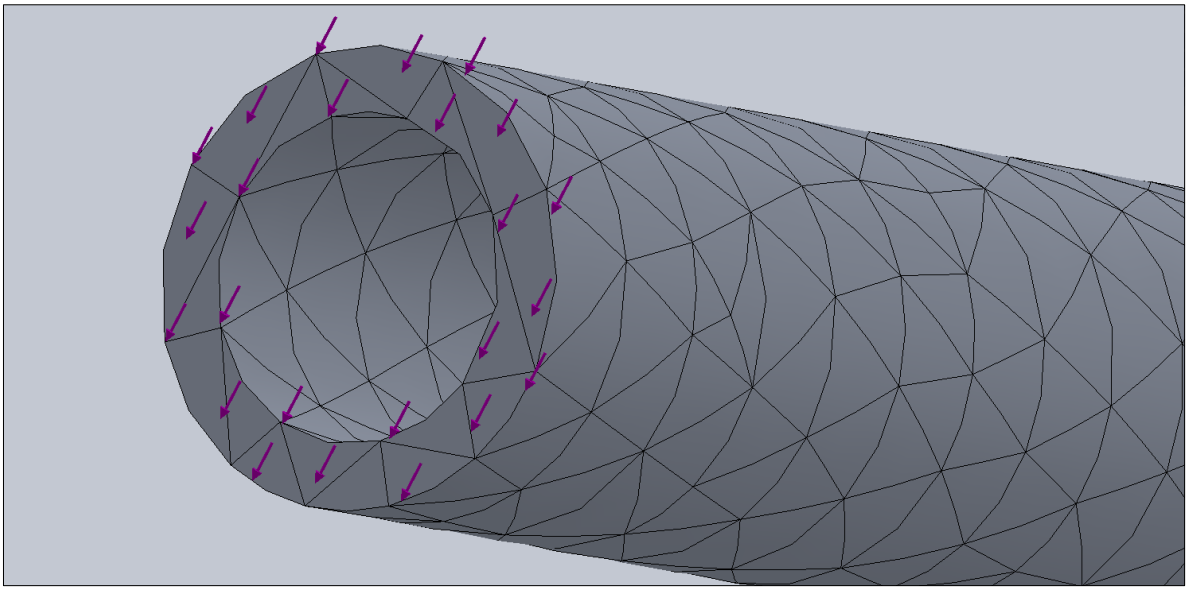

Figure 53: SolidWorks Simulation Curvature Based Mesh

The maximum stress concentration was analysed as 32.4 MPa with the von Mises stress theory as depicted in Figure 54. This gives a safety factor of 10.64.

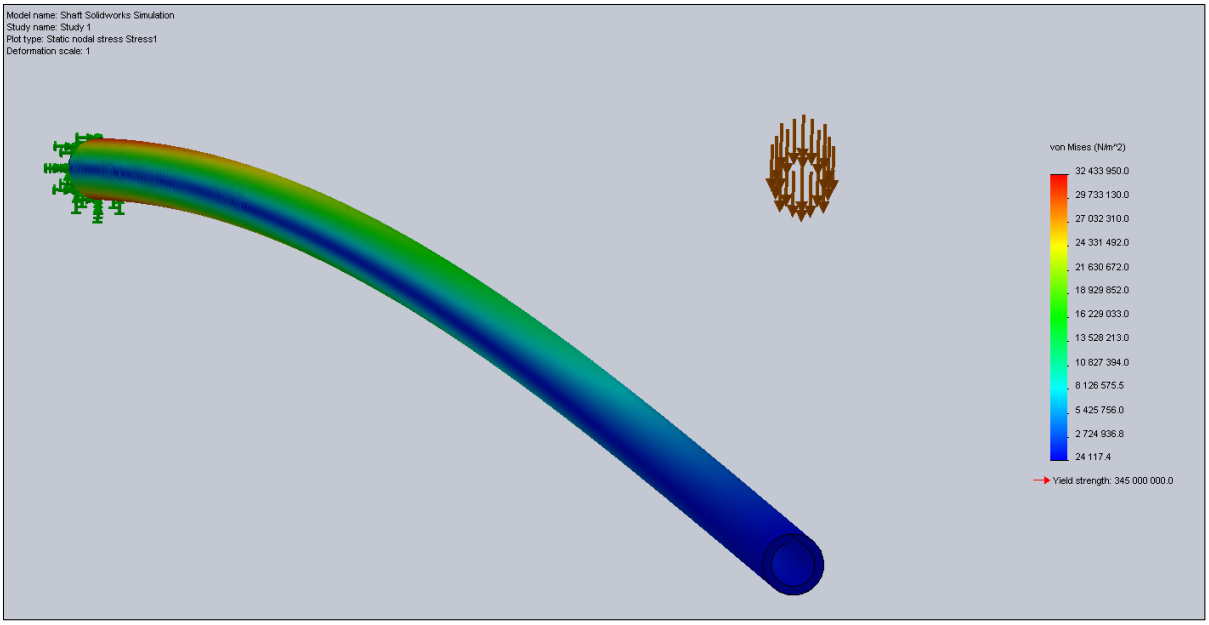

Figure 54: SolidWorks Simulation von Mises Plot

The deflection plot was plotted as depicted in Figure 55 shows the maximum deflection.

$$v_{max} = -0.2108\, m$$

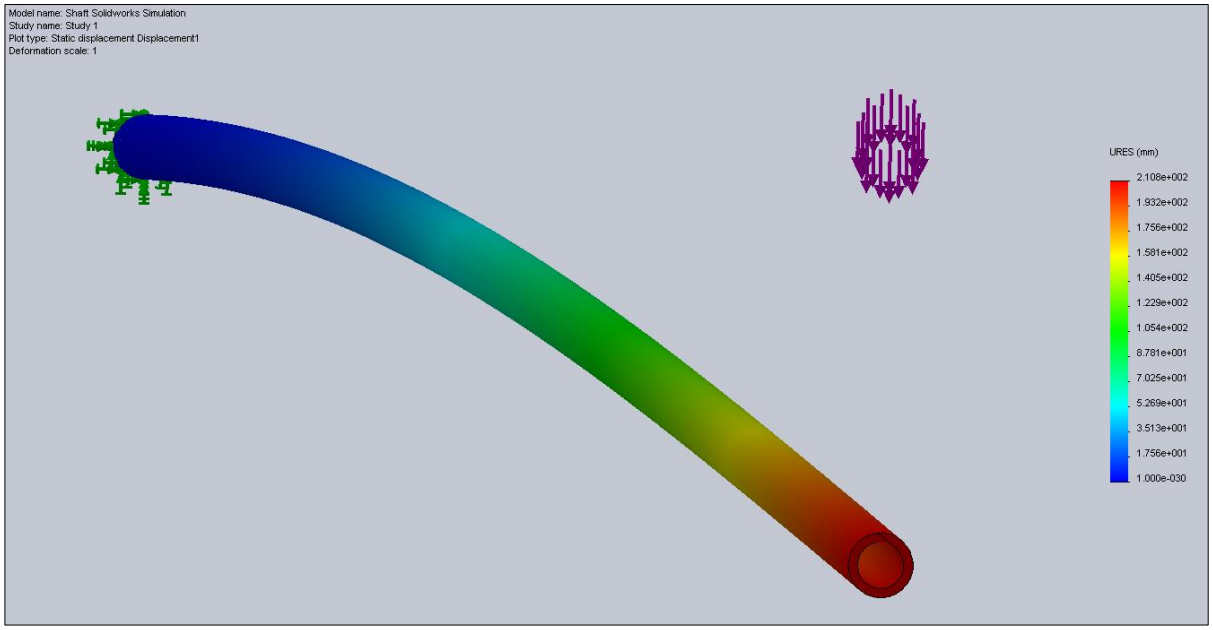

Figure 55: SolidWorks Simulation Displacement Plot

The maximum slope angle was sketched and dimensioned.

$$\theta_{max} = -0.0649\, rad$$

Analysis by PreVABS

The outer tube circumference was evenly divided into 100 points. The normalised coordinates of the cross-section were inserted into the airfoil geometric data file Sec_profile_shaft.input. This input file also included tube diameter (Chord length), twist angle, neutral axis, web number, chord line rotation angle and number of nods.

The cross-sectional lamina schema data file, Sec_Layup_Confg_shaft.input was setup by separating the nodes into segments. The segments specified the number of lamina, lamina thickness, fibre orientation of layer and material id per layer. The tube wall was modelled with a single lamina of thickness 5 mm. The fibre orientation was set at zero degrees, but would not have an effect as the material would be isotropic.

The material property data file, title_material_shaft.input was set up with title flags to request the Timoshenko model in VABS and use the isotropic material properties of Aluminium 2024-T3.

The control input file, Control.txt is run with PreVABS_Release_v202_Mar12_2012.exe to call the other input files and specify the following plotting and modelling parameters, plot_profile, Is_plot_area, plot_glbelm_mesh and Rel_mesh_size as shown in

Figure 56. The relative mesh size specifying the relative ratio of the element width to minimum layer thickness was set to 8.

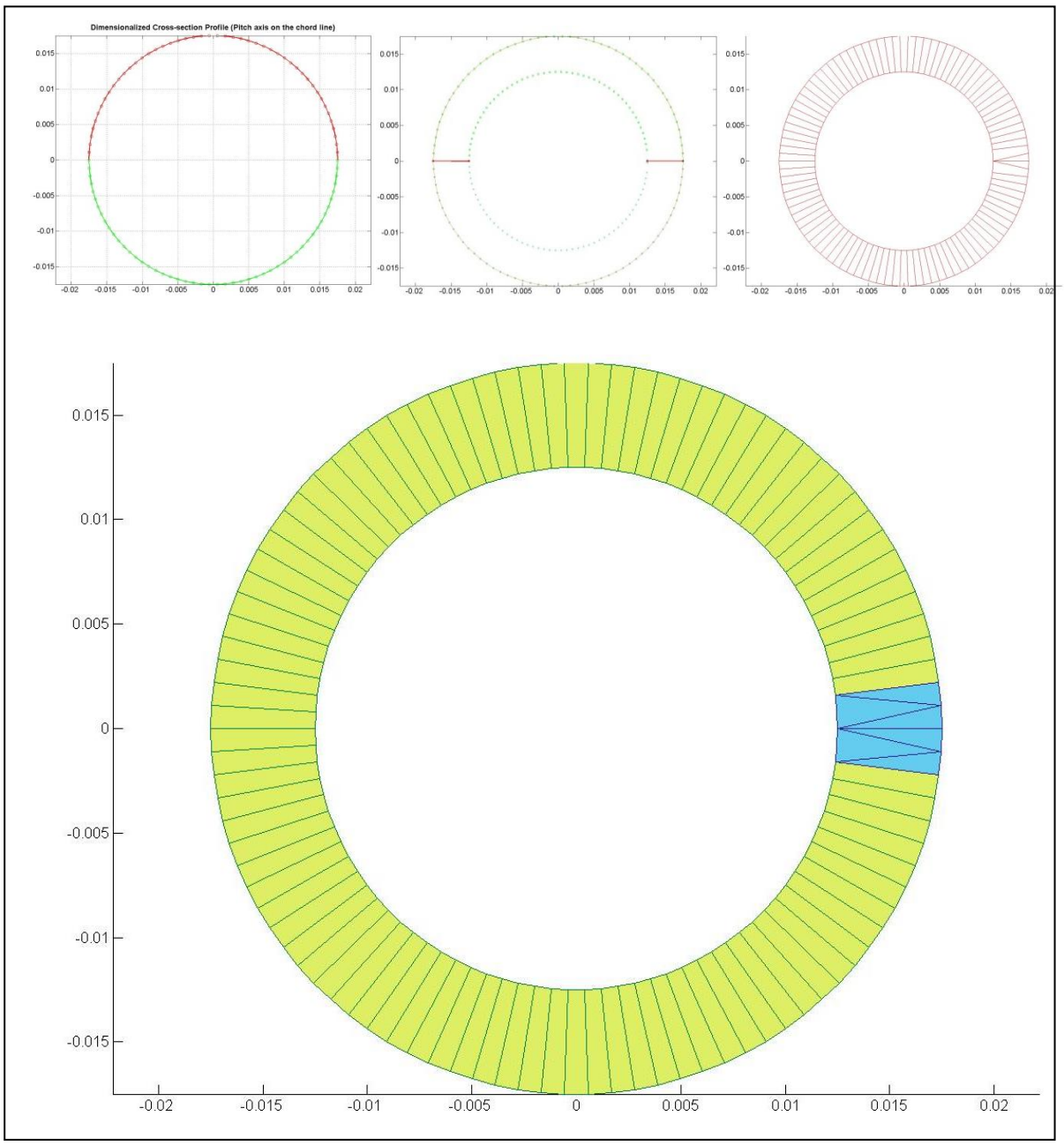

Figure 56: Mesh processing plots

PreVABS wrote an output file Shaft_output_for_VABS with all the data compiled for VABS with node coordinates, node connectivity, lamina properties etc.

Analysing with VABS

The Shaft_output_for_VABS was run in VABS with the generalized Timoshenko model, which outputs a 6x6 flexibility matrix needed for GEBT.

The VABS program was re-run with the updated results from the GEBT output data.

The displacements, rotations, forces and moments at the fixed point of the cantilever beam were taken from GEBT's results and inserted back into the VABS input file. This recovered the 3D point wise displacements, strains, and stress fields of the VABS cross-sectional nodes and Gaussian points.

For VABS to output 3D point wise displacements a direction cosine matrix is required to transform the 1D beam's un-deformed base vectors triad into the deformed triad.

The author created a geometrical model in SolidWorks to output the 3 x 3 direction cosine matrix as depicted in Figure 57 using mathematical theory (Starlino Electronics, 2011). This cross-checked the Matlab program that creates the cosine direction matrix coded by G. Grundling based on Chandrupatla and Belegundu (2002).

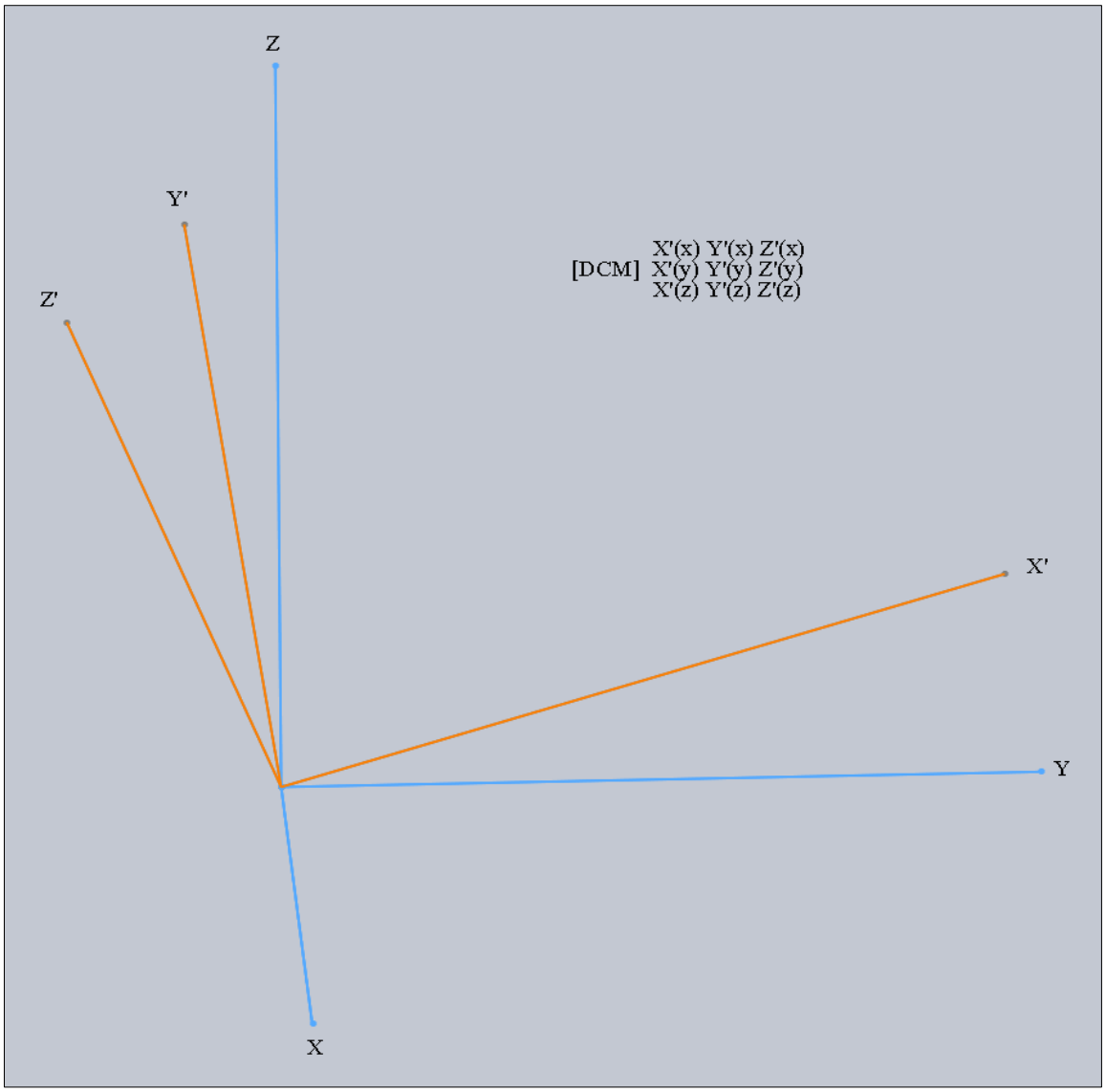

Figure 57: Direction Cosine Calculator

The 1D beam point rotations output from GEBT are entered into the calculator. The x, y, z values can be read from each point and entered into the cosine direction matrix.

The recovery outputs of VABS were compared to previous results as follows:

- The highest stress was calculated as 30.7 MPa using a Gaussian point expressed in the beam coordinate system.
- The highest stress using stress results at the highest stressed node expressed in the beam coordinate system is 33.1 MPa.

Analysing with GEBT

The GEBT input file is prepared with a 1D beam with two points depicting the VABS cross-sectional positions. The point coordinates are defined and have prescribed conditions giving a fixed point and a point with the 20 N load. The 1D beam has a 6x6 flexibility matrix defined by VABS. The parameters and mathematical models need to also be defined in the input file.

COMPARISON OF RESULTS

The maximum stress value difference from the hand calculation and SolidWorks FEM was calculated as 0.93%.

The displacement difference from the hand calculation and SolidWorks FEM was calculated as 0.21%. The maximum slope value difference from the hand calculation and SolidWorks FEM was calculated as 2.3%.

The maximum stress at the Gaussion points of the tube’s value difference from the hand calculations and VABS is 4.46%. The maximum stress of the tube’s value difference from the hand calculations and VABS is 3.07%.The output values from GEBT were compared as follows:

- The maximum displacement value difference from the hand calculation is 0.047%.
- The maximum slope value difference from the hand calculation is 0.096%.

- The results from PreVABS/VABS/GEBT showed good agreement with the hand calculations and SolidWorks FEM Simulation as shown in Table 6.

Table 6: Hand calculations compared to Tailor.m and SolidWorks FEM Simulation

	Hand Calculations	**Tailor.m**	**Percentage Diff.**	**SolidWorks Simulation FEM**	**Percentage Diff.**
$\boldsymbol{v_{max}}$	$-0.211245\ m$	$-0.211145\ m$	0.047%	$-0.2108\ m$	0.21%
$\boldsymbol{\theta_{max}}$	$-0.0634\ rad$	$-0.06334\ rad$	0.096%	$-0.0649\ rad$	2.3%
$\boldsymbol{\sigma_{max}}$	32.1 MPa	30.7 MPa (Gaussion point) 33.1 MPa (nod)	4.46% 3.07%	32.4 MPa	0.93%

APPENDIX B - MATLAB PROGRAM USER INTERFACE TO INTERGRATE PREVABS, VABS AND GEBT

Tailor.m

```
clc, clear all
path('C:\Program Files\MATLAB\R2010b\bin',path)
PreVABScalc=0;      %If PreVABS calculation done 1 otherwise 0
VABScalc=0;         %If VABS calculation done 1 otherwise 0
GEBTcalc=0;         %If GEBT calculation done 1 otherwise 0
GEBTgetresults=0;    %If GEBT results are not needed 1 otherwise 0
Plot1Dvar=1;         %Plots the variables VS the displacement
Plottwisttailor=0;   %Plots twist angle vs layup angle
Recover3D=1;
Recover3DVABS=1;
Recover3Dgetresults=1;
Model3D=1;
Calc=120; % Number of iterations for a specific variable (Variable must be
specified in controlfile.m)
Calc1D=1; % Number of iterations for a specific variable (Variable must be
specified in GEBTprep.m)
Secchange=2; % Number of different specified cross-sections
(controlfilesec1..2..3 etc to be created)
            % Remember to update GEBTprep.m with the cross section numbers
ProfileChord=[68.00 45.00]; %Profile chord of crossections
%ProfileChord=[68.00 67.15 66.30 65.44 64.59 63.74 62.89 62.04 61.19 60.33 59.48
58.63 57.78 56.93 56.07 55.22 54.37 53.52 52.67 51.81 50.96 50.11 49.26 48.41
47.56 46.70 45.85 45.00];
Tw=0;
Ang=linspace(15,25,10);
La=0;
for tw=1:Calc;
    Tw=Tw+1;
    if (Tw>0)&&(Tw<=30);
    Twistang(1,Tw)=0; %wing twist angle in deg 4deg
    Twistang(2,Tw)=1; %wing twist angle in deg 4deg
    end
    if (Tw>30)&&(Tw<=60);
    Twistang(1,Tw)=0;%wing twist angle in deg 4deg
    Twistang(2,Tw)=2; %wing twist angle in deg 4degg
    end
    if (Tw>60)&&(Tw<=90);
    Twistang(1,Tw)=0; %wing twist angle in deg 4deg
    Twistang(2,Tw)=3; %wing twist angle in deg 4deg
    end
    if (Tw>90)&&(Tw<=120);
    Twistang(1,Tw)=0; %wing twist angle in deg 4deg
    Twistang(2,Tw)=4; %wing twist angle in deg 4deg
    end
    if
(Tw==11)||(Tw==21)||(Tw==31)||(Tw==41)||(Tw==51)||(Tw==61)||(Tw==71)||(Tw==81)||
(Tw==91)||(Tw==101)||(Tw==111);
   La=0;
    end
```

```
   La=1+La;
    Layang(Tw,1)= Ang(La); %layers layup angle in degrees
    Layang(Tw,2)= Ang(La); %layers layup angle in degrees
    Layang(Tw,3)= Ang(La); %layers layup angle in degrees
    if
(Tw>10)&&(Tw<=30)||(Tw>40)&&(Tw<=60)||(Tw>70)&&(Tw<=90)||(Tw>100)&&(Tw<=120);
    Layang(Tw,2)= 45; %layers layup angle in degrees
    end
    if
(Tw>20)&&(Tw<=30)||(Tw>50)&&(Tw<=60)||(Tw>80)&&(Tw<=90)||(Tw>110)&&(Tw<=120);
    Layang(Tw,3)= 45; %layers layup angle in degrees
    end
end

LPS=[36 34];
HPS=[38 34];
%LPS=[36 36 36 36 36 36 36 36 36 36 36 36 36 36 36 36 36 36 34 34 34 34 34 34
34 34 34];   %2nd last node points on profile allowing layer convergence LPS
upper profile HPS lower profile
%HPS=[38 38 38 38 36 35 35 35 35 35 35 35 35 35 35 35 35 35 35 35 35 35 35 35
35 35 34];

E3=8000E6;%linspace(1000, , Calc);
G23=3000E6;%linspace(300, , Calc);

if PreVABScalc==0;
[k]=controlfilesec1(Calc,E3,G23,Secchange,LPS,HPS,ProfileChord,Twistang,Layang);
secs=1;
Secnum=Secchange-1;
%if 1 < Secchange ;
        %for i=1:Secnum;
        %secs=1+secs;
        %funcname=[func2str(@controlfilesec) , num2str(secs)];
        %funcname=str2func(funcname);
        %[k]=funcname(Calc,E3,G23,Secchange,LPS,HPS,ProfileChord);
       % end
%end
end
if VABScalc==0;
[k]=VABS(Calc,Secchange);
end
Beam1Dpt=Secchange;%Number of points in the 1D beam
LengthF=2.168;
Section1pt=1:2;
Section2pt=0:0;
pts=1;
Beam1Dptloc(1)=0.0;
T1(1:Secchange)=0
%T1(28)=4.238
%T1(2)=-2.938129509 %hand calculation distributed load
tae=1
if tae==0
T1(1)=  -0.142258174    ;
T1(2)=  -0.137413765    ;
T1(3)=  -0.132679538    ;
T1(4)=  -0.128054241    ;
T1(5)=  -0.123536622    ;
T1(6)=  -0.11912543 ;
T1(7)=  -0.11481941 ;
```

```
T1(8)=  -0.110617313    ;
T1(9)=  -0.106517884    ;
T1(10)= -0.102519873    ;
T1(11)= -0.098622026    ;
T1(12)= -0.094823093    ;
T1(13)= -0.09112182 ;
T1(14)= -0.087516955    ;
T1(15)= -0.084007247    ;
T1(16)= -0.080591442    ;
T1(17)= -0.07726829 ;
T1(18)= -0.074036537    ;
T1(19)= -0.070894932    ;
T1(20)= -0.067842222    ;
T1(21)= -0.064877155    ;
T1(22)= -0.061998479    ;
T1(23)= -0.059204942    ;
T1(24)= -0.056495292    ;
T1(25)= -0.053868275    ;
T1(26)= -0.051322642    ;
T1(27)= -0.048857138    ;
T1(28)= -0.497238772    ;

end

for p1=2:Beam1Dpt;
    pts=pts+1;
    Beam1Dptloc(pts)=(LengthF/(Beam1Dpt-1))+Beam1Dptloc(pts-1);
end
if GEBTcalc==0;
[k]=GEBTprep(Calc,Secchange,Beam1Dpt,Beam1Dptloc,Section1pt,Section2pt,T1);
end

if GEBTgetresults==0;
     [k,X,U,Rot,F,M]=GEBTresults(Calc,Beam1Dpt);
save('Wingtwist.mat','Rot')
end

if Plot1Dvar==0;
plot(E3(1:Calc),U(1:Calc,3,7));
title('Young''s z Modulus VS Displacement');
ylabel('z-Displacement (m)');
xlabel('Young''s Moudulus (Pa)');
end

if Plottwisttailor==0;
    Pl=0;
    PL1=Pl;
    Pl=Pl+10;
    PL1=PL1+11;
    plot(Ang(1:10),rad2deg(Rot(PL1-10:Pl,1,2)));
    hold on
    for PL=2:12;
    PL1=Pl;
    Pl=Pl+10;
    PL1=PL1+11;
    plot(Ang(1:10),rad2deg(Rot(PL1-10:Pl,1,2)));
    end

    title(' Bend-twist couple angle VS Layer Layup angle');
```

```
    ylabel(' Tailored Twist(deg)');
    xlabel(' Layup angle(deg)');
end
Sec1pt=max(Section1pt);
Sec2pt=max(Section2pt);
sec=0;
for f2=1:Secchange;
        sec=sec+1;
    if sec==1;
        pt=0;
        for f3=1:Sec1pt;
             pt=1+pt;
                Secptmat(pt,:)=[pt sec];
        end
    end
    if sec==2;
        for f5=Sec1pt+1:Sec2pt;
             pt=1+pt;
                Secptmat(pt,:)=[pt sec];

        end
    end
end

if Recover3D==0;

  [k]=Recover(Calc,Section1pt,Section2pt,Secchange,X,U,Rot,F,M,Secptmat);
end

if Recover3DVABS==0;
    [k]=VABSrecover(Calc,Secchange,Secptmat,Section2pt);
end

if Recover3Dgetresults==0;
    [k,Disp3D]=RecoveryResults(Calc, Secchange,Beam1Dpt,Secptmat,Section2pt);
end
%,Strain3D,Stress3D,Stressaverage3D
if Model3D==0;
    f=0;
    for f1=1:Beam1Dpt;
        f=f+1;
        Disp3d1=Disp3D{f,1,1};
        Disp3dy(f,:)=str2double(Disp3d1{2});
        Disp3dz(f,:)=str2double(Disp3d1{3});
        dDisp3dx(f,:)=str2double(Disp3d1{4});
        dDisp3dy(f,:)=str2double(Disp3d1{5});
        dDisp3dz(f,:)=str2double(Disp3d1{6});
        nodel=length(Disp3d1{1});
        Disp3dx(f,1:nodel)=Beam1Dptloc(f);
    end
        p1=surfl(Disp3dx(:,1:nodel),Disp3dy(:,1:nodel),Disp3dz(:,1:nodel));
        axis([0 2.5 -1.25 1.25 -1.25 1.25]);
        shading interp
        colormap copper
        hold on;
        TDisp3dx=Disp3dx+dDisp3dx;
        TDisp3dy=Disp3dy+dDisp3dy;
        TDisp3dz=Disp3dz+dDisp3dz;
        p2=surfl(TDisp3dx(:,1:nodel),TDisp3dy(:,1:nodel),TDisp3dz(:,1:nodel));
```

```
        shading interp
        colormap gray
        %set(p1,'Color','yellow');
        %set(p1,'Color','blue');
End
```

Controlfilesec1.m

```
function [k] =
controlfilesec1(Calc,E3,G23,Secchange,LPS,HPS,ProfileChord,Twistang,Layang)

s2=0;
for s1=1:Secchange;
    s2=1+s2;
    %Variables
sec=['sec', num2str(s2)];
k=0;
format('longEng');
for i=1:Calc;
    k=k+1;
    fid1=fopen('c:\PreVABS\1', 'w');
    Sec_profile=['Sec_profile_JS1_21m_Flaperon_3_', num2str(s2), '.Input \n'];
    fprintf(fid1, Sec_profile);
    Sec_Layup=['Sec_Layup_Confg_JS1_21m_Flaperon_3_', num2str(s2), '.Input \n'];
    fprintf(fid1, Sec_Layup);
    fprintf(fid1, 'title_material_JS1_21m_Flaperon_3_root.input \n');
    OutVABS=['Flaperon3VABSoutput', num2str(k), sec, ' \n'];
    fprintf(fid1, OutVABS);
    fprintf(fid1, 'no \n');
    fprintf(fid1, 'no \n');
    fprintf(fid1, 'no \n');
    fprintf(fid1, '3 \n');
    fclose(fid1);
    pls=['c:\PreVABS\Sec_profile_JS1_21m_Flaperon_3_', num2str(s2), '.Input'];
    fid4=fopen(pls, 'w');
    % Sec_profile_JS1_21m_Flaperon_3_().input

%=========================================================================
% (1)  Chord length (m)   twisted angle (deg)          pitch axis location (x y)
(m)
%=========================================================================
%
    fprintf(fid4, ['     ', num2str(ProfileChord(s2)/1000), '           ',
num2str((Twistang(s2,Calc))), '      0.00635319357980358    -0.00148599912394642
\n']);

%=========================================================================
% (2)  (a) Nondimensional positions for Web centers ((x,y) position for the
center of each web)
%      (b) webs' tittling angles (w.r.t. chord line)
%      Web center should be on the cord line (y=0.0)
%=========================================================================

% Total number of webs in this cross section
%     Nwebs
    fprintf(fid4,'      0    \n');
```

```
%     Webi_nd_x, Webi_nd_y     Web_tl_angles (deg)
%   0.819202971 0.0 90
%   0.833680072 0.0 90
%   0.848700885 0.0 90
%   0.863938277 0.0 90
%   0.879441    0.0 90
%   0.895466003 0.0 90
%   0.912274191 0.0 90
%   0.929122269 0.0 90
%   0.945761058 0.0 90
%   0.963212533 0.0 90
%
%
%=========================================================================
% (3)  Nondimensional profile data for low pressure surface (LPS)
%=========================================================================
%
%  chord line status  'Tilt' or 'Regular'
%  Currently (8/08) always 'Regular' -->: farthest trailing edge point lies on
the
    fprintf(fid4, '    Regular  \n');
%
%   chord line rotation angle (deg)  (0 deg if cord line is on x axis)
  fprintf(fid4, '      0.0 \n');
%
%       number of knods @ LPS   (top surface)
%
 fprintf(fid4, [num2str(LPS(s2)), ' \n']);
%
%       x       y (nondimensional)
%
coor = [0   0
0.001010373 0.012165449
0.004044832 0.022782518
0.009088956 0.032802577
0.016122837 0.042064249
0.025118717 0.05056482
0.036041092 0.057432662
0.048846858 0.062461434
0.063485475 0.065615071
0.079899171 0.067074696
0.09802317  0.067574901
0.117785944 0.06680477
0.141822973 0.064168226
0.161909678 0.061774815
0.186096503 0.058887592
0.211574517 0.055846236
0.238243171 0.052637994
0.265997216 0.049379232
0.29472712  0.046170809
0.324319497 0.042985926
0.354657562 0.039793504
0.385621583 0.036558161
0.417089359 0.033272947
0.451237024 0.029750959
0.481037925 0.026749283
0.513266339 0.023603592
0.545494752 0.020584741
0.577595975 0.017737267
0.609443318 0.015110272
```

```
0.640911095 0.012735172
0.671875116 0.010615996
0.70221318  0.008755551
0.731805558 0.007173499
0.760535461 0.005887187
0.788289506 0.004895894
0.812197526 0.004247501
0.826208417 0.003954129
0.841151728 0.003726756
0.856250042 0.003590786
0.871626512 0.003484651
0.887255489 0.003360637
0.903676516 0.003218484
0.920871865 0.003135869
0.937372673 0.003078772
0.954149443 0.003012972
0.972275623 0.002941801
0.977234464 0.002922331
0.982959455 0.002899082
0.987025358 0.002815339
0.990700682 0.00258265
0.993945375 0.002216152
0.996403875 0.001781269
0.998243523 0.001281896
0.999255325 0.00084762
0.999918633 0.000282937
1   0];
nod1=0;
for nodcoor=1:(LPS(s2)-1);
 nod1=nod1+1;
    fprintf(fid4, [num2str(coor(nod1,1)), '    ', num2str(coor(nod1,2)), '
\n']);
end
fprintf(fid4, '1   0 ');
%
%=========================================================================
% (5)  Nondimensional profile data for high pressure surface (HPS)
%=========================================================================
%
% number of knods @ HPS         (bottom surface)
%
 fprintf(fid4, [num2str(HPS(s2)), ' \n']);
%
%       x       y (nondimensional)
%
hcoor=[0    0
0.001010345 -0.010362635
0.004044804 -0.021741556
0.009088929 -0.032968397
0.016122811 -0.043786914
0.025118691 -0.05392862
0.036041068 -0.063103505
0.048846834 -0.070997108
0.063485453 -0.077267958
0.079899151 -0.081544521
0.098023151 -0.084240943
0.117785927 -0.086489189
0.137660827 -0.088091626
0.161909666 -0.089209594
0.186096493 -0.089474496
```

```
0.21157451  -0.088902905
0.238243167 -0.087440933
0.265997215 -0.085290779
0.294727121 -0.083002939
0.324319502 -0.080601558
0.354657569 -0.078087544
0.385621593 -0.075465086
0.417089373 -0.072739722
0.450967113 -0.069732906
0.481037946 -0.066994731
0.513266362 -0.063975791
0.545494779 -0.060842867
0.577596005 -0.057578257
0.609443352 -0.054159931
0.640911131 -0.050566928
0.671875155 -0.046805811
0.702213223 -0.042915504
0.731805604 -0.038947295
0.76053551  -0.034987176
0.788289558 -0.031120111
0.814045667 -0.027519544
0.827999604 -0.025561836
0.842902181 -0.023462312
0.857916592 -0.021337534
0.873137419 -0.019179436
0.888585019 -0.016997215
0.904848072 -0.014723509
0.921894002 -0.012376175
0.938222511 -0.010199251
0.954848856 -0.007938098
0.972797085 -0.00569002
0.977234464 -0.005134223
0.982959441 -0.004599082
0.987025358 -0.003854106
0.990700682 -0.003203437
0.993945375 -0.002556139
0.996403875 -0.001919015
0.998243523 -0.001285989
0.999255325 -0.000847698
0.999918633 -0.000283018
1   0];
nod2=0;
for nodcoor=1:(HPS(s2)-1);
 nod2=nod2+1;
    fprintf(fid4, [num2str(hcoor(nod2,1)), '    ', num2str(hcoor(nod2,2)), '
\n']);
end
fprintf(fid4, '1   0 ');



    fclose(fid4);
    fid2=fopen('c:\PreVABS\title_material_JS1_21m_Flaperon_3_root.input', 'w');
   % VABS title flags
%=====================================================
% Timoshenko_flag   recover_flag  thermal_flag
    fprintf(fid2, '1   0   0 \n');
%  curve_flag (k1 (deg/in), k2, k3)   oblique_flag   Trapeze_flag   Vlasov_flag
```

```
    fprintf(fid2, '0                                    0               0
0 \n');

%=========================================================
% MAterial Properties
%=========================================================

% number of material ids
    fprintf(fid2, '5 \n');

% Material Properties
%
% material ID 1      orth_flag 1

    fprintf(fid2, '1   1 \n');
%       E1   96000       E2             E3     (lb/in^2)
    mat1E=['96000E+06       8000E+06      8000E+06  \n'];
    fprintf(fid2, mat1E);

%       G12         G13            G23    (lb/in^2)
    mat1G=['3000E+06       3000E+06      3000E+06   \n'];
    fprintf(fid2, mat1G);

%       nu12        nu13           nu23
    fprintf(fid2, '0.2        0.2           0.2 \n');
    fprintf(fid2, '1445 \n');


% material ID 2      orth_flag 2

    fprintf(fid2, '2   1 \n');
%       E1          E2             E3     CHANGE to see effect
    mat2E=['55000E+06       55000E+06       0  \n'];
    fprintf(fid2, mat2E);


%       G12         G13            G23    (lb/in^2)
    mat2G=['4000E+06      4000E+06       0 \n'];
    fprintf(fid2, mat2G);

%       nu12        nu13           nu23
    fprintf(fid2, '0.08        0.08           0.2 \n');
%  rho  (lb-sec^2/in^4)
    fprintf(fid2, '1445 \n');

% material ID 3      orth_flag 3 check if carbon_____________

    fprintf(fid2, '3   1 \n');
%       E1          E2             E3     (lb/in^2)
    mat3E=['10000E+06       10000E+06      10000E+06  \n'];
    fprintf(fid2, mat3E);

%       G12         G13            G23    (lb/in^2)
    mat3G=['1000E+06      1000E+06       1000E+06   \n'];
    fprintf(fid2, mat3G);

%       nu12        nu13           nu23
```

```
    fprintf(fid2, '0.3        0.3           0.3 \n');
%  rho  (lb-sec^2/in^4)
    fprintf(fid2, '100 \n');
% material ID 4      orth_flag 4 AIR
   fprintf(fid2, '4   1 \n');
%       E1
    fprintf(fid2, '1.493900000e+002 1.493900000e+002    1.493900000e+002  \n');

%      G12
    fprintf(fid2, '1.160300000e+002     1.160300000e+002    1.160300000e+002
\n');

%       nu12
    fprintf(fid2, ' 0.3     0.3     0.3      \n');
%  rho
    fprintf(fid2, '0.000155705  \n');
  % material ID 5      orth_flag 5

    fprintf(fid2, '5   1 \n');
%       E1          E2             E3     CHANGE to see effect
    mat2E=['100E+06       100E+06       100E+06  \n'];
    fprintf(fid2, mat2E);


%       G12         G13            G23    (lb/in^2)
    mat2G=['10E+06      10E+06        10E+06 \n'];
    fprintf(fid2, mat2G);

%       nu12        nu13           nu23
    fprintf(fid2, '0.08        0.08           0.2 \n');
%  rho  (lb-sec^2/in^4)
    fprintf(fid2, '1445 \n');

    fclose(fid2);



    fid3=fopen(['c:\PreVABS\Sec_Layup_Confg_JS1_21m_Flaperon_3_', num2str(s2),
'.Input'], 'w');
   % Sec_Layup_Confg_JS1_21m_Flaperon_3_root.input

%=====================================================================
%  (1)  Chordwise lamina data for low press surface (LPS, top surface)
%       (thickness or offset, ply angle, and material ID)
%=====================================================================
%
%Surface indicator ('Low_PS' or 'High_PS', (top/bottom surface))  Id_Hig_low_PS
%
        fprintf(fid3, '  Low_PS   \n');
%
% Total number of chordwise segments (N_segm)
        fprintf(fid3, '  3   \n');
%
% Segment number
% Segment number for a particular cross section must run from leading edge to
trailing edge
% and in that order.
%
```

```
%       LE  UD Tape  aft  10mm 5mm end          TE
        fprintf(fid3, '  1     2        3     \n');
%
%-------------------------------------
% Segment No. 1 (LE)
%---------------------
%
% Starting and ending node number of Segment No. #1
% node here refers to the spline node used generate the foil cross section
profile.
%
% starting node             ending node
      fprintf(fid3, '  1                         13   \n');
%
% Number of lamina in this segment
      fprintf(fid3, '  4   \n');


%
% thickness (m)   fiber orientation (deg)   material id
%
        fprintf(fid3, '  0.00010    0   3   \n');
        fprintf(fid3, ['  0.00030   ', num2str(Layang(k,1)), '    2   \n']);
        fprintf(fid3, ['  0.00030   ', num2str(Layang(k,2)), '  2   \n']);
        fprintf(fid3, ['  0.00030   ', num2str(Layang(k,3)), '  2   \n']);

%
%-------------------------------------
% Segment No. 2 (Sand_1)
%-------------------------------------
%
% Starting and ending node number of Segment No. #2
% node here refers to the spline node used generate the foil cross section
profile.

% starting node             ending node
      fprintf(fid3, '  13                        24   \n');
% Number of lamina in this segment
      fprintf(fid3, '  4   \n');

% thickness (in)   fiber orientation (deg)   material id

     fprintf(fid3, '  0.00010   0   3   \n');
     fprintf(fid3, ['  0.00030  ', num2str(Layang(k,1)), '    2   \n']);
     fprintf(fid3, ['  0.00030  ', num2str(Layang(k,2)), '  2   \n']);
     fprintf(fid3, ['  0.00030  ', num2str(Layang(k,3)), '  2   \n']);


      %fprintf(fid3, '  0.00045     0   1   \n');
%
%-------------------------------------
% Segment No. 3 (Spar_Cap)
%-------------------------------------
%
% Starting and ending node number of Segment No. #3
% node here refers to the spline node used generate the foil cross section
profile.
%
% starting node             ending node
      fprintf(fid3, ['  24                        ', num2str(LPS(s2)), '  \n']);
```

```
%
% Number of lamina in this segment
    fprintf(fid3, '  4   \n');
%
% thickness (in)   fiber orientation (deg)   material id
%
    fprintf(fid3, '  0.00010    0   3   \n');
     fprintf(fid3, ['  0.00030  ', num2str(Layang(k,1)), '    2   \n']);
     fprintf(fid3, ['  0.00030  ', num2str(Layang(k,2)), '  2   \n']);
     fprintf(fid3, ['  0.00030  ', num2str(Layang(k,3)), '  2   \n']);




%=====================================================================
%  (2)  Chordwise lamina data for high press surface (HPS, bottom surface)
%       (thickness or offset, plyer angle, and material ID)
%=====================================================================
%
%Surface indicator ('Low_PS' or 'High_PS')  Id_Hig_low_PS
%
    fprintf(fid3, '          High_PS   \n');
%
% Total number of chordwise segments (N_segm)
       fprintf(fid3, '  3   \n');
%
% Segment number
% Segment number for a particular cross section must run from leading edge to
trailing edge
% and in that order.
%
%       LE  UD Tape  aft  10mm 5mm end          TE
       fprintf(fid3, '  1     2        3      \n');
%
%-------------------------------------
% Segment No. 1 (LE)
%---------------------
%
% Starting and ending node number of Segment No. #1
% node here refers to the spline node used generate the foil cross section
profile.
%
% starting node            ending node
     fprintf(fid3, '  1                        13   \n');
%
% Number of lamina in this segment
     fprintf(fid3, '  4   \n');


%
% thickness (m)   fiber orientation (deg)   material id
%
       fprintf(fid3, '  0.00010    0   3   \n');
     fprintf(fid3, ['  0.00030  ', num2str(-1*Layang(k,1)), '    2   \n']);
     fprintf(fid3, ['  0.00030  ', num2str(-1*Layang(k,2)), '   2   \n']);
     fprintf(fid3, ['  0.00030  ', num2str(-1*Layang(k,3)), '   2   \n']);


%
%-------------------------------------
```

```
% Segment No. 2 (Sand_1)
%-------------------------------------
%
% Starting and ending node number of Segment No. #2
% node here refers to the spline node used generate the foil cross section
profile.

% starting node             ending node
      fprintf(fid3, '  13                        24    \n');
% Number of lamina in this segment
      fprintf(fid3, '  4    \n');

% thickness (in)   fiber orientation (deg)   material id

    fprintf(fid3, '  0.00010    0    3    \n');
     fprintf(fid3, ['  0.00030  ', num2str(-1*Layang(k,1)), '    2    \n']);
     fprintf(fid3, ['  0.00030  ', num2str(-1*Layang(k,2)), '    2    \n']);
     fprintf(fid3, ['  0.00030  ', num2str(-1*Layang(k,3)), '    2    \n']);
    %fprintf(fid3, '  0.00045   0    1    \n');
%
%-------------------------------------
% Segment No. 3 (Spar_Cap)
%-------------------------------------
%
% Starting and ending node number of Segment No. #3
% node here refers to the spline node used generate the foil cross section
profile.
%
% starting node             ending node
      fprintf(fid3, ['  24                        ', num2str(HPS(s2)), '  \n']);
%
% Number of lamina in this segment
    fprintf(fid3, '  4    \n');
%
% thickness (in)   fiber orientation (deg)   material id
%
    fprintf(fid3, '  0.00010    0    3    \n');
     fprintf(fid3, ['  0.00030  ', num2str(-1*Layang(k,1)), '    2    \n']);
     fprintf(fid3, ['  0.00030  ', num2str(-1*Layang(k,2)), '    2    \n']);
     fprintf(fid3, ['  0.00030  ', num2str(-1*Layang(k,3)), '    2    \n']);

%=====================================================================
%  (3)  Webs layup configuration data
%       (thickness or offset, plyer angle, and material ID)
%=====================================================================
%

% Total number of webs in this cross section
    fprintf(fid3, '          0    \n');
%
% (3.1) lamina layup configuration of Web 1: main shear web
%
%-----------------------------------------
% Number of lamina: Nweb1
   % fprintf(fid3, '  1    \n');

%
% thickness (in)   fiber orientation (deg)   material id
%
```

```
 %   fprintf(fid3, '  0.0005    0   5   \n');



%
% (3.2) lamina layup configuration of Web 2: aft shear web
%
%-----------------------------------------
%
% number of lamina: Nweb 2
   % fprintf(fid3, '  1   \n');

%
% thickness (in)   fiber orientation (deg)   material id
%fprintf(fid3, '  0.001 0   5   \n');

% (3.3) lamina layup configuration of Web 3
%-----------------------------------------
%
% number of lamina: Nweb 3
    %fprintf(fid3, '          1   \n');
%
%thickness (in)  fiber orientation (deg)   material id

    %fprintf(fid3, '  0.001     0   5   \n');

%
% (3.4) lamina layup configuration of Web 4
%-----------------------------------------
%
% number of lamina: Nweb 4
   % fprintf(fid3, '          1   \n');
%
%thickness (in)  fiber orientation (deg)   material id
%
   % fprintf(fid3, '  0.001      0  5   \n');
% (3.4) lamina layup configuration of Web 5
%-----------------------------------------
%
% number of lamina: Nweb 5
  % fprintf(fid3, '          1   \n');
%
%thickness (in)  fiber orientation (deg)   material id
%
  % fprintf(fid3, '  0.001  0   5   \n');
% (3.4) lamina layup configuration of Web 6
%-----------------------------------------
%
% number of lamina: Nweb 6
    %fprintf(fid3, '          1   \n');
%
%thickness (in)  fiber orientation (deg)   material id
%
   % fprintf(fid3, '  0.001 0   5   \n');
% (3.4) lamina layup configuration of Web 7
%-----------------------------------------
%
% number of lamina: Nweb 7
   %fprintf(fid3, '          1   \n');
```

```
%
%thickness (in)  fiber orientation (deg)   material id
%
   % fprintf(fid3, '  0.001     0   5   \n');
% (3.4) lamina layup configuration of Web 8
%-----------------------------------------
%
% number of lamina: Nweb 8
    %fprintf(fid3, '          1   \n');
%
%thickness (in)  fiber orientation (deg)   material id
%
   % fprintf(fid3, '  0.001 0   5   \n');
% (3.4) lamina layup configuration of Web 9
%-----------------------------------------
%
% number of lamina: Nweb 9
%    fprintf(fid3, '          1   \n');
%
%thickness (in)  fiber orientation (deg)   material id
%
%    fprintf(fid3, '  0.001     0   5   \n');
% (3.4) lamina layup configuration of Web 10
%-----------------------------------------
%
% number of lamina: Nweb 10
%    fprintf(fid3, '          1   \n');
%
%thickness (in)  fiber orientation (deg)   material id
%
%    fprintf(fid3, '  0.001     0   5   \n');

    fclose(fid3);
    cd c:\PreVABS;
    system('PreVABS.exe');
end
end
end
```

VABS.m

```
function [k]=VABS(Calc,Secchange)

sec=0;
for s=1:Secchange;
    sec=sec+1;
    VABSext=['sec', num2str(sec)];
    k=0;
  for i=1:Calc;
    k=k+1;
    VABSe=['c:\VABS\VABS.exe c:\PreVABS\Flaperon3VABSoutput',  num2str(k),
VABSext];
    cd c:\VABS;
    system(VABSe);
  end
end
 end
```

GEBTprep.m

```
function
[k]=GEBTprep(Calc,Secchange,Beam1Dpt,Beam1Dptloc,Section1pt,Section2pt,T1)
format('longEng');
sec=0;
for s=1:Secchange;
    sec=sec+1;
    VABSext=['sec', num2str(sec)];
    k=0;

    for i=1:Calc;
        k=k+1;
        VABSK=['c:\PreVABS\Flaperon3VABSoutput', num2str(k), VABSext, '.K'];

        fid=fopen(VABSK,'r');
        C=textscan(fid, '%s%s%s%s%s%s');
        %('Timoshenko Flexibility Matrix');
        startString=['Timoshenko', 'Flexibility'];
        p=0;
        t=0;
    while t==0;
        p=p+1;
        tline = strcat(C{1}(p), C{2}(p));

    % Break if we hit end of file, or the start marker
        t=strcmp(tline, startString);

    end

    line=p+2;
    for q=1:6;
        for r=1:6;

            Flex(r,q,sec,k)=str2double(C{q}(line+r));
        end
    end

    fclose(fid);
    end
end
k=0
for xd=1:Calc;
    k=1+k
    dat=strcat('c:\GEBT\Flap3c', num2str(k), '.dat');
    GEBTfid=fopen(dat, 'w');
    fprintf(GEBTfid, '0 100 40 #dynamic_flag, niter, nstep \n');



Memprop=[num2str(Beam1Dpt),'    ', num2str(Beam1Dpt-1), '   ',
num2str(Beam1Dpt), '   ', num2str(Secchange), '   0  0 0 0 0  #
npoint,nmemb,ncond_pt,nmate, nframe, ncond_mb,ndistrfun, ntimefun, ncurv,nvel
\n'];
fprintf(GEBTfid,Memprop);
```

```
pts1=0;
for ge=1:Beam1Dpt;
    pts1=pts1+1;
    fprintf(GEBTfid, [num2str(pts1), '     ', num2str(Beam1Dptloc(pts1)), '  0.0
0.0 # coordinates for each point \n']);
end

%NB!!! Set mate_no1 and mate_no2 according to section flex matrix and update
Section1pt etc.
pts2=0;
fstsec=(max(Section1pt))-1;
if max(Section2pt)>max(Section1pt);
fstsec2=(max(Section2pt))-1;
else
    fstsec2=fstsec;
end
for ge2=1:fstsec;
    pts2=pts2+1;
    fprintf(GEBTfid, [num2str(pts2), '     ', num2str(pts2), '     ',
num2str(pts2+1), '  ', num2str(pts2), ' ', num2str(pts2+1), ' 0 200  0  #
memb_no kp_1 kp_2 mate_no1 mate_no2 frame# #divisions, curvature# velocity#
\n']);
end
%if Section2pt>=1;
%for ge3=pts2+1:fstsec2;
   % pts2=pts2+1;
    %fprintf(GEBTfid, [num2str(pts2), '     ', num2str(pts2), '     ',
num2str(pts2+1), '  1 2 0 500  0  # memb_no kp_1 kp_2 mate_no1 mate_no2 frame#
#divisions, curvature# velocity# \n']);
%end
%end
fprintf(GEBTfid, '1    #point conditions \n');
fprintf(GEBTfid, '1 2 3 4 5 6 \n');
fprintf(GEBTfid, '0 0 0 0 0 0 # corresponding value \n');
fprintf(GEBTfid, '0 0 0 0 0 0 # corresponding time functions \n');
fprintf(GEBTfid, '0 0 0 0 0 0 # indicate whether it is a follower condition
\n');
pts3=1;

for ge4=1:fstsec2;
    pts3=1+pts3;
    fprintf(GEBTfid, [num2str(pts3),' \n']);
    fprintf(GEBTfid, '7 2 3    10 11 6 \n');
    fprintf(GEBTfid, ['0 0 0.07 ', num2str(T1(pts3)), '  0 0  \n']);
    fprintf(GEBTfid, '0  0 0    0  0  0 \n');
    fprintf(GEBTfid, '0 0 0   1  0  0 \n');
end
ss2=0
for section=1:Secchange
    ss2=ss2+1
fprintf(GEBTfid, [num2str(ss2), ' # section No. ', num2str(ss2), ' \n']);
for x=1:6;
Flex1=[' ', num2str(Flex(x,1,ss2,k)), ' ' ,num2str(Flex(x,2,ss2,k)), ' ',
num2str(Flex(x,3,ss2,k)), ' ', num2str(Flex(x,4,ss2,k)), ' ',
num2str(Flex(x,5,ss2,k)), ' ', num2str(Flex(x,6,ss2,k)), ' \n'];
fprintf(GEBTfid, Flex1);
end
end
%if Secchange == 2;
    %fprintf(GEBTfid, '2 # section No. 2 \n');
```

```
    %for v=1:6;
        %Flex2=[' ', num2str(Flex(v,1,2)), ' ' ,num2str(Flex(v,2,2)), ' ',
num2str(Flex(v,3,2)), ' ', num2str(Flex(v,4,2)), ' ', num2str(Flex(v,5,2)), ' ',
num2str(Flex(v,6,2)), ' \n'];
        %fprintf(GEBTfid, Flex2);
    %end
%end
fclose(GEBTfid);

end

k=0;
for xds=1:Calc;
    k=k+1;
    GEBTdat=['c:\GEBT\gebt.exe c:\GEBT\Flap3c', num2str(k), '.dat'];
    cd c:\GEBT;
    system(GEBTdat);
end
```

DCMRad.m

```
function [A] = DCMRad(Alpha,Beta,Gamma)
% Calculates the direction cosine matrix given three orthagonal angles of
rotation in radians
format('longEng')
A=[1 0 0;0 cos(Alpha) -sin(Alpha);0 sin(Alpha) cos(Alpha)]...
            * ...
            [cos(Beta) 0 sin(Beta);0 1 0;-sin(Beta) 0 cos(Beta)] ...
            * ...
            [cos(Gamma) -sin(Gamma) 0;sin(Gamma) cos(Gamma) 0;0 0 1];
End
```

GEBTresults.m

```
function [k,X,U,Rot,F,M]=GEBTresults(Calc,Beam1Dpt)
format('longEng');
k=0;
for n1=1:Calc;
    k=k+1;
    pointno=0;
  for n2=1:Beam1Dpt;

        pointno=pointno+1;

        GEBTout=strcat('c:\GEBT\Flap3c', num2str(k), '.dat.out');

        GEBTfid=fopen(GEBTout,'r');
        Results=textscan(GEBTfid, '%s%s%s%s%s%s');
        %('Timoshenko Flexibility Matrix');
        Pointloc=['Point#:', num2str(pointno)];
        p=0;
        t=0;
        while t==0;
```

```
            p=p+1;
            pline = strcat(Results{1}(p), Results{2}(p), Results{3}(p));

           % Break if we hit end of file, or the start marker
           t=strcmp(pline, Pointloc);


        end

        line=p+2;
        for q=1:3;

            X(k,q,pointno)=str2double(Results{q}(line));
            U(k,q,pointno)=str2double(Results{q}(line+1));
            Rot(k,q,pointno)=str2double(Results{q+3}(line+1));
            F(k,q,pointno)=str2double(Results{q}(line+2));
            M(k,q,pointno)=str2double(Results{q+3}(line+2));
        end
        fclose(GEBTfid);
  end
end
```

Recover.m

```
function [k]=Recover(Calc,Section1pt,Section2pt,Secchange,X,U,Rot,F,M,Secptmat)
format('longEng');
k=0;

Sec1pt=max(Section1pt);
Sec2pt=max(Section2pt);

for n=1:Calc;
    k=k+1;
    sec=0;
    for n2=1:Secchange;
        sec=sec+1;
    VABSfile{1}=['c:\PreVABS\Flaperon3VABSoutput', num2str(k), 'sec',
num2str(sec)];
    VABSfile{2}=['c:\PreVABS\Flaperon3VABSoutput', num2str(k), 'sec',
num2str(sec),'.ech'];
    VABSfile{3}=['c:\PreVABS\Flaperon3VABSoutput', num2str(k), 'sec',
num2str(sec), '.K'];
    VABSfile{4}=['c:\PreVABS\Flaperon3VABSoutput', num2str(k), 'sec',
num2str(sec), '.opt'];
    VABSfile{5}=['c:\PreVABS\Flaperon3VABSoutput', num2str(k), 'sec',
num2str(sec), '.v0'];
    VABSfile{6}=['c:\PreVABS\Flaperon3VABSoutput', num2str(k), 'sec',
num2str(sec), '.v1S'];

    if sec==1;
        pt=0;
        for n3=1:Sec1pt;
             pt=1+pt;
              pop=0;
                VABSfileo{1}=['c:\PreVABS\Flaperon3VABSoutput', num2str(k),
'sec', num2str(1), 'pt', num2str(pt)];
```

```
                VABSfileo{2}=['c:\PreVABS\Flaperon3VABSoutput', num2str(k),
'sec', num2str(1), 'pt', num2str(pt), '.ech'];
                VABSfileo{3}=['c:\PreVABS\Flaperon3VABSoutput', num2str(k),
'sec', num2str(1), 'pt', num2str(pt), '.K'];
                VABSfileo{4}=['c:\PreVABS\Flaperon3VABSoutput', num2str(k),
'sec', num2str(1), 'pt', num2str(pt), '.opt'];
                VABSfileo{5}=['c:\PreVABS\Flaperon3VABSoutput', num2str(k),
'sec', num2str(1), 'pt', num2str(pt), '.v0'];
                VABSfileo{6}=['c:\PreVABS\Flaperon3VABSoutput', num2str(k),
'sec', num2str(1), 'pt', num2str(pt), '.v1S'];

                for n4=1:6;
                    pop=pop+1;

                     copyfile(VABSfile{pop},VABSfileo{pop});
                end
        end
    end
    if sec==2;
        for n5=Sec1pt+1:Sec2pt;
             pt=1+pt;
              pop=0;
                VABSfileo{1}=['c:\PreVABS\Flaperon3VABSoutput', num2str(k),
'sec', num2str(2), 'pt', num2str(pt)];
                VABSfileo{2}=['c:\PreVABS\Flaperon3VABSoutput', num2str(k),
'sec', num2str(2), 'pt', num2str(pt), '.ech'];
                VABSfileo{3}=['c:\PreVABS\Flaperon3VABSoutput', num2str(k),
'sec', num2str(2), 'pt', num2str(pt), '.K'];
                VABSfileo{4}=['c:\PreVABS\Flaperon3VABSoutput', num2str(k),
'sec', num2str(2), 'pt', num2str(pt), '.opt'];
                VABSfileo{5}=['c:\PreVABS\Flaperon3VABSoutput', num2str(k),
'sec', num2str(2), 'pt', num2str(pt), '.v0'];
                VABSfileo{6}=['c:\PreVABS\Flaperon3VABSoutput', num2str(k),
'sec', num2str(2), 'pt', num2str(pt), '.v1S'];

                for n6=1:6;
                    pop=pop+1;

                    copyfile(VABSfile{pop},VABSfileo{pop});
                end
        end



    end
    end




end


k=0;
for t1=1:Calc;
    k=k+1;
    ptmat=0;
```

```
    for s1=1:Sec2pt;
        ptmat=ptmat+1;

        VABSinput1=['c:\PreVABS\Flaperon3VABSoutput', num2str(k), 'sec',
num2str(Secptmat(ptmat,2)), 'pt', num2str(Secptmat(ptmat,1))];

        VABSCHECK=fopen(VABSinput1,'r');
        Check=textscan(VABSCHECK, '%s%s%s%s%s%s%s');
         %('recovery');
        Checkloc='110';
        fclose(VABSCHECK);
        rline = strcat(Check{1}(2), Check{2}(2), Check{3}(2));
        z=0;
        % Break if we hit end of file, or the start marker
        z=strcmp(rline, Checkloc);

            if z==1;

            else


%Remember to write a code to change VABS input file's second line from 1 0 0
%to 0 1 0 for recovery



                VABSrecover=fopen(VABSinput1,'r+');


% call fseek between read and write operations
                fseek(VABSrecover, 0, 'bof');

% print the new values
                 fprintf(VABSrecover, '0 0 \n');
                 fprintf(VABSrecover, '1 1 0 \n');
                 fprintf(VABSrecover, '0 0 0 0 \n');
% close the file
                fclose(VABSrecover);



                 A=zeros(3);
                 VABSR=fopen(VABSinput1,'a');
                   U123=['   ', num2str(U(k,1,Secptmat(ptmat,1))), '   ',
num2str(U(k,2,Secptmat(ptmat,1))), '   ', num2str(U(k,3,Secptmat(ptmat,1)))
,'\n'];
                fprintf(VABSR, U123);
                A=DCMRad(Rot(k,1,Secptmat(ptmat,1)), Rot(k,2,Secptmat(ptmat,1)),
Rot(k,3,Secptmat(ptmat,1)));
                e=0
                    for a=1:3;
                        e=1+e;
                        DCM=['   ', num2str(A(e,1)), ' ', num2str(A(e,2)), ' ',
num2str(A(e,3)), ' \n'];

                         fprintf(VABSR, DCM);
```

```
                    end
                F1M123=['    ', num2str(F(k,1,Secptmat(ptmat,1))), ' ',
num2str(M(k,1,Secptmat(ptmat,1))), ' ', num2str(M(k,2,Secptmat(ptmat,1))), ' ',
num2str(M(k,3,Secptmat(ptmat,1))), ' \n '];
                fprintf(VABSR, F1M123);
                F2F3=['    ', num2str(F(k,2,Secptmat(ptmat,1))), '    ',
num2str(F(k,3,Secptmat(ptmat,1))), ' \n '];
                fprintf(VABSR, F2F3);
                fprintf(VABSR, '    0 0 0 0 0 0 \n');%f1  f2  f3  m1  m2  m3
                fprintf(VABSR, '    0 0 0 0 0 0 \n');%f1' f2' f3' m1' m2' m3'
                fprintf(VABSR, '    0 0 0 0 0 0 \n');%f1" f2" f3" m1" m2" m3"
                fclose(VABSR);
            end
    end
    end
    end          %add a function to run VABS recovery for every 1D beam point
and draw a 3Dend%plot
```

VABSrecover.m

```
function [k]=VABSrecover(Calc,Secchange,Secptmat,Section2pt)

sec=0;
Sec2pt=max(Section2pt);
    k=0;
  for i=1:Calc;
    k=k+1;
     ptmat=0;

    for s1=1:Sec2pt;
        ptmat=ptmat+1;

        VABSext=['c:\PreVABS\Flaperon3VABSoutput', num2str(k), 'sec',
num2str(Secptmat(ptmat,2)), 'pt', num2str(Secptmat(ptmat,1))];



    VABSe=['c:\VABS\VABS.exe ', VABSext];
    cd c:\VABS;
    system(VABSe);
  end
  end
end
```

RecoveryResults.m

```
function [k3d,Disp3D]=RecoveryResults(Calc,
Secchange,Beam1Dpt,Secptmat,Section2pt)
format('longEng');
sec=0;
Sec2pt=max(Section2pt);
    k3d=0;
  for i=1:Calc;
    k3d=k3d+1;
```

```
     ptmat=0;
    %Strain3D,Stress3D,Stressaverage3D
    for s1=1:Sec2pt;
        ptmat=ptmat+1;

        Displacement3D=['c:\PreVABS\Flaperon3VABSoutput', num2str(k3d), 'sec',
num2str(Secptmat(ptmat,2)), 'pt', num2str(Secptmat(ptmat,1)), '.U'];
         fid=fopen(Displacement3D,'r');
        Disp3D{ptmat,:,k3d}=textscan(fid, '%s%s%s%s%s%s');
        fclose(fid);

        %Strain13D=['c:\PreVABS\Flaperon3VABSoutput', num2str(k3d), 'sec',
num2str(Secptmat(ptmat,2)), 'pt', num2str(Secptmat(ptmat,1)), '.E'];
         %fidS=fopen(Strain13D,'r');
        %Strain3D{ptmat,:,k3d}=textscan(fidS, '%s%s%s%s%s%s%s%s');
        %fclose(fidS);

        %Stress13D=['c:\PreVABS\Flaperon3VABSoutput', num2str(k3d), 'sec',
num2str(Secptmat(ptmat,2)), 'pt', num2str(Secptmat(ptmat,1)), '.S'];
         %fidSt=fopen(Stress13D,'r');
        %Stress3D{ptmat,:,k3d}=textscan(fidSt, '%s%s%s%s%s%s%s%s');
        %fclose(fidSt);
         %Stressa3D=['c:\PreVABS\Flaperon3VABSoutput', num2str(k3d), 'sec',
num2str(Secptmat(ptmat,2)), 'pt', num2str(Secptmat(ptmat,1)), '.S'];
         %fidSa=fopen(Stressa3D,'r');
        %Stressaverage3D{ptmat,:,k3d}=textscan(fidSa,
'%s%s%s%s%s%s%s%s
```